This is to certify that the

thesis entitled

Residual Stress Factors in Torsional
Failure Modes of Induction-Hardened
Steel Axial Shafts

presented by

Stephen A. Zayac

has been accepted towards fulfillment
of the requirements for

Ph.D. degree in Materials Science

Robert Summitt
Major professor

Date 8 November 1979

O-7639

RESIDUAL STRESS FACTORS IN TORSIONAL FAILURE MODES OF INDUCTION-HARDENED STEEL AXLE SHAFTS

By

Stephen Adam Zayac

A DISSERTATION

Submitted to
Michigan State University
in partial fulfillment of the requirements
for the degree of

DOCTOR OF PHILOSOPHY

Department of Metallurgy,
Mechanics and Material Science

1979

ABSTRACT

RESIDUAL STRESS FACTORS IN TORSIONAL FAILURE MODES
OF
INDUCTION-HARDENED STEEL AXLE SHAFTS

BY

Stephen Adam Zayac

A quantitative relation between surface residual stress and ultimate torsional strain of induction-hardened SAE 1038 steel axle shafts has been established experimentally. Shafts which met the same heat treatment specifications and had comparable ultimate torsional strengths exhibited a wide variation in shear strain at failure. Two distinct failure modes were observed: a brittle mode, controlled by a maximum shear strain criterion; and a ductile mode, controlled by void coalescence. No correlation was found between the bulk properties and the ultimate torsional strain.

Residual stress measurements, obtained using a dual diffractometer technique prior to torsional testing, revealed that large local gradients exist in the surface residual stress distribution. Nevertheless, a mean residual stress level could be associated with each axle shaft. This mean residual stress level, determined by an average of eight equispaced measurements on a transverse cross section, was constant along the shaft except at the flange, where heat treatment conditions vary, and at the spline, where the material was severely cold worked. Comparison of these mean residual stress measurements revealed that the angle-of-twist at failure increased as the compressive residual stress level increased, and that the failure mode was a function of this

residual stress level. Analysis demonstrated that this mean residual stress level, and consequently, the angle-of-twist at failure, can be controlled by process selection and quench conditions.

To my Father and Mother

whose love and sacrifices

have been a source of strength

throughout my life.

ACKNOWLEDGMENTS

Dr. Robert Summitt, my academic advisor, whose persistent pursuit of excellence weathered this investigation to completion and whose studies of surface properties suggested the direction of this research;

The late Dr. Denton McGrady, my previous academic advisor, for invaluable assistance on the practical aspects of industrial metallurgy, and for unmeasurable support, patience and a positive attitude whenever needed;

Mr. Carl Langenberg of Oldsmobile Division, General Motors Corporation, for suggesting initial research areas, and for providing materials and research facilities;

Mr. Jack LaBelle of Detroit Diesel Allison Division, General Motors Corporation, for technical advice and experimental assistance;

Dr. Terry Triffet, for guidance in developing an understanding of continuum models and dislocation theory;

Dr. K. N. Subramanian, for guidance in structural aspects of fracture and in fractography;

Dr. Nicholas Altiero, for his assistance in fracture mechanics;

Dr. Chuan-Tseng Wei, for developing fundamental approaches to material behavior;

Dr. Donald Montgomery, whose technology assessment group provided the techniques for evaluating real-time production problems;

Mr. Leo Tankersley, for sharing his practical expertise and for assistance with the scanning electron microscopic studies;

Mr. Edison Searles, for his assistance in photography and final preparation,

Mrs. Mary Wood, for the care and patience that she displayed in preparing this manuscript;

Mrs. Thelma Liszewski, without whose experience and last-minute assistance publication would still be pending;

Finally, to my friends and family, without whose love, encouragement and assistance, this work could not have been completed, and, especially to my wife, Marilyn, who sustained us through the simultaneous genesis of this thesis and births of our daughters, Nicole and Elise.

TABLE OF CONTENTS

LIST OF TABLES

LIST OF FIGURES

Page

NOMENCLATURE

A_{c_3}	upper critical temperature for non-equilibrium heating
$A_{c_3}', A_{c_3}'', A_{c_3}'''$	A_{c_3} for heating rates of 100, 500 and 1000 °F/sec
A_{e_1}	lower critical temperature for equilibrium
A_{e_2}	magnetic transition (Curie) temperature
A_{e_3}	upper critical temperature for equilibrium
$\vec{B}$	magnetic field vector
D_I	ideal critical diameter
E	Young's modulus
G	slope of linear region of torque-twist curve ~ shear modulus
I	electrical current
K	material toughness
K_{IIIc}	critical value of material toughness in torsion
K'	stress constant
R	electrical resistance
R_c	Rockwell "C" hardness
R_{CORE}	R_c measured on flange
R_{50}, R_{150}	R_c measured 0.050 and 0.150 inch below surface
TUS	torsional ultimate strength
TYP	torsional yield point
TYS	torsional yield strength
V	coefficient of variation
Z	ductile-brittle residual stress level
Z_{10}	ductile limit--10% of transition
Z_{90}	brittle limit--90% of transition
a	flaw size
a_o	inherent flaw size

d	lattice spacing
d_o	equilibrium lattice spacing
$d_z, d_{\psi_x}, d_{\psi_z}$	lattice spacing for grains oriented perpendicular to the z, ψ_x and ψ_z axes
f	frequency
r	radius
t	time
δ	reference depth
ε	nominal strain
$\varepsilon_x, \varepsilon_t, \varepsilon_z, \varepsilon_{\psi_x}, \varepsilon_{\psi_y}$	components of strain in x, y, z, ψ_x, ψ_z directions
θ	diffraction angle
θ_o	diffraction angle for equilibrium spacing
$\theta_z, \theta_{\psi_x}, \theta_{\psi_y}$	diffraction angle for grains oriented perpendicular to z, ψ_x, ψ_y directions
θ_F	angle-of-twist-at-failure
λ	wavelength
μ	magnetic permeability
ν	Poisson's ratio
π	a constant--3.1416 . . .
σ	nominal stress, electrical conductivity
σ_c	stress required for stable crack growth
σ_m	maximum interatomic stress
σ_{pp}	perfect plastic fracture stress
$\sigma_x, \sigma_y, \sigma_z$	components of stress in x, y, z, directions
ys	unflawed yield strength
$\bar{\sigma}_{RES}$	mean compressive residual stress level
τ	nominal shear stress
ψ	angular displacement of oblique detector from normal
ω	surface energy
ω_p	plastic component of ω
ω_α	elastic component of ω

I. INTRODUCTION

> "In our description of nature the purpose is not to disclose the real essence of the phenomena but only to track down, so far as it is possible, relations between the manifold aspects of our experience."
>
> Niels Bohr
> "Atomic Theory and Description of Nature" (1934)

Relations between the conditions under which a component fails and its properties are a major aspect of materials science. A good engineering design must specify not only a material which will withstand the required design loads, but also must consider the material response if stressed to failure.

A major cause of failure in components is the presence of unanticipated residual stress. Such stresses may result from design flaw, inappropriate processing, or poor material selection. More insidious sources are variations inherent within the manufacturing process and material specification. The effect of these process variables on the residual stress state must be examined critically. Unfortunately, the effect of the various mechanical, chemical and thermal manufacturing processes on the residual stress state is not understood quantitatively for most materials and manufacturing processes.

Residual stresses produced during the manufacturing process may be either tensile or compressive. Newton's Law of equilibrium for a free body under no external load, however, requires that the sum of these internal stresses be zero. This fundamental principle requires that the residual stresses generated cannot be uniform, but does not stipulate what distribution will result. This inhomogeneity necessitates

a quantitative analysis of the residual stress distribution if its importance in failure is to be established, and suggests that a single measurement may be insufficient.

From the Greco-Roman period[1] to contemporary times [2], cold working on forgings, bronze swords to alloy pinions, has improved component durability and ability to withstand impact. Myriad examples of fatigue life improvement exist with perhaps the World War II National Defense Research Committee Report (NA-115) being the most extensive early investigation. This report attributes fatigue life improvements of up to 700,000% to compressive residual stresses on the surface. Unfortunately, this report contains no residual stress measurements. Furthermore, no quantitative analysis is currently available which successfully correlates residual stress variations and fracture resistance.

Industrial applications and theoretical analyses, conducted by Almen at the General Motors Research Laboratories [3] show that the maximum beneficial effect is obtained with components whose surfaces bear the maximum stress. In torsion, for example, the stress, zero at the neutral axis, increases linearly to a maximum at the surface for circular shafts elastically loaded. Horger and Maulbetsh [4] report that cold-rolled railroad axles exhibit doubled fatigue life and attribute the increase to the presence of compressive residual stresses on the surface. Similarly, Osborn [5] and Shklyarov [6] credit compressive residual surface stresses induced by induction heat treatment with doubling the fatigue life of the case-hardened rear axle shafts over that of alloy shafts which possessed equivalent maximum yield strengths. Unfortunately, a quantitative evaluation of the role residual stress plays in torsional failure is not available.

In this study we analyzed the proposition that for a given set of similarly processed, induction-hardened axle shafts, the residual stress variation is significant and is critical in defining the conditions of torsional overload failure. Measurements were made on commercially available automotive rear axle shafts. Residual stress measurements, prior to testing, were compared with the results of the standard torsion test, metallurgical and failure analysis. This choice of subject exploits the inherent symmetry and geometric simplicity of the component, the surface hardened layer, and the applied loading to reduce the complexity of the stress analysis. Furthermore, since the vase majority of rear axle shafts manufactured since World War II have been surface hardened by induction heat treatment[5], any potential cost savings or reliability improvement is important commercially. In the 1978 automotive model year, production of induction-hardened rear axle shafts, sold in the United States market, totals thirty million units with an estimated value of approximately one half billion dollars[7].

II. BACKGROUND

2.1 Induction Heat Treatment

2.1.1 Heat Treatment Effects

The primary effect of induction heat treatment, which must be isolated if the residual stress effects are to be understood, is the production of a case-hardened surface layer. Properly processed, this exterior case consists almost entirely (> 99%) of martensite. The extent of the case is indicated by the distance from the surface to the reference depth, δ , where the structure is 50% martensite. For quantitative analysis, this 50% martensitic structure is measured by a Rockwell "C" hardness reading of 45. The importance of this hardened case, other than providing wear resistant bearing surfaces, is a dramatic increase in the yield strength of the case material.

The effect of this increased yield strength is to provide load-bearing capabilities comparable with more expensive materials. Under torsional load, the surface experiences the maximum stress. The results of stress analysis for a circular shaft [8], illustrated in Figure 1, reveal that the stress is not constant on a cross-section but decreases linearly to zero on the central axis. Consequently, choosing a material whose yield strength matches the maximum elastic design stress is not necessary. It is sufficient that the yield strength of the material chosen exceed the stress level at every point on the cross-section.

Induction hardening provides the most flexibility in selecting a yield strength distribution. Regulation of process parameters determines whether yielding occurs initially at the surface, Figure 1a, or in the transition zone at the case-core interface, Figure 1b. The

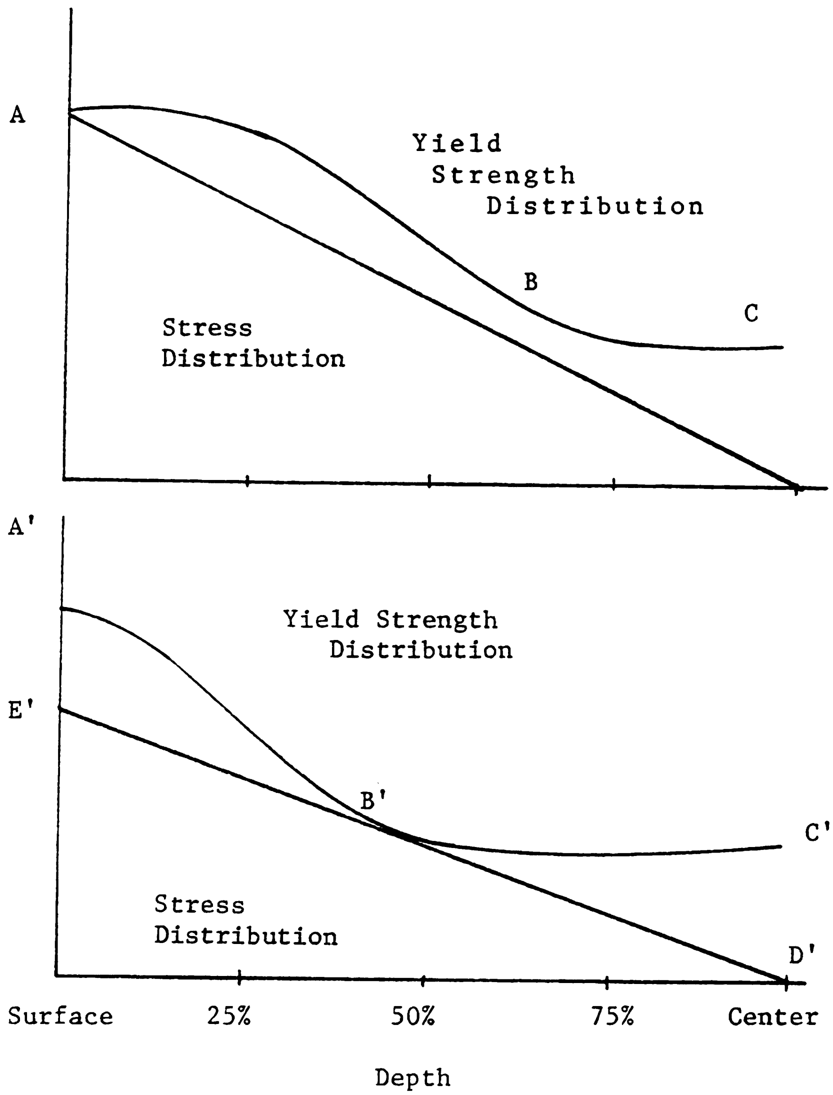

Figure 1. Torsional Stress vs Yield Strength

a. Curve ABC represents shear yield strength distribution for a deep hardened shaft. Curve AD represents the maximum stress distribution for which the shaft responds elastically. Yielding initiates at the surface (A).

b. Curve A'B'C' represents shear yield strength distribution for a shallow hardened shaft. Curve E'D' represents the maximum stress distribution for which the shaft responds elastically. Yielding initiates at the core (B').

shaft's response beyond initial yielding has been analyzed by Olszak[9] for various yield strength distributions and by Klosowicz[10,11] to determine the optimum yield strength distribution. Their analyses, however, terminate with the shaft fully plastic and consider only stress and strain-rate relations. Behavior at failure is not considered; although, the important variables of the analyses, yield strength, case depth, and plastic rigidity, must be considered if the importance of residual stress at failure is to be determined.

2.1.2 Process Parameters

Induction heat treatment of hardenable steels provides flexibility in obtaining optimum hardness and yield strength distributions. Heating is direct and selective throughout a cross-section rather than dependent on thermal transfer and diffusion mechanisms at the surface. With induction, heating results from the power dissipation of electrical currents induced to flow in the workpiece (I^2R losses). These currents, limited by the magnetic diffusion equation,

$$\frac{1}{\mu\sigma} \nabla^2 \vec{B} = \frac{\partial \vec{B}}{dt} , \tag{1}$$

diminish exponentially with distance below the surface. The exponential constant or reference depth, δ , where

$$\delta = 3160(\mu\sigma f)^{-1/2}, \tag{2}$$

defines the region within which 85% of the heating occurs.

Extensive research has been done to characterize the temperature distribution for various geometries[12,13,14]. Figure 2 displays the temperature distribution which should result if the optimum heating rates as suggested by the ASM Metals Handbook [15], are employed in

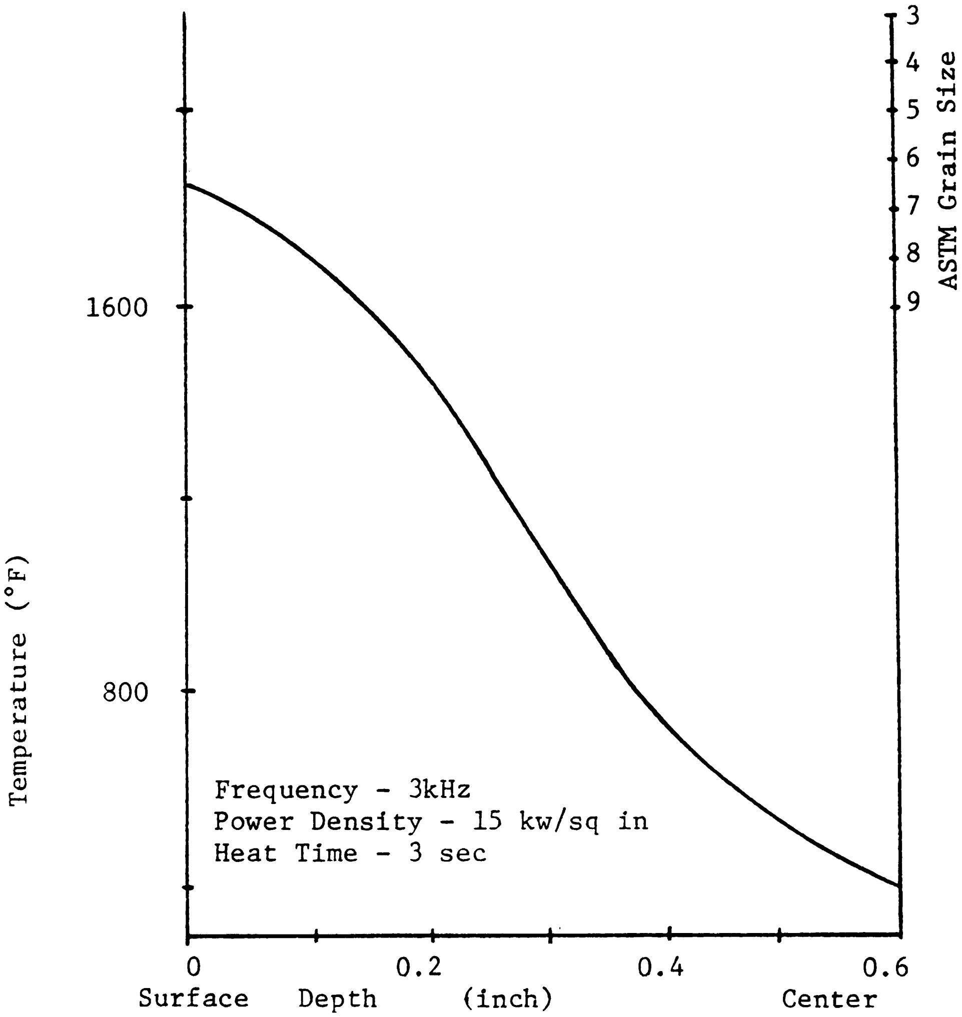

Figure 2. Temperature after Induction Heat Treat

(a) Temperature distribution for axle shaft with circular cross section as calculated using Kasper's equation (15), a 1700°F surface temperature and setup data recommended by ASM(14).

(b) The martensitic grain size is determined by the maximum temperature reached during this process. The correspondence between temperature and grain size was measured by Wuerfel (21).

Kasper's calculations [14] for a circular shaft with a 1.2 inch O.D. and which reaches a maximum surface temperature of 1700°F. This prediction compares favorably with the experimental measurements of Ishii *et al* [16]. This controlled temperature profile enhances the steel's hardenability and increases the maximum hardness obtainable [17] because minimal heat is retained within the core to temper the surface throughout the quench cycle.

Induction heating, normally at rates between 100 and 1000°F per second, supresses the diffusion controlled transformations A_{e_3} and A_{e_1}. This results in higher solution temperatures than are common with furnace heat treatments. Figure 3 illustrates the increase which Feurstein and Smith [18] measured in the A_{e_3} upper critical temperature [19] for heating rates of 100, 500, and 1000°F per second. The A_{e_3} transition temperature increases to A_{c_3}', A_{c_3}'' and A_{c_3}''' respectively for these normalized 0.38% carbon steel forgings. Material preparations that alter a steels electrical conductivity or magnetic susceptibility also yield different solution temperatures [18]. These higher solution temperatures, however, do not result in grain coarsening. The high energy input during induction heating, as opposed to the interface regulated thermal diffusion of isothermal heat treatments, requires only 0.5 to 1.0 seconds at solution temperatures to uniformly disperse the dissolved carbon [20] and thus produces a structure with fine grain size [21].

The best steels for induction hardening contain between 0.35 and 0.40% carbon and enough manganese to harden to the required depth [22]. Lower carbon content produces a less saturated martensite which restricts the maximum surface hardness [23], and consequently, the maximum yield

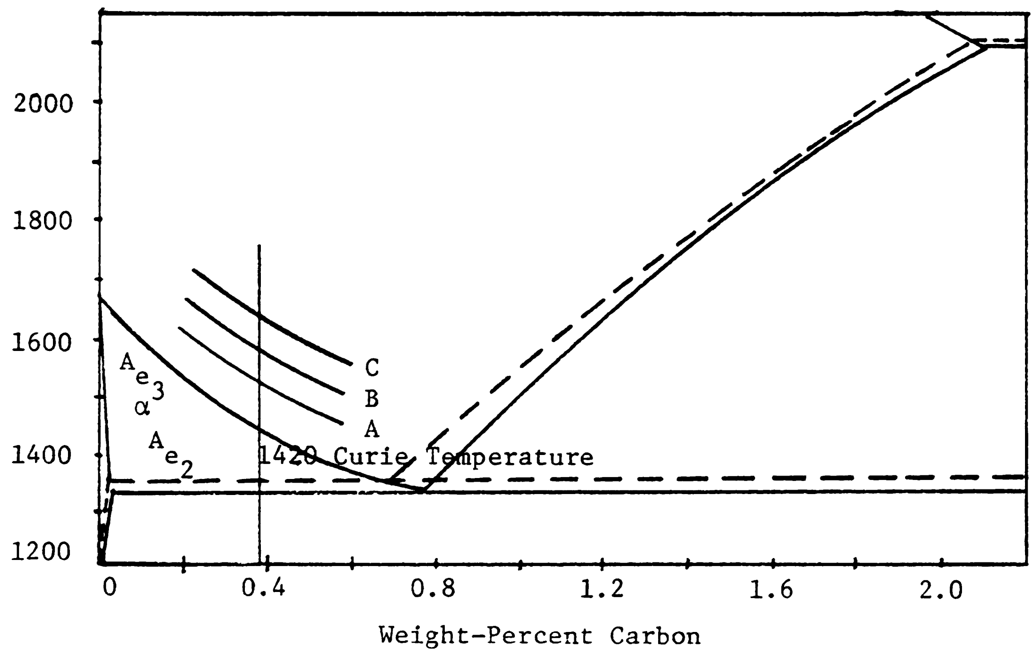

Figure 3. Austenitic Region of the "Iron-Carbon" Phase Diagram

Austenitic region of the iron-carbon phase diagram [19] modified to illustrate the effect of rapid heating on the upper critical temperature. The A_{e_3} equilibrium transition temperature increases to A_{c_3}' (A) for a heating rate of 100°F/sec, to A_{c_3}'' (B) for 500°F/sec, and to A_{c_3}''' (C) for 1000°F/sec, for the 0.38% carbon steel indicated [18].

strength obtainable [24]. Higher carbon content results in lower strength because the resulting structures contain retained austenite [22]. Higher carbon may be required for large cross-section parts, however, if additional hardenability is required. The optimum tempering cycle, a trade-off between retaining high strength and reducing quench embrittlement, which typifies the extreme heating and cooling rates of most induction heating processes, requires one hour at temperatures between 300 and 350°F [22].

2.1.3 Process Description

Two separate induction processes produce similar results--progressive and single-shot hardening. With progressive hardening equipment, the axle rotates constantly and moves through a circular, water-cooled copper coil, called an inductor, which establishes the heating magnetic field. The hot zone, once established, moves along the length of the shaft. A spray quench follows and progressively hardens the workpiece. This system, alternately referred to as scan hardening, provides considerable flexibility in hardening shafts of various lengths without complicated tooling changes. A schematic representation of this process is shown in Figure 4.

With single-shot hardening equipment, the axle rotates constantly, heats and quenches in position. Two hot zones, induced by a focused magnetic field of a laminated, water cooled copper tube (the inductor), positioned along the length of the shaft, pass around the axle as it is rotated. Once the shaft reaches the austenitizing temperature, heating ceases and quenching, accomplished by pressurized spray along the entire length of the shaft, hardens the entire shaft simultaneously. Single-shot

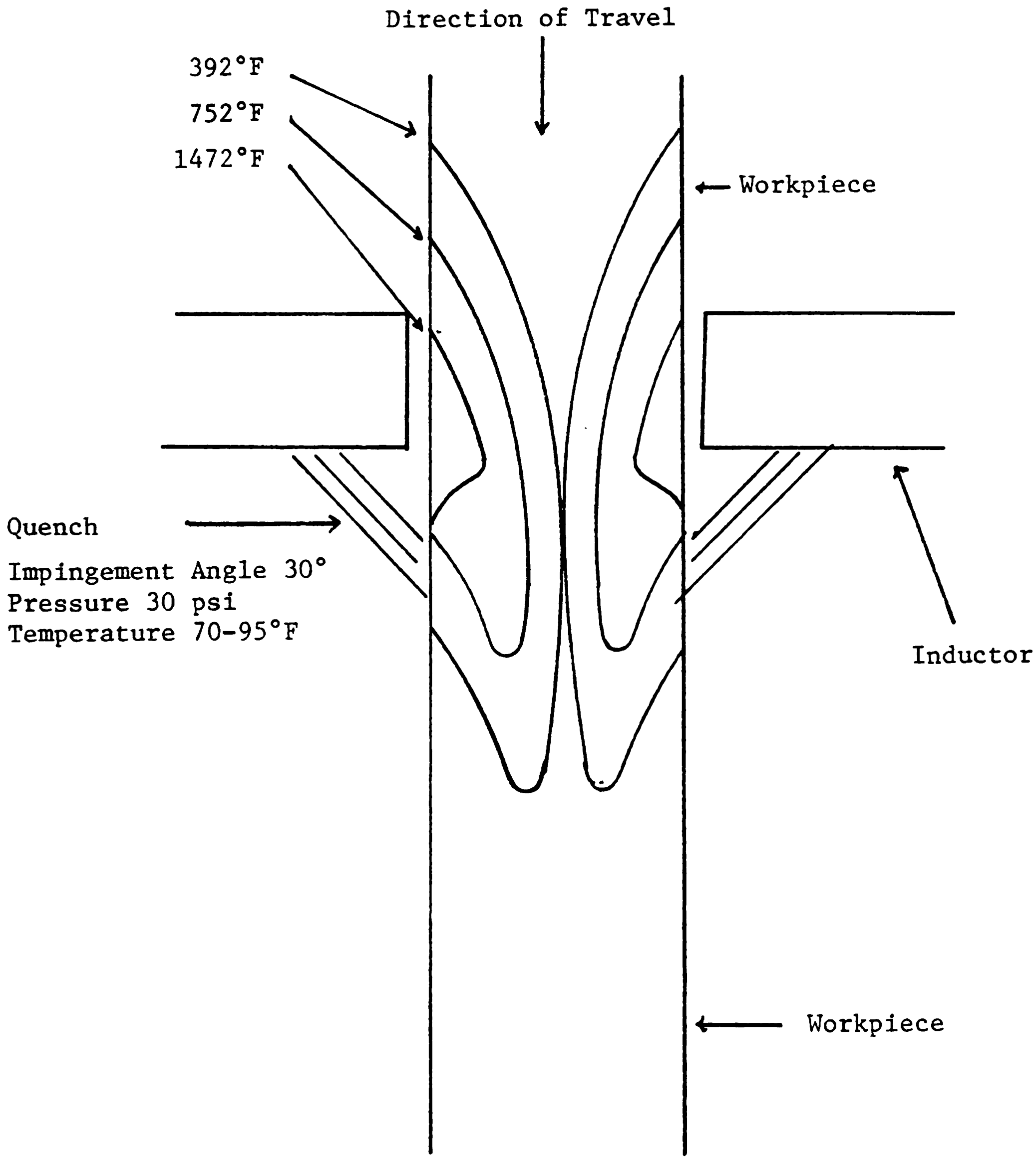

Figure 4. Progressive Hardening Process

Isotherms after Ishii, Iwamato, Shiriawa and Sakamoto [16].

hardening reduces induction heating times by up to 80% and allows rapid subsequent induction tempering. Tooling costs and change-over time, however, limit application to product lines which require minimal flexibility. A schematic representation of the single-shot process is provided in Figure 5.

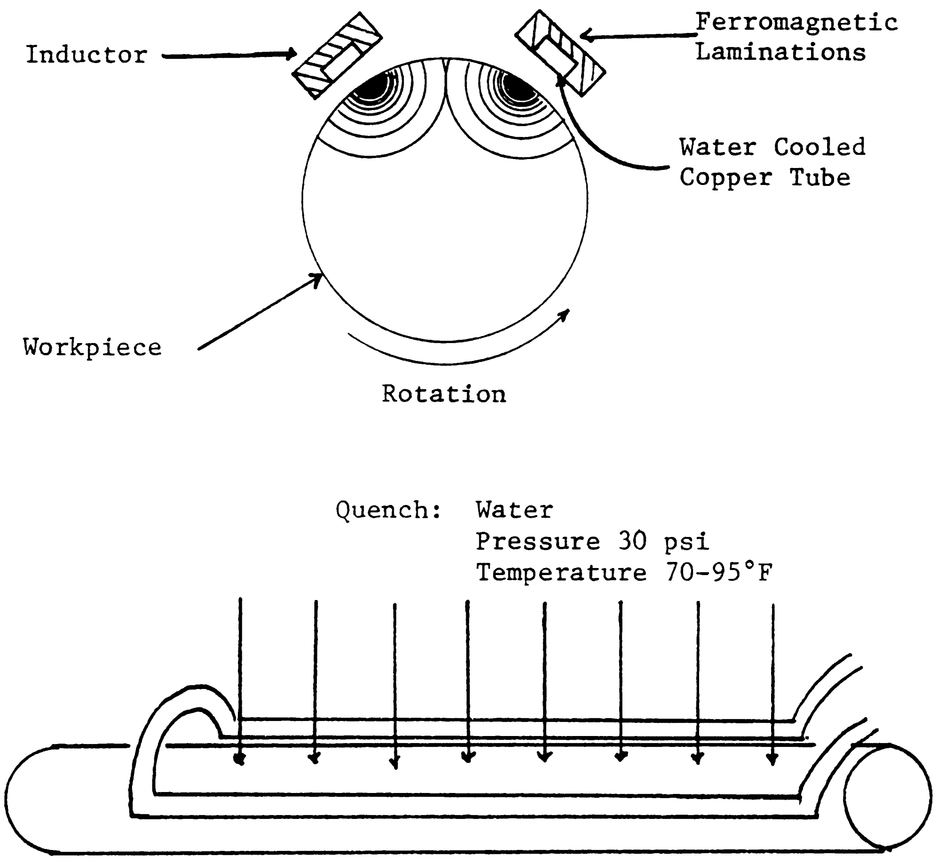

Figure 5. Single-Shot Process

Density of lines on upper drawing is proportional to the heating rate.

2.2 Residual Stress

2.2.1 Origins of Residual Stress

A primary source of failure of components is the presence of unanticipated residual stress. Residual stress develops in induction hardened axle shafts as the result of rapid metallurgical changes in the exterior structure of the shafts. Localized geometric misfit, one source of residual stress, arises from variation in the specific volumes among the various microconstituents (Figure 6)[25] and from insufficient relaxation time at grain boundaries [26]. Large thermal gradiants, inherent in the process, provide another source.[27]

Dilatometric measurements (Figure 7) by Bühler and Scheil [28] indicate that the relative coefficients of thermal expansion and the various transformation temperatures determine whether any strain results from heat treatment. Their data reveal the importance of material selection--the addition of 16% Ni to their plain carbon steel switched the strain from tension to compression. This strain in a transformed exterior case acts upon the non-transformed interior core structure to produce residual stresses within an axle shaft.

The maximum residual stress that can be generated by heat treatment is a function of the material's high temperature yield strength. Plastic flow acts to relieve stresses that are induced beyond yielding. The maximum value that residual stress can reach is a function of the thermal diffusivity of the material, the characteristic temperature distribution of the process, and the time at transformation temperature. With induction heat treatment, the temperature distribution can be controlled to allow minimal time-at-temperature and rapid heat extraction.

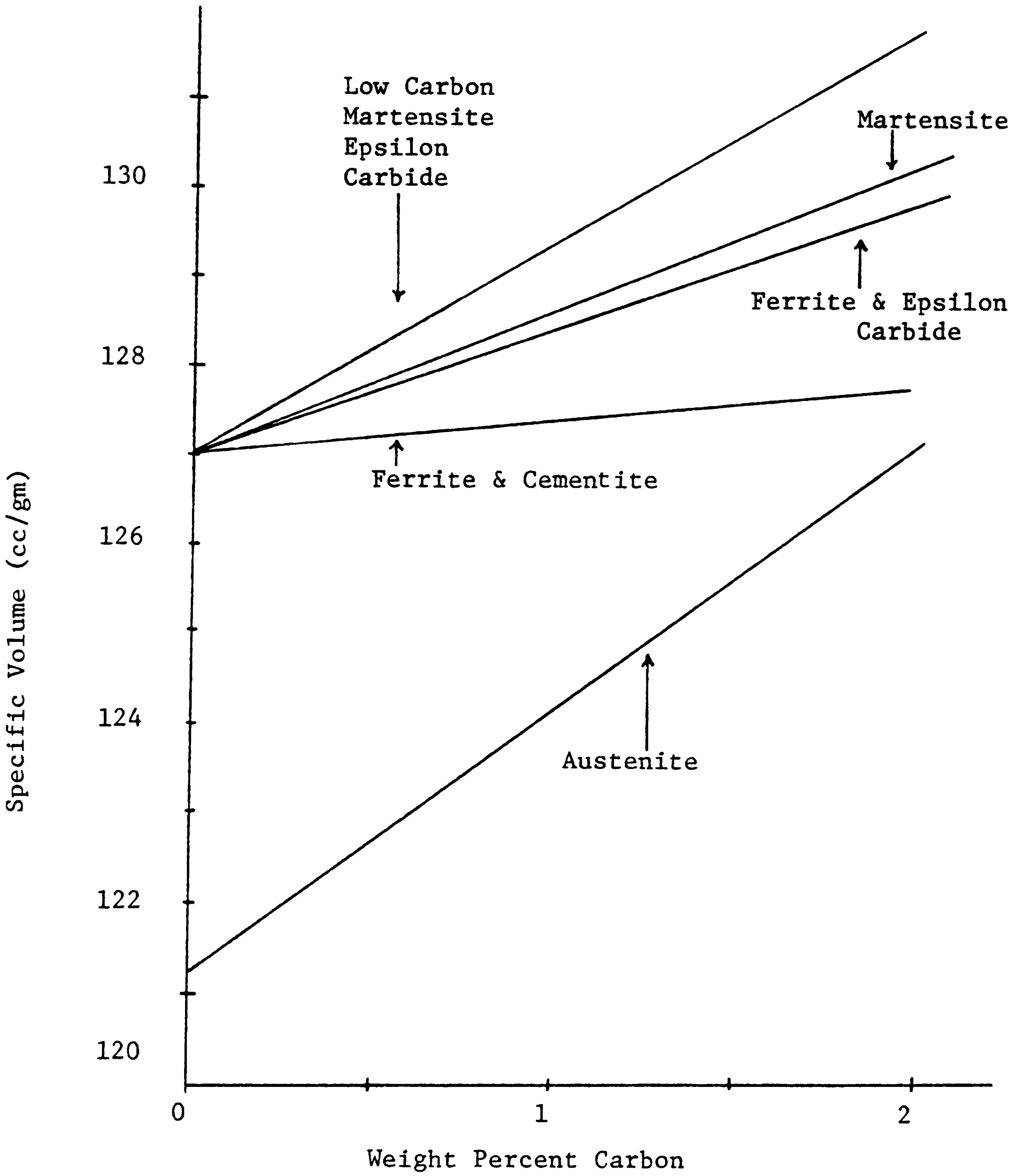

Figure 6. Specific Volumes of Steel *Versus* Carbon Content (25)

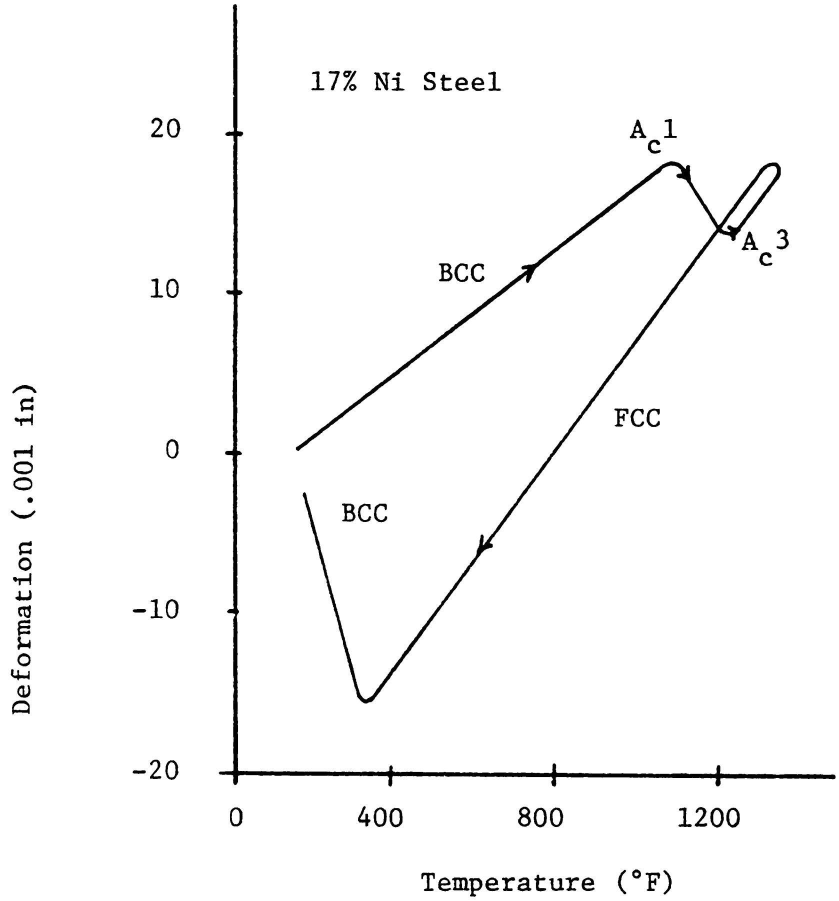

Figure 7. Dilatometric Measurements During Heat Treatment (28)

This process choice inhibits plastic flow and tempering of the case to produce maximum values of residual stress.

2.2.2 Residual Stress Distribution

The residual stress distributions which result from induction hardening--both scan and single-shot processes--have been measured by Vatev [29]. Vatev analyzed 0.45% C, plain carbon steel shafts. His measurements, illustrated in Figure 8, indicate that the residual stress varies smoothly. Tangential and longitudinal components are comparable throughout the hardened zone. Both of these components range from a high compressive stress on the surface to zero stress at the boundary of the heat-affected zone. Tensile stresses are present in the core region. The hardness transverse also indicates that the depth to 50% martensite, as indicated by R_c45, corresponds to a 50% reduction in the maximum compressive residual stress. The radial component, zero on the surface and tensile in the interior, does not exhibit a strong dependence on the cross-section structure. These measurements indicate that increases in the case depth yield increases in the value of the resultant residual stresses. It should be noted, however, that this residual stress-case depth relation was achieved by varying heating times and solution temperatures, not by varying penetration depth.

Vatev's experiments also isolate residual stress variations between scan and single-shot hardening [29] and between furnace and single-shot tempering [31]. Between the hardening processes, the major difference observed is in the radial component. The axles which were single-shot hardened possess significantly higher radial stresses

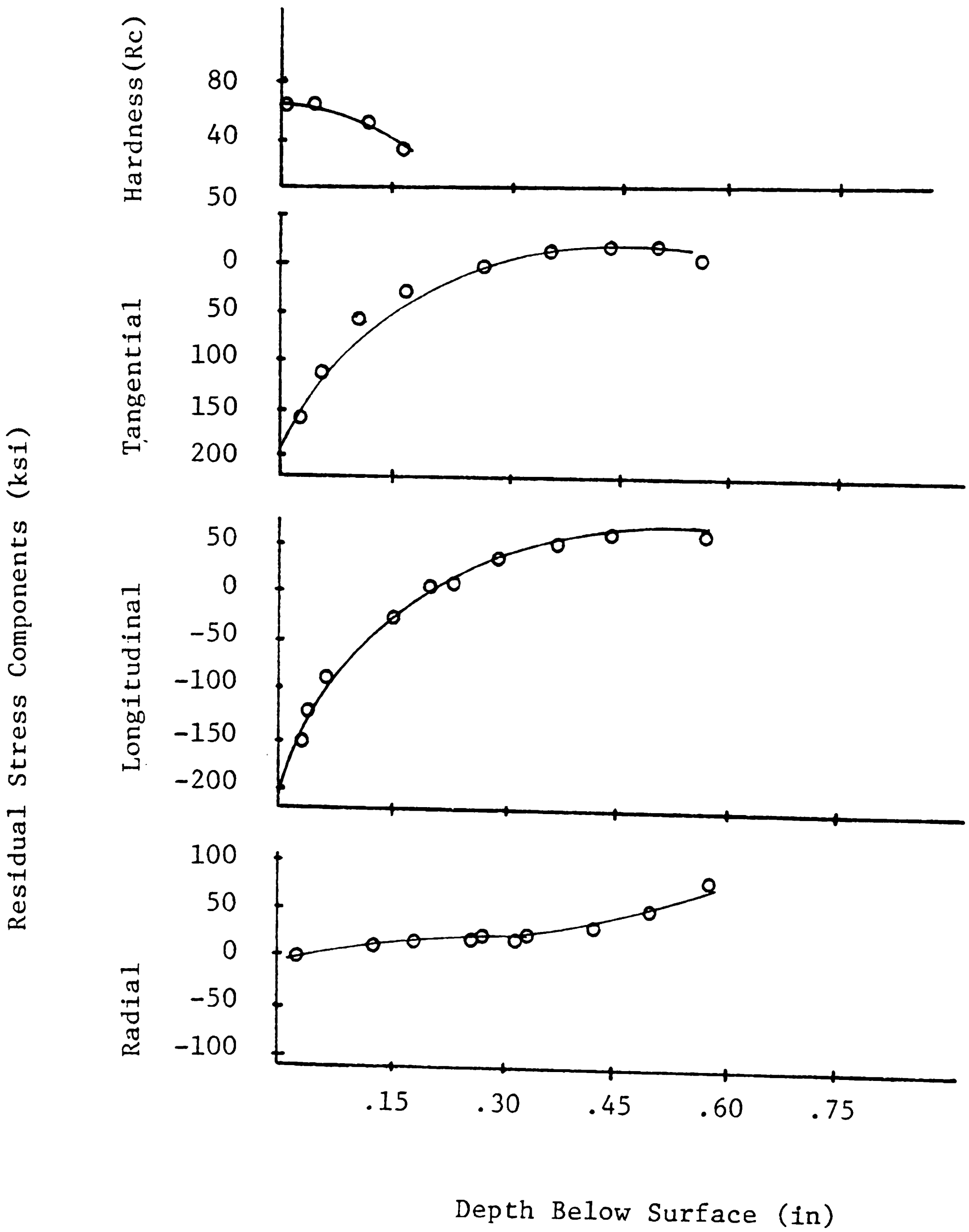

Figure 8. Residual Stress on Axle Cross-section

A 1.6 in O.D. plain carbon steel of 0.45C, axle single-shot hardened with 69 kHz source to depth of 0.10 in. Electroetch and x-ray diffraction techniques of Christenson [30] were used to measure residual stress.

throughout the cross section. The tangential and longitudinal components also differ. The single-shot hardened axles obtain higher levels of compressive stress; however, the decrease throughout the heat affected zone is more abrupt. The single-shot hardened axles also possess a less pronounced maximum in the tensile stress in the core. Between the axles tempered using the two different methods, no significant differences were observed for comparable processing. The net effect of the tempering process is a general decrease in both compressive and tensile residual stress values. Vatev's experiments, however, underline the complexity in achieving this equivalence.

The effects that variations in shaft diameter, quench conditions and surface structure cause in the residual stress distribution have been investigated by Liss, Massieon and McKloskey [32] at Caterpillar Tractor Research. Their experiments were conducted on as-quenched shafts of circular cross-section that had been austenitized for one hour under a protective atmosphere. Residual stress was determined by x-ray diffraction techniques [30] and only the longitudinal component of the surface stress was analyzed. Figure 9 summarizes their results.

For equivalent quench conditions, the compressive stress on the surface increased with increases in the shaft diameter. The increases are attributed to increased thermal plastic strains that result as the ratio of core-to-case cross-sectional area increases. This hypothesis is based on their calculation that stresses produced by the specific volume differences between martensite and ferrite-carbide aggregates in a 0.50% C steel should not exceed 100,000 psi. For equivalent steels, the compressive stresses on the surface increased with increases in quench severity. Nonuniform quench resulted in variations

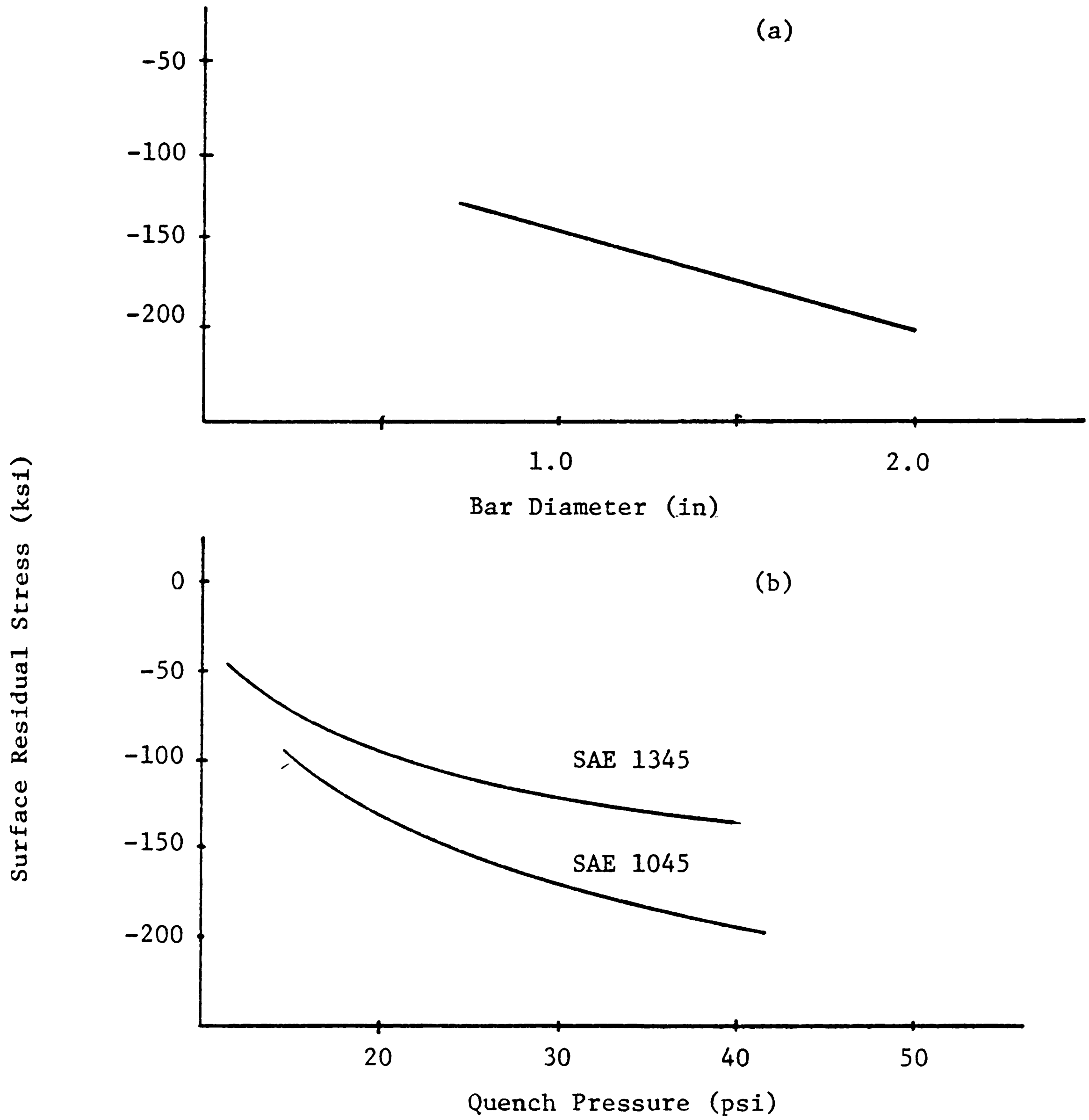

Figure 9. Factors Affecting Residual Stress

Experimental measurements by Liss (32) indicating that increasing (a) bar diameter and (b) quench rate increases the maximum residual stress on a shaft's surface.

in surface hardness and a corresponding variation in residual stress. For similar grade steels, surface decarburization drastically diminished the compressive stress obtainable on the surface. A thin layer of free ferrite on the surface reduced the surface residual stress to approximately one-third of that measured on a fully martensitic surface.

2.2.3 Residual Stress Effects

The major improvement associated with the use of induction-hardened axle shafts is the fatigue life increase which case-hardened plain carbon steels exhibit over alloy steels with comparable yield strength. Industrially reported improved service life, as cited by Osborn [5], has been verified by Shklyarov [6] in a series of controlled torsion experiments. Shklyarov's experiments compare the static and fatigue properties of induction-hardened 0.40-0.45%C plain carbon steels with alloy steels of similar carbon content. Fatigue results indicate that the plain carbon, induction-hardened axles can withstand a 100% increase in loading without decreasing fatigue life. Static torsion tests results, however, indicate no apparent residual stress dependence. Failure loads are comparable to Olszak's predictions [9] and are correspondingly less than the alloy axles. Strain variation is not considered.

Fatigue life improvement also can be measured by the endurance limit - the maximum stress at which continuous cycling produces no failure. Liss *et al.*[32] analyzed the comparative importance of carbon content and surface residual stress on the endurance limit of steel bars. The longitudinal component of the residual stress, determined by x-ray diffraction, was utilized in the comparison. Constant moment, reverse bending fatigue tests were conducted on notched circular bars 1.750 inch in diameter. As illustrated in Figure 10a, their tests indicated that surface residual stress, and not carbon content, is critical in controlling the endurance limit. Their analysis, however, does not exclude dependence on hardenability or yield strength distribution. Their experiments, as illustrated in Figure 10b, do analyze what effects tempering causes in fatigue. As-quenched SAE 1045 steel shafts exhibited a higher endurance limit, whereas tempered SAE 1045 steel shafts demonstrated a capacity to withstand more severe loads.

Although no relation between residual stress and failure in static torsion has been observed for induction-hardened axle shafts, experimental evidence exists which relates static fracture and residual stress. Littleton's experiments [33] demonstrated a four-fold increase in the bending strength of glass when properly quenched. Photoelastic comparison of annealed and quenched glass indicated the surface of the quenched glass is in a state of compression, approximately 25 ksi, higher than the annealed glass. Littleton attributes this change in fracture resistance to the residual stress difference.

Experiments by Kaplan and Rowell [34], investigating the shear constraint and macroscopic fracture crietrion for ductile metals, reveal anomalous behavior in the angle-of-twist-at-failure. Their torsion measurements, conducted with 2024-T3 aluminum tubing, produced failure strains which varied from 0.17 to 0.30 on the outside diameter for equivalently machined tubes. Further testing, conducted with similarly machined tubes, which were chemically treated to diminish the effect of surface finish, produced strains which varied from 0.31 to 0.33 on

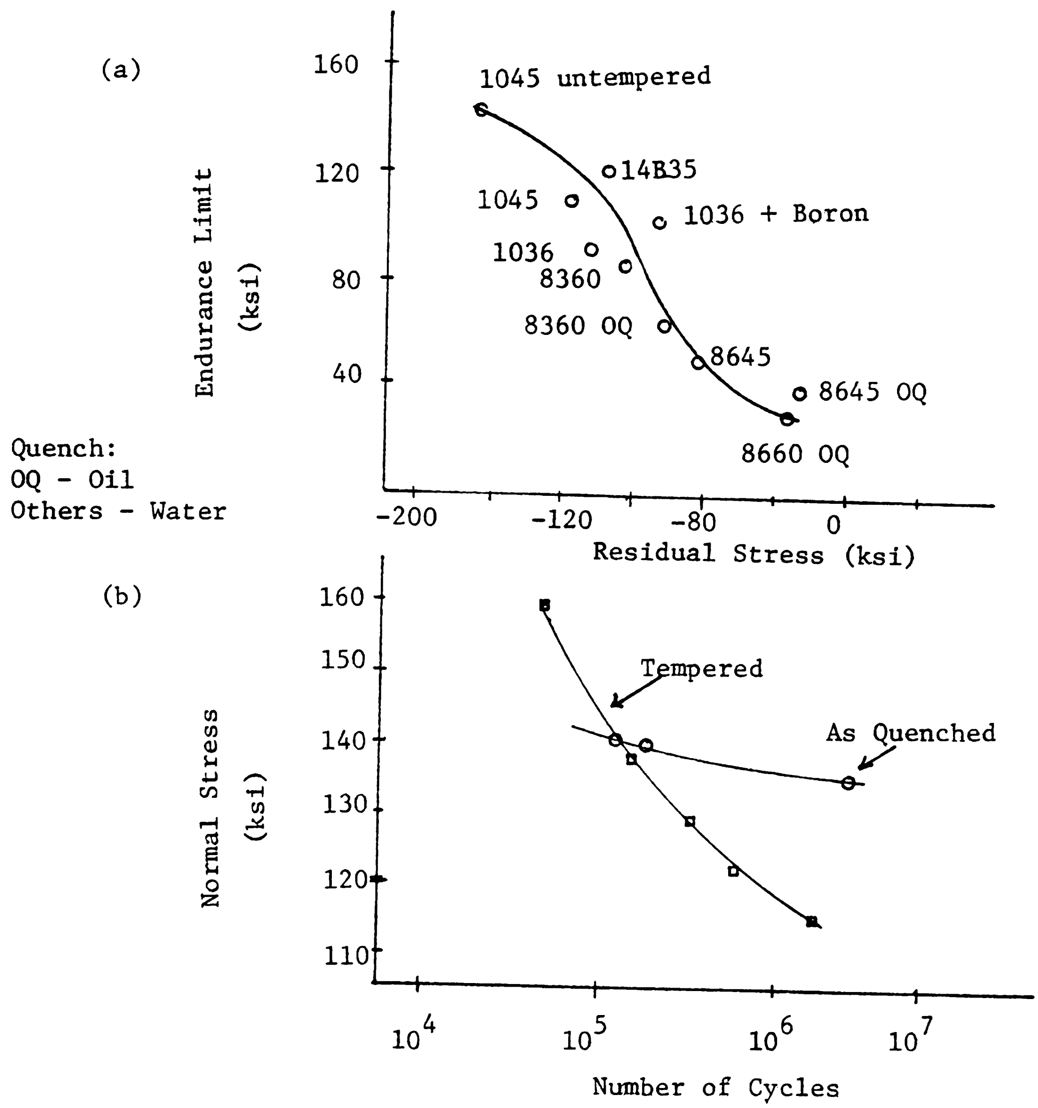

Figure 10. Residual Stress Fatigue Effects

Experimental measurements by Liss (32) indicating;

(a) Increased compressive residual stress on the surface increases endurance limit (carbon content not related to endurance limit); and,

(b) Tempering increased fatigue life at high loads.

the outside diameter. Kaplan and Rowell purported that residual stresses introduced by machining were the source of the variation.

2.3 Fracture

2.3.1 General Concepts

Ultimate strength is determined by the strength of interatomic bonds. Theoretically, the maximum resistance to fracture can be represented as the stress required to separate adjacent planes of atoms. A model, developed by Orowan [35], equates the energy required to overcome the lattice binding energy or the potential barrier with the surface energy required to form the two new surfaces. The fracture energy is calculated by integrating the stress-displacement curve from the equilibrium position, d_o, to infinity. Orowan approximates the actual distribution with a triangular barrier. Then, the separation energy is equal to $\sigma_m \Delta d$ where σ_m is the maximum stress and Δd is the displacement at this peak stress. A strain, $\varepsilon = \Delta d/d_o$, can be introduced so that the separation energy becomes $d\varepsilon\sigma_m$. For materials whose deformation can be modelled as elastic, the separation energy becomes $\sigma_m^2 d_o/E$ where E is Young's modulus. At rupture, the energy input to separate the material is equated to the surface energy, $2\omega_\alpha$, on the two new surfaces. Using this energy balance,

$$\sigma_m^2 d_o/E = 2\omega_\alpha, \tag{3}$$

the maximum fracture stress is given as

$$\sigma_m = \frac{2E\omega_\alpha}{d_o} . \tag{4}$$

The predictions of this model correspond closely to the fracture strength measured by Brenner [36] for single crystal "whiskers."

Predictions, based on this model, however, grossly overestimate both yield and ultimate strengths for commercially prepared materials. This discrepancy, recognized by Griffith [37], results from imperfect atomic order. Using continuum arguments to model the fracture resistance of glass, Griffith's analysis employs a similar energy balance argument. The application of uniform stress does not produce a homogeneous stress distribution. Pre-existing flaws--dislocations, voids, grain boundaries, inclusions, microcracks--act as stress concentrators. The strain energy released as cracks grow is equated to the surface energy of the crack. Griffith's calculations assume an elliptical flaw and produce a result similar to the atomistic approximation,

$$\sigma = K\frac{2E\omega}{a_o} , \tag{5}$$

where K is a geometric constant, a_o is the inherent flaw size, and ω is the surface energy term. Griffith's model considers only fracture following elastic behavior and sets $\omega = \omega_\alpha$. Irwin [38] and Orowan [38] extended Griffith's model to consider fracture following plastic behavior. Their results are similar except that $\omega = \omega_\alpha + \omega_p$ where ω_p is the energy irreversibly consumed as plastic flow per unit area. Usually, $\omega_p >> \omega_\alpha$, so letting $\omega = \omega_p$ introduces minimal error. Predictions, based on this Griffith-Orowan-Irwin model, conform closely to observed fracture behavior [39] and form the basis of fracture mechanics.

The effect of residual stress on the Griffith-Orowan-Irwin criterion has been studied analytically by Jahsman and Field [40] and experimentally by Ebert, Krotine and Troiano [41]. Jahsman *et al.* proposed that the residual stress directly affects the surface energy term, W. Their calculations for the effects of residual stress in tempered glass under tension indicated a general decrease in critical stress level. Ebert *et al.* proposed that residual stress produces triaxial stress below the surface in tension. Their experiments with through-hardened tensile bars indicated temperature embrittlement similar to tests conducted with notched tensile bars. Both analyses indicated the presence of residual stresses, whether tensile or compressive on the surface, decrease the critical fracture stress. These analyses, however, did not consider the effect of residual stress in either bending or torsion.

For torsional loading of a circular shaft [42], fracture mechanics analysis establishes a failure criterion which is based on the size of the pre-existing flaws (a_o), the material's toughness (K_{IIIc}), and the unflawed yield strength (σ_{ys}). Fracture occurs by unstable crack growth of pre-existing flaws if the local stress, σ, equals the critical stress σ_c, where

$$\sigma_c = \frac{K_{IIIc}}{\sqrt{2\pi a_o}} \quad . \qquad (6)$$

Comparison with Orowan's and Irwin's equation suggest K_{IIIc} is dependent on the surface energy. If the flaw size is sufficiently small, the crack stability criterion breaks down and the material fractures if its unflawed yield strength is exceeded.

2.3.2 Static Torsion

Modelling of the fracture behavior of induction-hardened axle shafts under severe torsional loads must consider the possible effects of the inherent residual stress distribution. An analytical model of the combined stress state which would include both pure torsional loading and the actual residual stress distribution is beyond the scope of this investigation. Relationships between measurable material characteristics and observable fracture conditions are sought. The actual stress state will be modelled as a simple state of combined compression (or tension) and torsion. This approximation allows utilization of well-developed analyses.

Makky [44] derives a torsional failure criterion based on the potential for slip instability along the planes of principle stress--longitudinal, transverse, and inclined at an angle of 45° to the shaft generatrix. She dismisses fracture along the shaft's axis as not realizable; and although this surface does not seem important for static torsion, the ASM Metals Handbook [4] presents examples that demonstrate its importance in torsional fatigue. Makky finds that for rigid-plastic materials, the surface of slip instability coincides with the principle planes which intersect the shaft's axis at 45° . This rigid-plastic assumption requires minimal strain before failure and corresponds to the behavior of brittle materials [45]. Makky, however, advises [46] that if the small strain condition breaks down, triaxial stresses, generated if expansion along the longitudinal axis is restrained, cause the surface of latent instability to coincide with the principle planes perpendicular to the shaft's axis. This loosening of constraints to allow large strains simulates the behavior of ductile materials [43].

Nadai [47] cites the experimental work of Böker, who explored the influence of hydrostatic and axial compression on the torsional failure of solid marble cylinders. Under torsion alone, the cylinders fractured along a surface which intersects the surface of the cylinder in a helix inclined at an angle of 45° with respect to the longitudinal axis. This fracture occurred by cleavage on a principle plane of maximum tensile stress. Under the application of compression during torsional tests, plastic deformation was recorded and fracture occurred on two surfaces which intersected at 45°. These fractures, one by cleavage and one by shear, corresponded to the directions of calculated principle stresses.

The influence of compressive stress on torsional failure, and possibly the effect of residual stresses on the torsional response of induction-hardened axle shafts, can be analyzed by strength of material arguments [48,39,49]. Consider the Mohr's envelope, which represents a combination of maximum shear stress and maximum tensile stress failure criteria, for a brittle material. For pure torsion, and for combined tension and torsion, failure, indicated as the point tangency of the maximum principle Mohr's circle and Mohr's envelope in Figure 11a, occurs by cleavage as the maximum tensile strength of the material is exceeded. For combined compression and torsion, if the compressive stress is sufficient, failure, as indicated in Figure 11a, occurs if the maximum shear strength is exceeded. Next, consider the Mohr's envelope for a ductile material. For combined compression and torsion, and for pure torsion, failure, as indicated in Figure 11b, occurs if the maximum shear strength is exceeded. For combined tension and torsion, if the tensile stress is sufficient, failure, as indicated in Figure 11b, occurs by cleavage if the maximum tensile strength of the material is exceeded.

2.3.3 Structural Aspects

Both fracture mechanics and continuum arguments allow that a variation in residual stress could change the fracture behavior of induction-hardened axle shafts. Both analyses predict the presence of dual failure modes--yield and crack controlled propagation. The occurrence of two independent fracture modes would have to be linked to the microstructural existence of competing mechanisms. For the torsional failure of steel shafts, experiments by Yokobori and Otsuka [50]

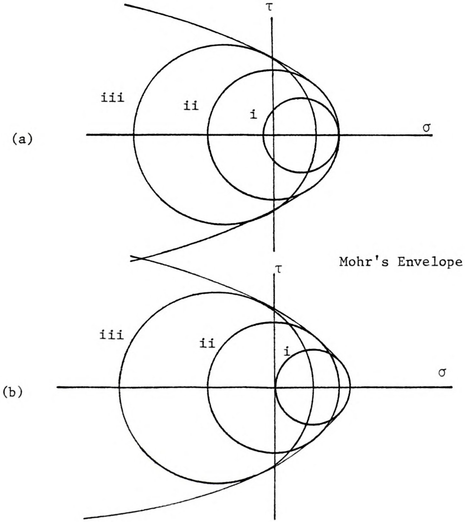

Figure 11. Mohr's Envelope and Combined Stress

Mohr's envelope indicates maximum shear stress criteria for failure. Failure represented as point of tangency between principle Mohr's circle and envelope.

(a) For brittle material. Combined tension and torsion (i) failures by maximum tensile stress. Pure torsion (ii) failure by maximum tensile stress. Combined compression and torsion (iii) failure by maximum shear stress.

(b) For ductile materials. Combined tension and torsion (i) failure by maximum tensile stress. Pure torsion (ii) failure by maximum shear stress. Combined compression and torsion (iii) failure by maximum shear stress.

demonstrate the existence of dual failure modes and the dependence of failure mode on ambient temperature.

Low temperature torsional failures appeared bright, crystalline and granular. The fractures occurred on a helical surface that was inclined at an angle of 45° to the shaft's generatrix. Etching the fracture surface with a 25% nitric acid solution produced square etch pits which indicate cleavage along the $\{100\}$ plane. Scanning electron micrographic studies by Yokobori *et al.* [51] revealed a plateau and ledge morphology typical of brittle fracture on the plane of maximum tensile stress. McClintock [52] proposed that this brittle fracture occurs as slip is blocked by pinning sites. Local stress increases until sessile dislocations break loose. Cleavage relieves the local stress and crack growth is arrested. As the applied torque increases, the local stress again increases until the shear strength is exceeded at the next barrier. The presence of these shear lips was not investigated by Yokobori.

High temperature torsional failures appeared grey, silky and fibrous. The fracture occurred on a transverse plane. Etching the fracture surface with a 25% nitric acid solution produced rectangular etch pits which indicate shear along the $\{110\}$ plane. Scanning electron microscopic studies cited by Hertzberg [51] indicated ductile fracture on the plane of maximum shear stress proceeds as mobile dislocations coalesce into voids. Final fracture occurs when the effective cross-sectional area can no longer support the applied load.

III. EXPERIMENTAL

3.0 Sample Preparation

The experimental work was performed on commercial grade S.A.E. 1038 steel axle shafts, forged, machined and heat-treated by Oldsmobile Division of General Motors Corporation. These shafts, illustrated in Figure 12, measured 30.5 inches in length. At the transverse section of minimal area, the spline, the outside diameter measured 1.22 inches. The spline contained 28 teeth which measured 0.050 inch deep with a minimal radius of curvature at the spline root circle, which measured 0.015 inch. These axle shafts were hardened to Rockwell "C" 50-58 on the surface and to Rockwell "C" 45 between 0.100 and 0.150 inch below the surface from the flange radius to the spline end of the shaft.

All shafts were processed similarly, except that either of two different induction hardening processes, progressive or single-shot, were utilized. The hardening cycles chosen represent the optimal heat treatment conditions as specified in the ASM Metals Handbook [15]. Both hardening cycles used three kHz power sources. For the progressive hardening process, the axle shafts were heated with an effective surface power density of fifteen kilowatts per square inch for three seconds. The hot zone was held at 1700°F for one second. Quenching was accomplished with a 30 psi, room temperature water spray incident at 30 degrees. Overall heating time was 52 seconds. For the single-shot hardening process, the axle shafts were heated with an effective surface power density of four kilowatts per square inch for twelve seconds. The hot zone was held at solution temperature for one second. Quenching was accomplished using a room temperature, 30 psi, water spray. Following

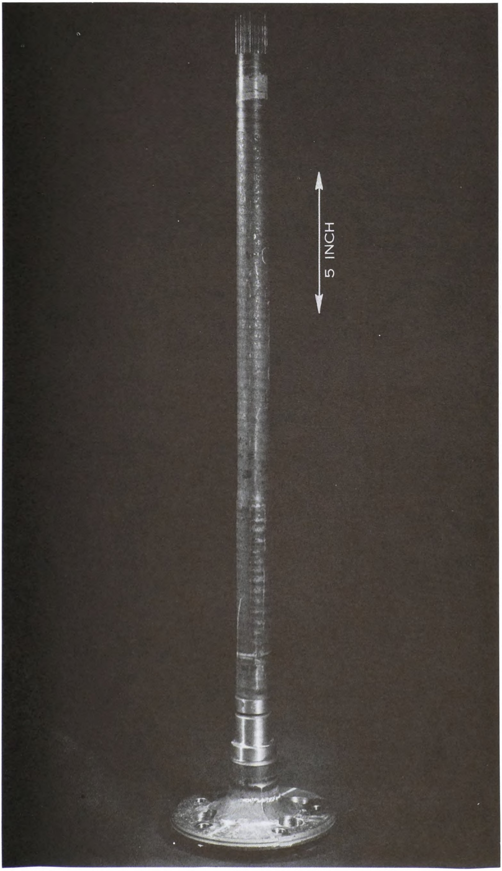

Figure 12 Rear Axle Shaft.

the hardening cycle the shafts were tempered, either one hour at 300°F ambient or equivalent induction cycle.

3.1 Physical Testing

3.1.1 Experimental Procedure

Test samples were selected randomly from commercially available axle shafts over a three-year period which commenced in September 1972. All shafts were induction hardened and subsequently tempered. A Tinius-Olson torsion testing machine was used to evaluate the torsional performance of each shaft. The shafts were bolted and twisted at the flange end. Torque was applied by holding the spline end rigid with a mating side gear. A strain rate of 0.2 degrees per second was used. This choice, according to the analysis of Kardos [54], should not introduce any dynamic effects and thus allows application of static analyses. Each shaft was twisted to failure. The test instrumentation provided a plot of applied torque versus angle-of-twist and a direct display of the maximum torque and strain. Since no change in cross-sectional area accompanied the deformation, these torque-twist curves were used to determine the yield point and the yield strength. The yield strength was identified as that point on the torque-twist curve at which a line parallel to the linear region of the curve but offset two degrees intersects the experimental trace.

Subsequent to failure, the extent of the hardened zone adjacent to the fracture zone was measured by a series of Rockwell "C" hardness measurements on each shaft. These measurements extended in 0.010 inch increments from a depth 0.010 inch to 0.150 inch below the surface. Case hardness was measured with a Brinell 3000 kg tester at the flange. These hardness data were used to assess the effect of the yield strength variation on failure.

For plain carbon steels, the relation between hardness and yield strength is well established [24]. The hardness 0.050 inch below the surface was used as a measure of the maximum yield strength. The hardness 0.150 inch below the surface and the depth to Rockwell "C" 45 were chosen as measures of the case depth. The core hardness was used as the measure of the core strength. In addition, the maximum torque, which each shaft should sustain if circular and perfectly plastic, was estimated using the hardness data. A step and a ramp approximation which measured torque in R_c-in^2 were used to evaluate the effect of the transverse yield strength variation.

The step approximation modelled the cross-sectional hardness variation as constant from the surface to the penetration depth with a value equal to that measured at a depth of 0.500 inch and as constant from the penetration depth to the shaft's midpoint with a value equal to that measured for the core. The penetration depth was taken as the depth to Rockwell "C" 45. The ramp approximation modelled the cross-sectional hardness variation as: first, constant from the surface to a depth of 0.050 inch; second, varying linearly between the depths of 0.050 inch and 0.150 inch with the endpoint hardness as measured; and, third, varying linearly between a depth of 0.150 and the central axis with the end point hardness as measured. Then, using the cross section of minimal area where the radius equals 0.610 inch, the maximum torque,

$$\sigma_{pp} = \int_0^{.610} \int_0^{2\pi} \sigma(r)\ r d\theta dr, \tag{7}$$

can be calculated. For the step approximation,

$$\sigma_{pp} = \pi \cdot 10^{-6}\{R_{50}(1220\delta-\delta^2) + R_{core}\ (610-\delta)^2\}\ , \tag{8}$$

and for the ramp approximation,

$$\sigma_{pp} = \pi \cdot 10^{-6}\{111{,}167R_{50} + 190{,}400R_{150} + 70{,}533R_{core}\} \tag{9}$$

where R_{50}, R_{150}, and R_{core} are the hardness measurements at depths of 0.050 inch, 0.150 inch and the core, respectively, and δ is the depth to Rockwell "C" 45.

Chemical analyses were performed on a random subset of the test axles. A Leco Carbon-Sulfur Analyzer was used to measure carbon and sulfur content. Spectrographic analysis was used to determine residuals. Based on the experimental work of Liss *et al.* [32], no direct link between chemical composition and failure should be expected, and was not evaluated. Since their analysis did not exclude failure dependence on hardenability, these chemical analyses and the algorithm of Jatczak [55] were used to determine the "ideal critical diameter" and this standard measure of hardenability was compared with the failure conditions.

3.1.2 Statistical Analyses

In-process variables were monitored and regulated to yield axle shafts with equivalent behavior under load. Since some variation within the heat treatment was unavoidable, the failure loads, the maximum deformations and the variables thought to affect failure were analyzed to determine whether their distributions were random. The mean, the standard deviation, the skewness, the kurtosis and the Kolmogorov-Smirnov "d" [56] were calculated for each distribution (Appendix I) by standard techniques (Appendix II). The "Errror" program compared the distribution with a normal distribution whose mean and standard distribution were similar, compared the actual range of the variable with the six-sigma limits, calculated the maximum confidence at which the Kolmogorov-Smirnov test indicated normality and plotted the actual distribution.

This Kolmogorov-Smirnov test for normality compares the actual distribution with the associated normal distribution. The Kolmogorov-Smirnov statistic represents the maximum difference between the normalized actual and Gaussian distributions. Based on Lilliefor's calculations [56], this statistic provides a more powerful test of normality than that provided by the standard chi-squared test. The "Errror" program tests at the .20, .15, .10, .05 and .01 levels of significance. The lowest level (.01) is tested first, and if accepted at this level, is tested at progressively higher levels to determine the maximum acceptance level.

Previous analyses [6,9] have established the ultimate torsional strength's dependence on the yield strength variation that induction hardening induces. Since no relation has been established for the ultimate torsional strain, linear regression analysis between the angle-of-twist-at-failure and those variables indicated by previous analysis as critical were performed (Appendix III) to isolate their effects. The "Compare" program calculated the correlation coefficient, standard deviation in predicted failure angle, and the coefficients for the least squares linear approximation. Scatter diagrams were plotted to insure the correlation calculations were not biased and to detect any trends not revealed by the calculations. Furthermore, the

coefficient of variation (V), determined by the ratio of the standard deviation to the mean, was used to compare the relative dispersion of the various distributions.

3.1.3 Data and Observations*

The deformation and load at failure for the test group exhibited dissimilar statistical behavior. The angle-of-twist-at-failure distribution (Table 1) did not meet the minimum Kolmogorov-Smirnov "d" criterion for normality. The individual data showed much scatter as indicated by the high coefficient of variation, V = 0.422, for the distribution. The torsional ultimate strength distribution (Table 2) met the most stringent Kolmogorov-Smirnov "d" criterion for normality. The individual data were grouped closely as indicated by the low coefficient of variation, V = 0.070, for the distribution. Correlation analysis (Table 12) between the angle-of-twist-at-failure and the torsional ultimate strength yielded a correlation coefficient of -0.076. Linear regression analysis yielded a standard deviation in the failure angle estimate, which was 19.5% of the actual distribution range, and a slope which indicated that increasing the ultimate strength decreases the failure angle. Analysis of the scatter diagram confirmed the apparent independence of these physical measures of failure.

The torsional yield strength distribution (Table 3) met the Kolmogorov-Smirnov "d" criterion for normality at the .01 significance level. The individual data were grouped closely as indicated by a low coefficient of variation, V = 0.093, for the distribution. Correlation

---

* References to tables in this section refer to tables in Appendix IV.

analysis (Table 13) between the angle-of-twist-at-failure and the torsional yield strength yielded a correlation coefficient of 0.010. Linear regression analysis yielded a standard deviation in the failure angle estimate that was 19.6% of the actual distribution range and a slope which indicated that increasing the yield strength decreases the failure angle. Analysis of the scatter diagram revealed no observable trend in the data.

The torsional yield point distribution (Table 4) met the Kolmogorov-Smirnov "d" criterion for normality at the .01 significance level. The individual data were grouped closely as indicated by a low coefficient of variation, V = 0.169, for the distribution. Correlation analysis (Table 14) between the angle-of-twist-at-failure and the torsional yield point yielded a correlation coefficient of 0.284. Linear regression analysis yielded a standard deviation in the failure angle estimate which was 18.8% of the actual distribution range and a slope which indicated that increasing the yield point increases the failure angle. Analysis of the scatter diagram revealed no observable trend in the data.

The surface hardness distribution (Table 5) did not meet the minimum Kolmogorov-Smirnov criterion for normality. The individual data, however, were grouped closely as indicated by a low coefficient of variation, V = 0.041, for the distribution. Correlation analysis (Table 15) between the angle-of-twist-at-failure and the surface hardness yielded a correlation coefficient of -0.085. Linear regression analysis yielded a standard deviation in the failure angle estimate which was 19.5% of the actual distribution range and a slope which indicated increasing the surface hardness decreases the failure angle. Analysis of the scatter diagram revealed no observable trend in the data.

The case hardness distribution (Table 6) met the Kolmogorov-Smirnov "d" criterion for normality at the .01 significance level. The individual data were grouped closely as indicated by a low coefficient of variation, V = 0.194, for the distribution. Correlation analysis (Table 16) between the angle-of-twist-at-failure and the case hardness yielded a correlation coefficient of -0.242. Linear regression analysis yielded a standard deviation in the failure angle estimate which was 18.4% of the actual distribution range and a slope which indicated that increasing case hardness decreases the failure angle. Analysis of the scatter diagram revealed no observable trend in the data.

The core hardness distribution (Table 7) did not meet the minimum Kolmogorov-Smirnov "d" criterion for normality. The individual data were not scattered as indicated by the coefficient of variation, V = 0.346, for the distribution. The distribution appears single-sided. Correlation analysis (Table 17) between the angle-of-twist-at-failure and the core hardness yielded a correlation coefficient of -0.265. Linear regression analysis yielded a standard deviation in the failure angle estimate which was 19.9% of the actual distribution range and a slope which indicated that increasing case hardness decreases the failure angle. Analysis of the scatter diagram revealed no observable trend in the data.

The case depth distribution (Table 8) did not meet the minimum Kolomogorov-Smirnov "d" criterion for normality. The individual data were not scattered as indicated by the coefficient of variation, V = 0.150, for the distribution. Correlation analysis (Table 18) between the angle-of-twist-at-failure and the case depth yielded a

standard deviation in the failure angle estimate which was 18.6% of the actual distribution range and a slope which indicated that increasing the case depth decreases the failure angle. Analysis of the scatter diagram revealed no observable trend in the data.

The hardenability distribution (Table 9) met the Kolmogorov-Smirnov "d" criterion for normality at the .05 significance level. The individual data were grouped closely as indicated by a low coefficient of variation, V = 0.103, for the distribution. Correlation analysis (Table 19) between the angle-of-twist-at-failure and the hardenability yielded a correlation coefficient of -0.345. Linear regression analysis yielded a standard deviation in the failure angle estimate which was 18.5% of the actual distribution range and a slope which indicated that increasing the hardenability decreases the failure angle. Analysis of the scatter diagram revealed no observable trend in the data.

The step approximation distribution (Table 10) met the Kolmogorov-Smirnov "d" criterion at the .01 significance level. The individual data were grouped closely as indicated by a low coefficient of variation V = 0.130, for the distribution. Correlation analysis (Table 20) between the angle-of-twist-at-failure and the step approximation yielded a correlation coefficient of -0.137. Linear regression analysis yielded a standard deviation in the failure angle estimate which was 19.2% of the actual distribution range and a slope which indicated that increases in the step approximation should result in decreases in the failure angle. Analysis of the scatter diagram revealed no observable trend in the data.

The ramp approximation distribution (Table 11) did not meet the minimum Kolmogorov-Smirnov "d" criterion for normality. The individual data, however, were grouped closely as indicated by a low coefficient of variation, V = 0.093, for the distribution. Correlation analysis (Table 21) between the angle-of-twist-at-failure and the ramp approximation yielded a correlation coefficient of -0.290. Linear regression analysis yielded a standard deviation in the failure angle estimate which was 18.2% of the actual distribution range and a slope which indicated that increases in the ramp approximation should result in decreases in the failure angle. Analysis of the scatter diagram revealed no observable trend in the data.

3.1.4 Test Results

No obvious correlation between the angle-of-twist-at-failure and the investigated parameters was apparent. Summarizing the test results (Table 1), however, revealed some interesting trends. Those variables that were affected by the heat treatment (i.e., all except the core hardness as measured at the flange) exhibited very little dispersion compared with the failure angle. This difference in data scatter suggested that perhaps some other variable had been overlooked. The variables, except those that specifically measured the elastic limit (i.e., both the torsional yield point and the torsional yield strength), possessed negative correlation coefficients. This difference indicated that increases in material hardness tends to reduce the ultimate twist that can be sustained, whereas raising the elastic limit tends to increase the twist that can be sustained. Since elastic limit increases usually accompany hardness increases, the difference in correlation trend was probably structure dependent. The slopes of the linear regression analyses corroborate these trends except for the torsional

Table 1.

Angle-of-Twist-at-Failure[1] Correlations

Variable	Units	Sample Size	Var.[2] Coef.	Corr. Coef.	Std. Dev. (deg)	Y-Int. (deg)	Slope
T.U.S.	kip	131	.070	-.076	62.5	216	-1.16
T.Y.S.	kip	131	.093	.010	62.7	155	-0.20
T.Y.P.	kip	131	.169	.284	60.1	43	4.24
Surface Hardness	R_c@.050	131	.041	-.085	62.5	276	-2.36
Case Hardness	R_c@.150	111	.194	-.242	58.9	239	-2.18
Core Hardness	R_c@Flg	131	.346	-.265	60.5	196	-4.02
Case Depth	in/1000	86	.150	-.278	59.5	270	-0.86
D_I	in/1000	43	.103	-.345	59.2	369	-0.32
Step Appx.	R_c-in^2	86	.130	-.137	61.4	183	-1.65
Ramp Appx.	R_c-in^2	111	.093	-.290	58.1	332	-3.93

1. Angle-of-twist-at-failure measured in degrees.
2. Angle-of-twist-at-failure distribution coefficient of variance, V = 0.422.

yield strength; however, the correlation coefficient and the slope of the least-squares linear approximation that are associated with this variable and the angle-of-twist-at-failure were so close to zero that the change is insignificant and no trend could be ascertained. The predicted errors in the failure angle estimate, varying from ±18.2% to ±19.6%, were remarkably consistant and quite large. This estimation error also suggested that other variables were necessary to explain the angle-of-twist-at-failure behavior.

3.2 Residual Stress

3.2.1 Sample Preparation

Fourteen rear axle shafts were removed from production for residual stress analysis and for physical testing. The shafts comprised three test troups. The first group, consisting of samples A and B, were from the same heat and were not tempered. Sample A was induction hardened using a vertical scanning process, and sample B was hardened using the single-shot technique. The second group, consisting of samples C, D, E, F, G, and H, were from the same heat as the first group but were furnace tempered. Samples C, D, and E were hardened using a vertical scanning process, and samples F, G, and H were hardened using the single-shot technique. The third group, consisting of samples I, J, K, L, M, and N, were from a heat different than the previous groups. These samples were induction tempered. Samples I, J, and K were induction hardened using a vertical scanning process, and samples L, M, and N were induction hardened using the single-shot process. Processing within each group was sequential to duplicate the heat treatment conditions.

3.2.2 Measurement Theory

The residual stress on the surface of the various induction hardened axle shafts, samples A through N, was evaluated by the normal-oblique x-ray diffractometer technique which was developed by Glocker [57]. This experimental procedure, applicable to polycrystalline materials, measured the position of the diffracted x-rays for two slightly different angular exposures. These two measured angles were

coupled with Hooke's law and the appropriate elastic constants to calculate the strain on grains with different crystallographic orientations with respect to the surface. These strains and the relative invariance of the diffracted planes determined the local residual stress.

In the schematic diagram (Figure 13) the residual stress is to be evaluated at point O. A rectangular coordinate system, chosen so that the x and y axes determine the tangent plane at O and coincide with the directions of the principle residual stresses, simplifies the calculation. Since the z direction is perpendicular to the surface at O and since stresses cannot act across a free surface, the z component of the residual stress is equal to zero at O. Further, since the x and y axes are the principle directions of residual stress and since this is a plane stress problem, Hooke's law yields the following relations between stress and strain for the usual conditions of homogeneity, isotropy and linear elasticity:

$$\varepsilon_{\psi x} = \sigma_x \cdot \frac{1+\nu}{E} \cdot \sin^2\psi - \frac{\nu}{E}(\sigma_x + \sigma_y), \tag{10}$$

$$\varepsilon_{\psi y} = \sigma_y \cdot \frac{1+\nu}{E} \cdot \sin^2\psi - \frac{\nu}{E}(\sigma_x + \sigma_y), \text{ and} \tag{11}$$

$$\varepsilon_z = -\frac{\nu}{E}(\sigma_x + \sigma_y). \tag{12}$$

Subtracting Equation 12 from Equation 10 in order to eliminate the stress and strain components in the y direction yields:

$$\varepsilon_{\psi x} - \varepsilon_z = \sigma_x \cdot \frac{1+\nu}{E} \cdot \sin^2\psi. \tag{13}$$

Solving for the x component of the shear stress gives:

$$\sigma_x = \frac{E}{1+\nu} \cdot \sin^2\psi \cdot (\varepsilon_{\psi x} - \varepsilon_z) . \tag{14}$$

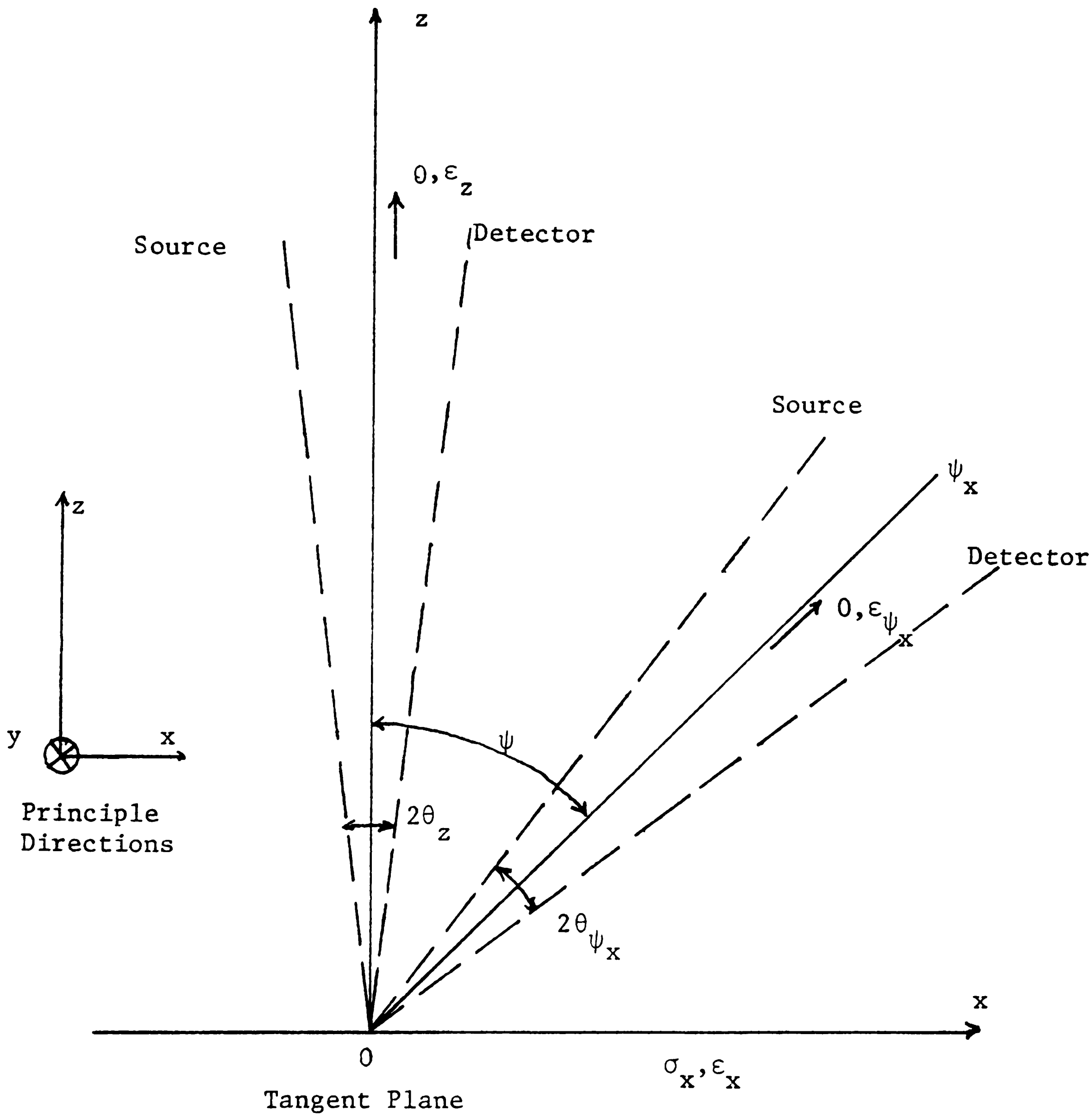

Figure 13. Residual Stress Analysis by the Normal-Oblique Technique

This means that measurement of the strain in the normal or z direction combined with measurement of the strain in an oblique direction determines the stress state uniquely.

In the neighborhood about point O, grains, oriented at the appropriate angle with respect to the surface, diffract the incident x-rays at an angle θ_z. Since the surface is stressed the lattice spacing differs from the standard lattice parameter. The residual strain in the normal direction, expressed in terms of the lattice parameter is:

$$\varepsilon_z = \frac{d_z - d_o}{d_o} \quad . \tag{15}$$

In the oblique direction, grains at a different orientation diffract the x-rays incident at angle θ_{ψ_x}. Since the stress that acts on these grains is the same, the lattice spacing, reflecting the change in orientation of the crystallographic planes, is different. Relating this change in spacing to the residual strain in this oblique direction yields:

$$\varepsilon_{\psi x} = \frac{d_{\psi x} - d_o}{d_o} \tag{16}$$

Combining Equations 15 and 16, the difference in strain between the normal and oblique directions is:

$$\varepsilon_{\psi x} - \varepsilon_z = \frac{d_{\psi x} - d_z}{d_o} \tag{17}$$

Previous x-ray experiments [58] that measured lattice parameter variation under stress indicate that the change in lattice parameter is less than 1%. Using the Bragg law,

$$d = \frac{\lambda}{2\sin\theta} , \tag{18}$$

to represent the lattice spacing in terms of the diffracted angle, the variation in lattice spacing may be represented by:

$$\delta d = \frac{\lambda}{2} \frac{\cot\theta}{\sin\theta} \delta\theta \ . \tag{19}$$

These relationships between the Bragg angle and the lattice spacing allow the residual stress to be written:

$$\varepsilon_{\psi x} - \varepsilon_z = \cot\theta_o \ (\theta_{\psi x} - \theta_z) \quad . \tag{20}$$

Substituting Equation 20 into Equation 14, the residual stress at 0 may be expressed:

$$\sigma_x = \frac{E}{1+\nu} \cdot \frac{\cot\theta_o}{\sin^2\psi} (\theta_{\psi x} - \theta_z) \quad . \tag{21}$$

For a specific material and experimental setup, E, ν, θ_o, and ψ are are constant and the residual stress' dependence on the diffraction angles, $2\theta_{\psi x}$ and $2\theta_z$, is simply:

$$\sigma_x = K'(2\theta_{\psi x} - 2\theta_z) \ , \tag{22}$$

where K', known as the stress constant, is a property of the material examined and the experimental setup only. Thus, evaluation of the residual stress on the surface requires measurements of two angles $2\theta_{\psi x}$ and $2\theta_z$ to determine σ_x and two angles $2\theta_{\psi y}$ and $2\theta_z$ to determine σ_y.

3.2.3 Experimental Apparatus

An American Analytical Fastress machine was utilized to measure the surface residual stress [59]. This device (Figure 14) used two chromium-source x-ray diffraction tubes with an effective penetration depth of 0.5 x 10^{-3} inch. The incident x-ray beams covered an area

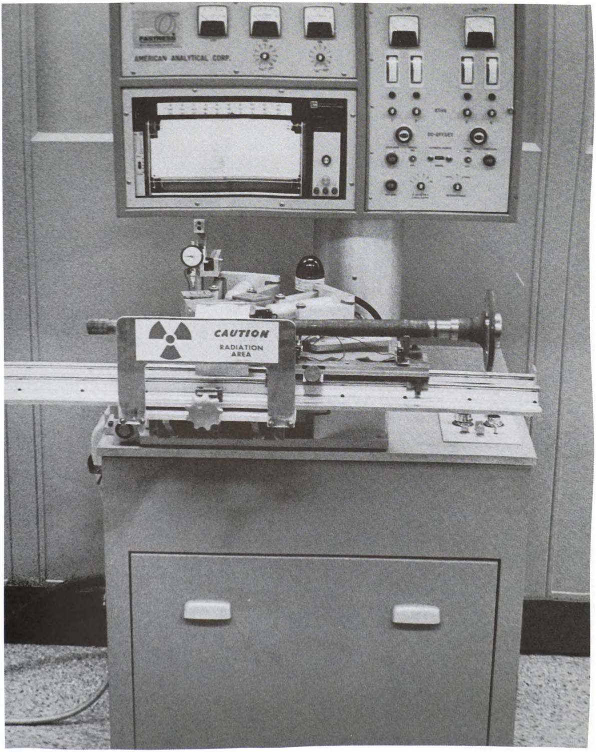

Figure 14 "Fastress" Automated Diffractometer.

which measured 0.090 inch in diameter. Appropriate shimming of the v-block fixtures insured that the plane which is determined by the x-ray beams normally intersects the plane which is tangent to the shaft. An indicator gauge, fixed with respect to the x-ray sources and graduated in 0.1×10^{-3} inch intervals, was used to position the shaft's surface in the focal plane of the x-ray beams. Linear and angular position along the shaft are referenced from the machined end surface that is adjacent to the spline.

The Fastress automates the normal-oblique diffractometer measurements. Two separate x-ray sources and detectors, illustrated in Figure 15, are positioned to measure the diffracted intensity from those planes which are oriented parallel to and 45° to the surface, and that are oriented normally to that plane which contains the incident x-rays. Each detector contains two x-ray sensors, co-planar with the incident x-ray beams and separated by an angular distance which corresponds to the width of the diffraction peak at half maximum. Each sensor generates a voltage proportional to the incident diffracted intensity. Within each detector unit, an error signal is generated if the diffracted beam is off center and the signal strength is proportional to the difference in diffracted intensities registered at the sensors. This error signal directs a servomotor angular drive which moves the detector toward the center of the diffraction peak. The control system is essentially critically damped so that the balance point is reached rapidly and without hunting.

Fastress is electronically calibrated to provide a graphical readout which plots residual stress in pounds per square inch. The residual stress is measured according to the prescription provided by

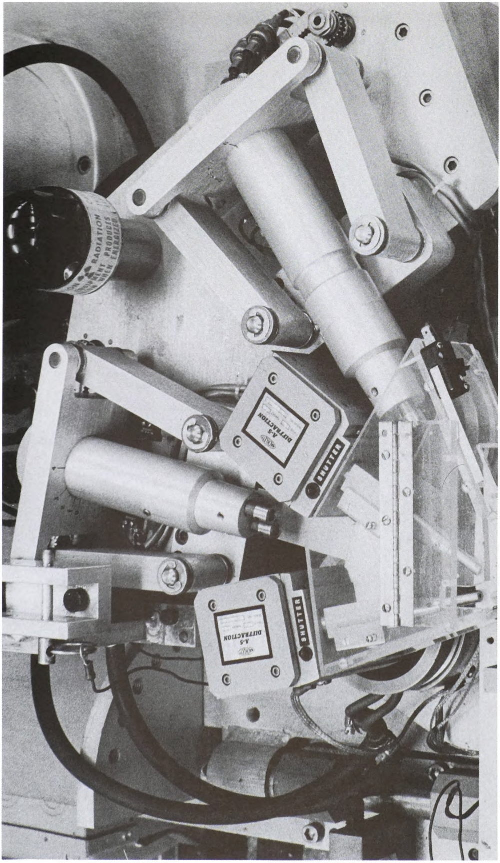

Figure 15 "Fastress" Test Set-Up,

Equation 22. The diffraction angles are determined from voltages that are proportional to the angular displacement of the detectors. The difference between these voltages is proportional to the residual stress. The output is calibrated experimentally through the use of two references. The zero stress level is established by blocking the x-ray sources and adjusting the output display to indicate zero. Calibration is established by adjusting the output to display the residual stress which corresponds to the calibrated standard supplied by the Timken Roller Bearing Company.

This calibrated voltage, used to plot the residual stress, is measured over intervals of at least five minutes. The residual stress at the point of measurement is taken to be the graphic average over this period. This measurement technique is illustrated in Figure 16. Previous experiments [60] indicate that this value is accurate to wihin $\pm$ 2000 to 3000 pounds per square inch.

3.2.4 Data and Observations

Initial experiments characterized the variation in the residual stress along the surface of the axle shafts. For all measurements, zero reference was established as the plane determined by the spline end of the axle shafts. No measurements were attempted at the spline because the surface irregularity in this region is large compared with the x-ray spot size and no measurements were made adjacent to the flange because the heat treatment differs in this region. The residual stress was measured in the longitudinal direction only. Although the fixturing of the Fastress prevented measurement of the corresponding tangential component, the longitudinal component itself proved significant.

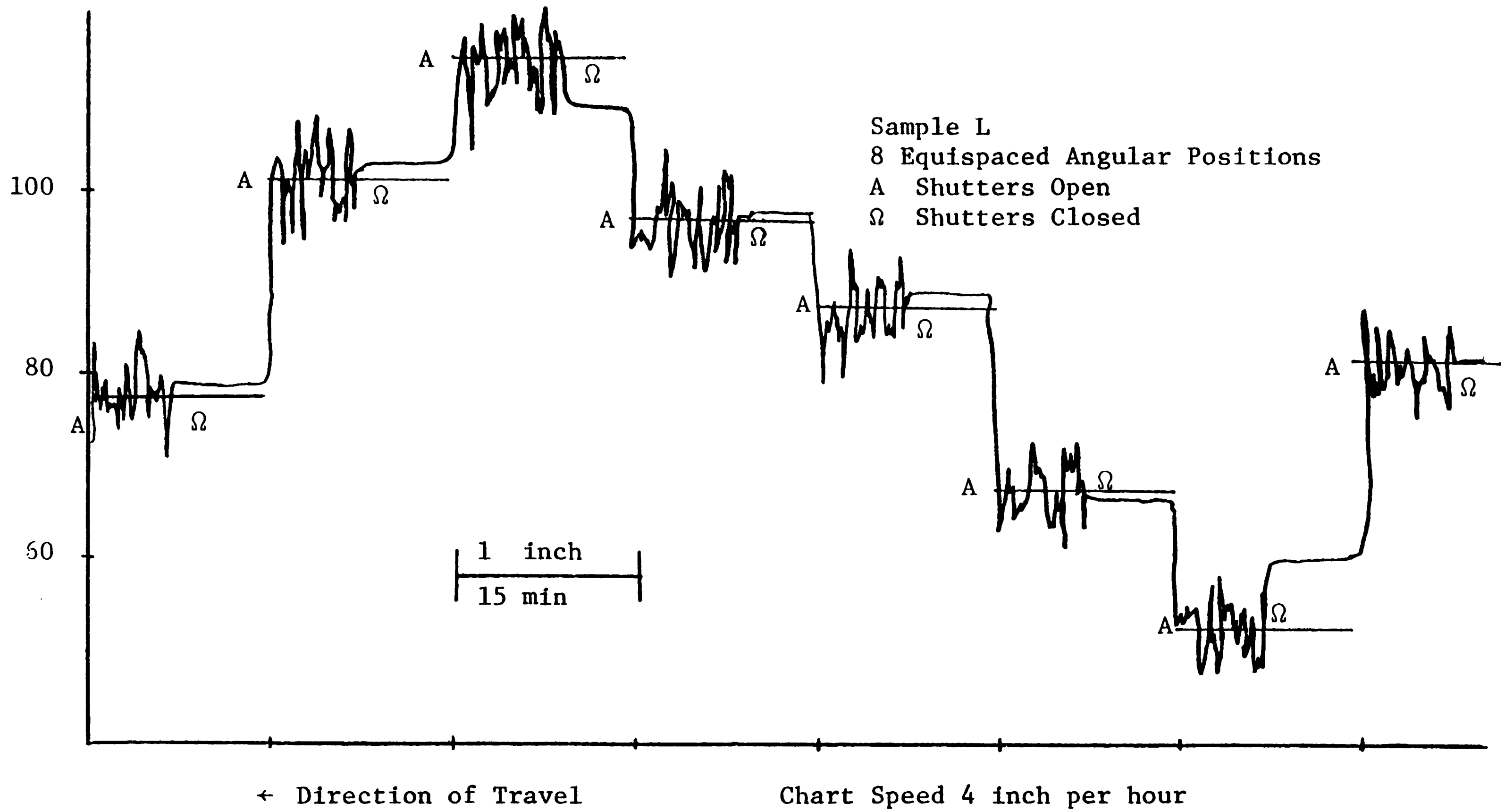

Figure 16. "Fastress" Output

Further, experiments by Vatev [29] imply that, for induction-hardened shafts of circular cross section, the longitudinal and tangential components of the residual stress at the surface are comparable.

The first group of samples was used to characterize the variation of residual stress that may be associated with the different induction hardening processes. Four measurements, spaced 90° apart, were made at each of the ten cross sections which were chosen. As shown in Figures 17 and 18, the residual stress was found to vary as much as 40 ksi from point-to-point. However, if the average value of the four residual stress measurements at each cross section are compared and if the measurements immediately adjacent to the spline are neglected, a mean value of residual stress may be associated with each shaft. For sample A, a comparison of the cross-sectional averages yielded a mean value of 92.3 ksi compressive for the residual stress with a standard deviation of 2.4 ksi for the nine cross-sectional averages. For sample B, a comparison of the cross-sectional averages yielded a mean value of 51.2 ksi compressive for the residual stress with a standard deviation of 5.4 ksi for the nine cross-sectional averages. The cross-sectional average adjacent to the spline was significantly higher in both cases.

The local variation of the surface residual stress for both samples was evaluated as close as possible to the most probable fracture surface. In the preliminary experiments all fractures occurred within the spline, so in these residual stress experiments the machined surface that borders the spline was examined. First, the longitudinal variation of the surface residual stress was determined by a series of twenty measurements that were spaces 0.10 inch apart. Second, the circumferential variation of the surface residual stress was determined by a

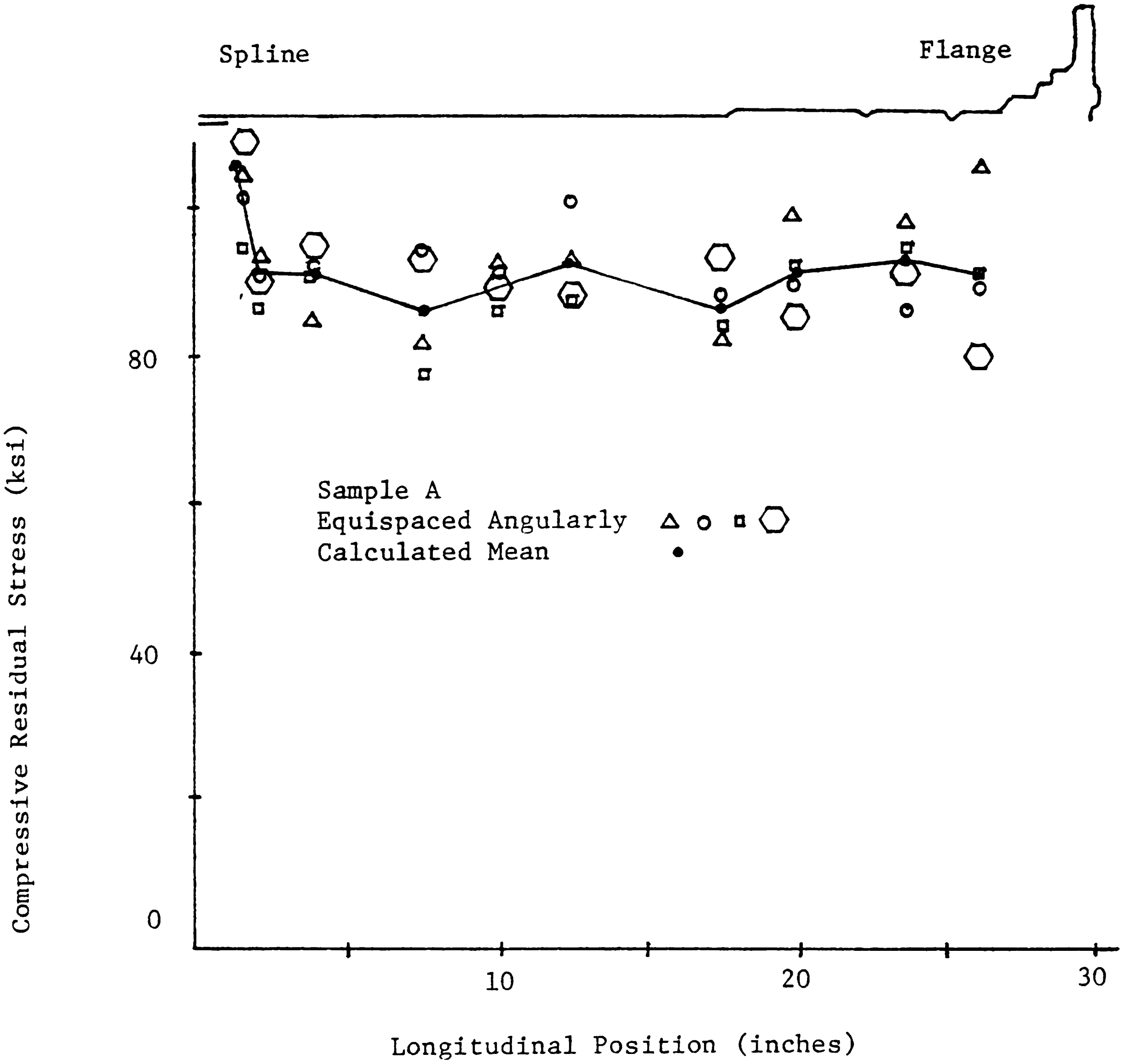

Figure 17. Consistency of Mean Residual Stress for Scan Hardened Shaft

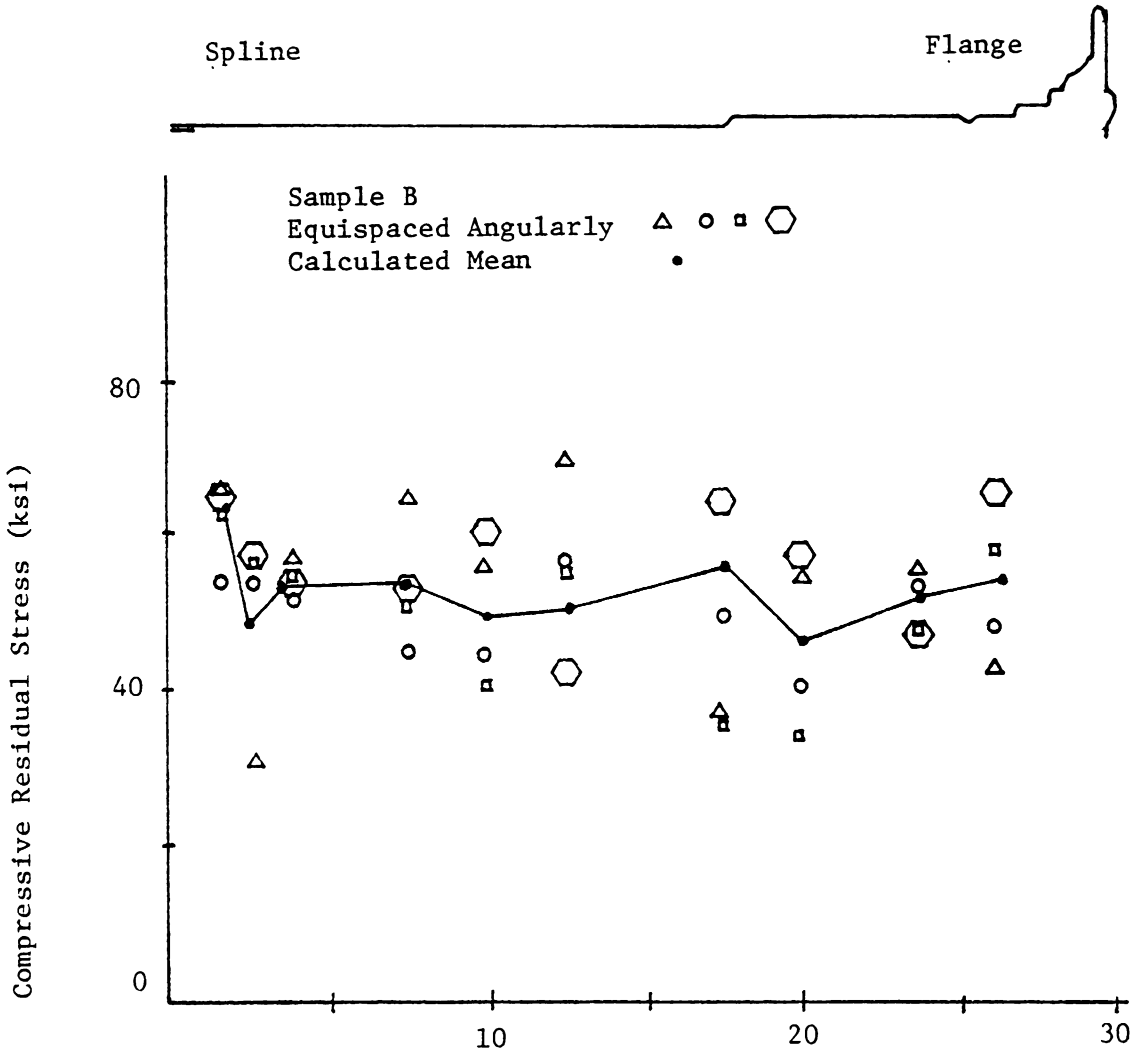

Figure 18. Consistency of Mean Residual Stress for Single-Shot Hardened Shafts

series of twenty-eight equispaced angular measurements. Observations from this data for sample A (Figure 19) indicated for the progressively hardened axle shaft that the residual stress varies sinusoidally. Since this pattern also repeats circumferentially (Figure 20A), the cross-sectional average should be valid. Observations from this data for sample B (Figure 21) indicated that for the single-shot hardened axle shaft, the residual stress varies with an irregular period along the length of the axle shaft but that the variation circumferentially (Figure 22B) provides a representative cross-sectional average. The data in Figures 19 and 21 revealed an increase in compressive residual stress level near the spline.

Subsequent experiments examined whether the maximum strain which can be sustained before failure can be related to the residual stress distribution. For each of the test samples C through N, eight residual stress measurements, spaced every 45° at a distance that is two inches from the spline end of the axle shaft, were used to establish a mean residual stress level for each axle shaft. For the initial test samples A and B, twenty eight equispaced measurements at the same longitudinal position were taken. The results, presented in Figures 20 and 22 showed: first, that the average residual stress level varied little for axle shafts subjected to the same induction hardening conditions; second, that, within each test group, induction hardening by the vertical scanning process produced less variation in residual stress than by the single-shot process; and third, that, within the first group, the standard deviation of those samples which were not tempered was significantly larger than the standard deviation of those samples in the second group which were similarly processed but tempered.

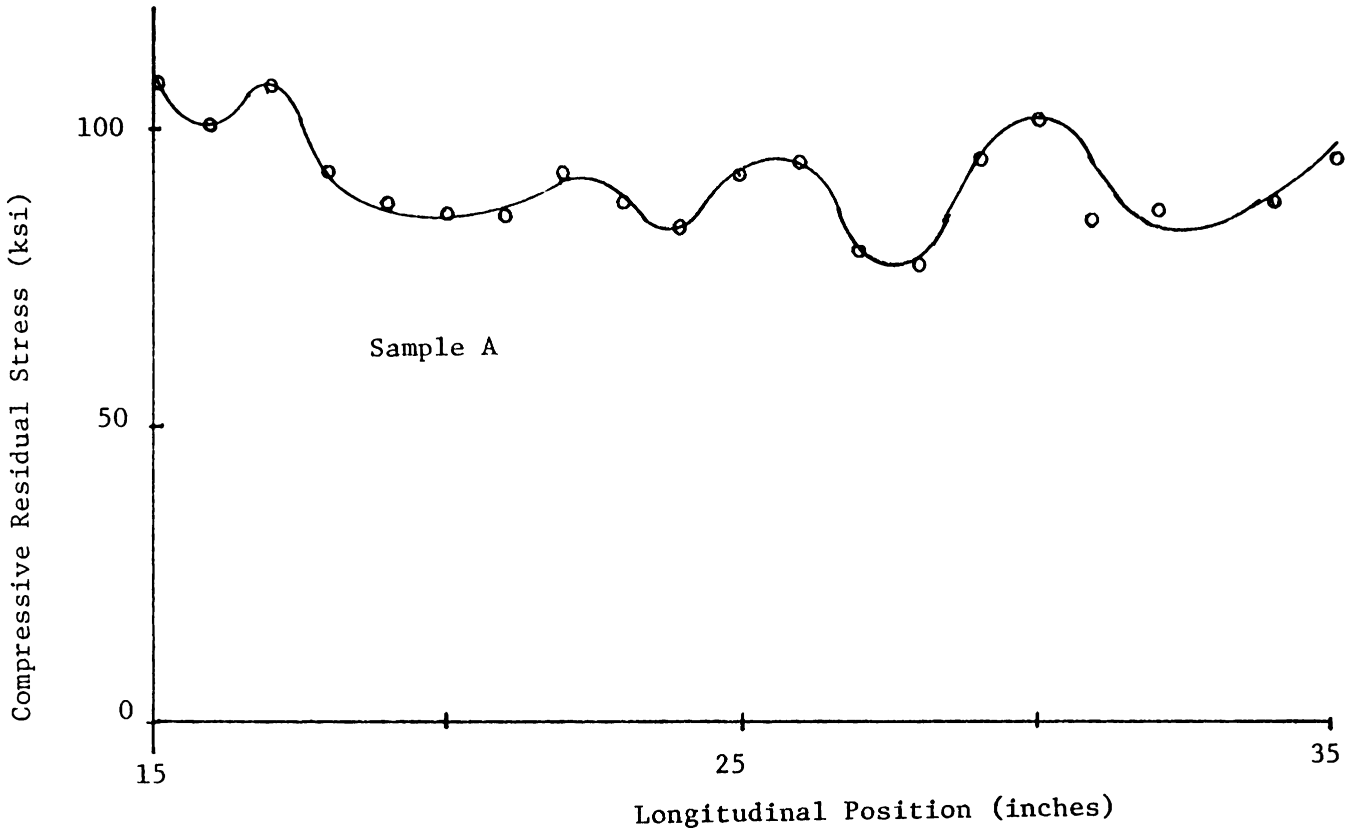

Figure 19. Local Residual Stress Variation for Scan Hardened Shaft

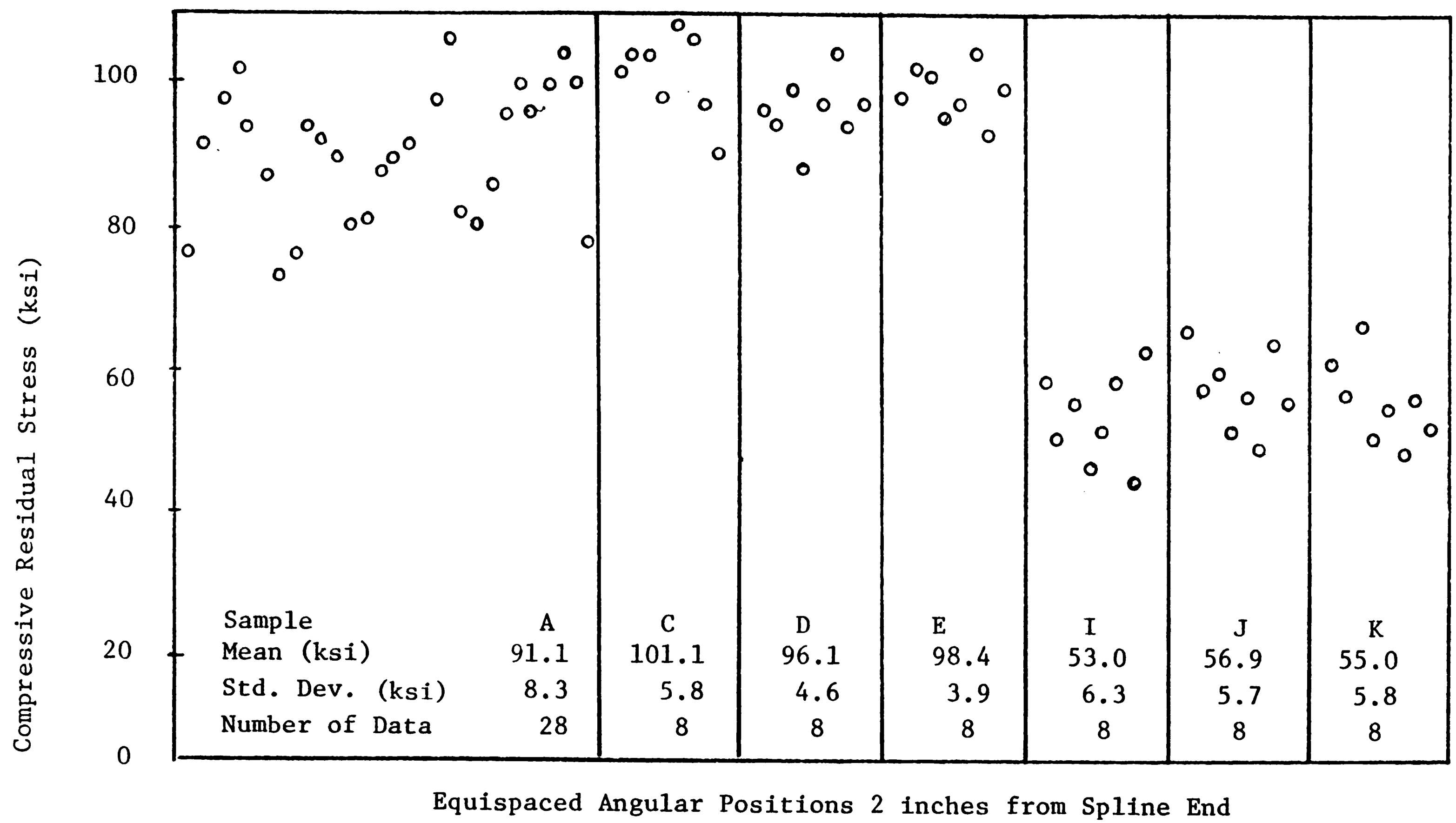

Figure 20. Data Establishing Mean Residual Stress for Scan Hardened Shafts

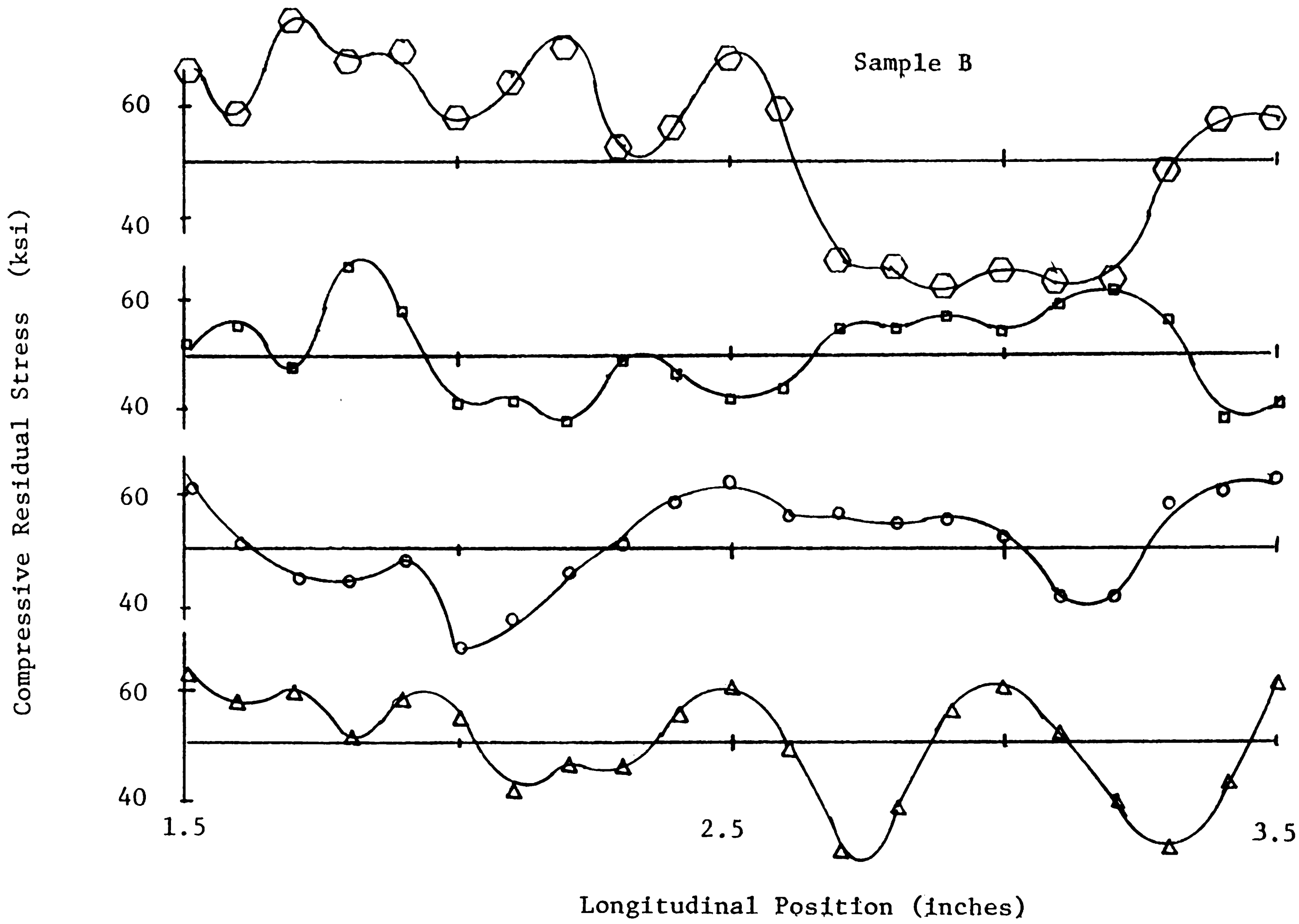

Figure 21. Local Residual Stress Variation for Single-Shot Hardened Shaft

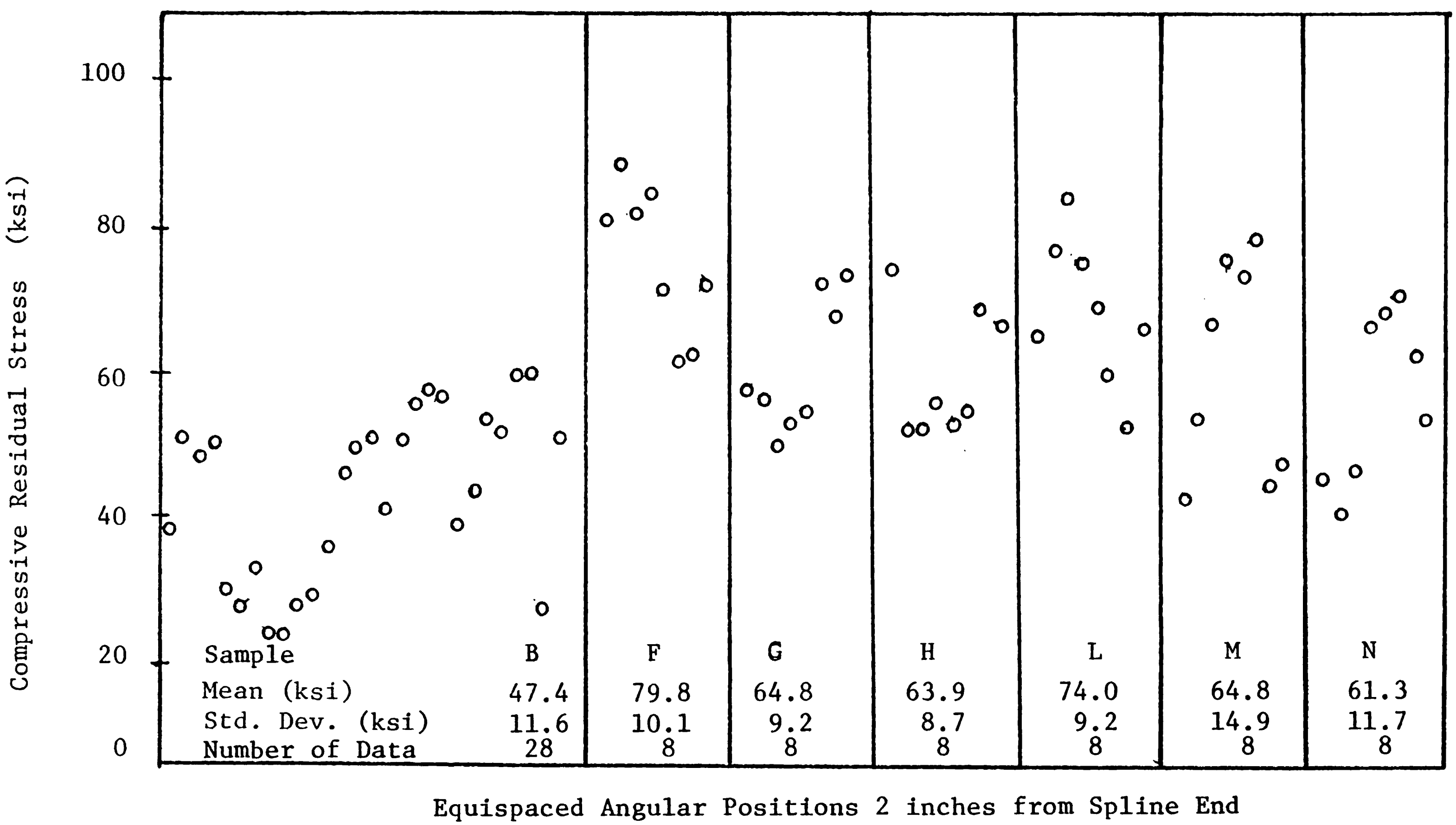

Figure 22. Data Establishing Mean Residual Stress for Singel-Shot Hardened Shafts

Following the residual stress determination, the test samples were torsion tested to failure. Torque-twist plots are presented in Figure 23 for the furnace-tempered group and in Figure 24 for the induction-tempered group. Next, the extent of the metallurgical transformation was measured on a transverse section through the test shafts' splines. This data, Rockwell "C" hardness traverses, are presented in Figure 25 for the furnace-tempered shafts and in Figure 26 for the induction tempered shafts. Finally, the chemical composition of each shaft was determined and used to evaluate its hardenability through the ideal critical diameter calculations.

3.2.5 Test Results

These test results, summarized in Table 2, indicate a correspondence between the angle-of-twist-at-failure and the mean residual stress level. A comparison of the mean residual stress level and its variation with angle-of-twist-at-failure is presented in Figure 27. The indicated level represents the mean value and the error bar represents the two sigma deviation for each shaft. This correspondence suggests that for induction-hardened axle shafts which meet the same heat treatment specifications, the mean residual stress level determines the maximum strain which can be sustained.

Furthermore, these data (Figure 27) indicate that a ductile-brittle transition may exist. For comparison purposes, three limits were identified. A lower limit, chosen at the 10% point in the transition region, was identified as Z_{10} and should represent a brittle fracture limit for lower levels of compressive residual stress. An upper limit, chosen at the 90% point in the transition region, was

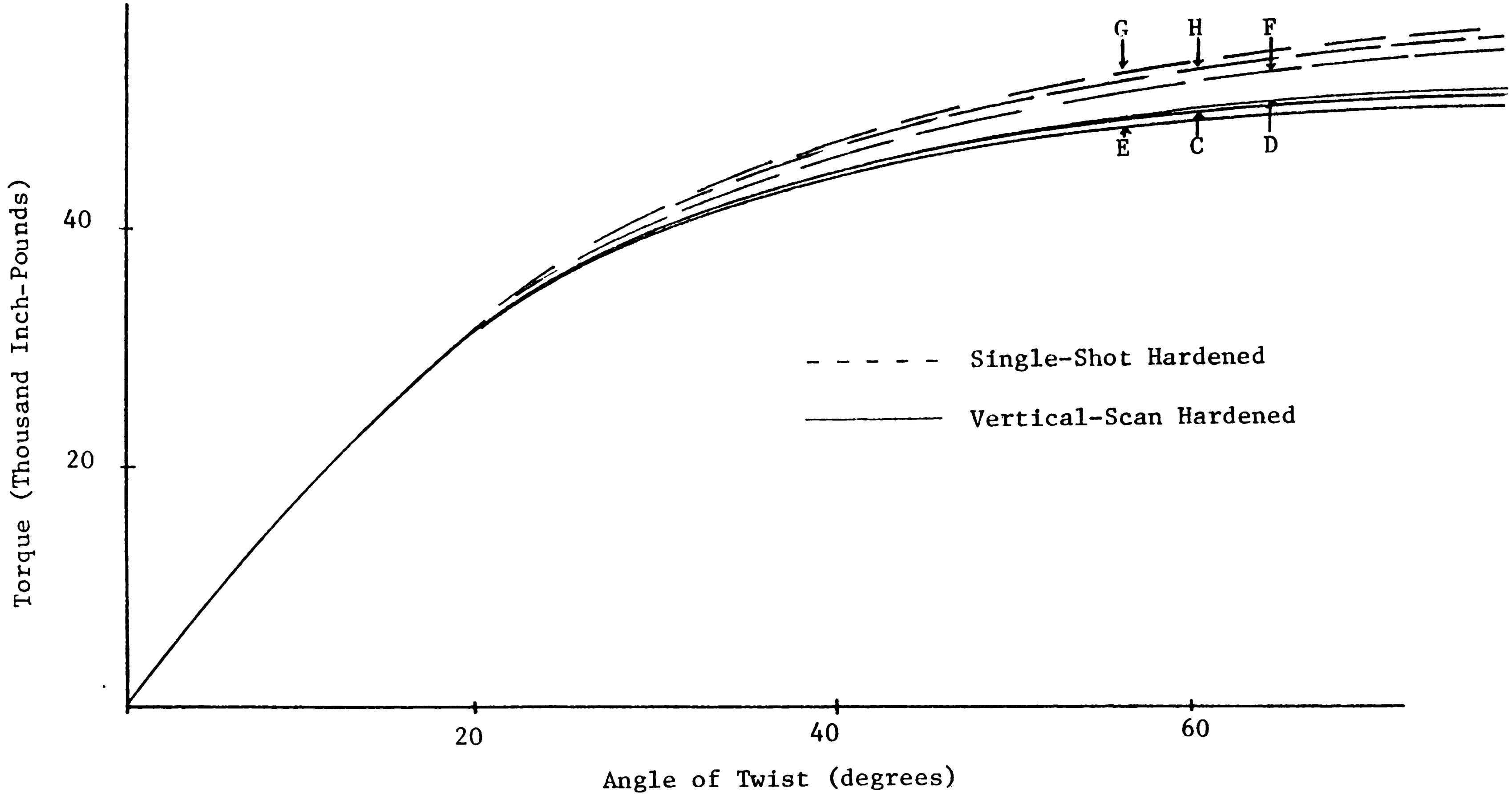

Figure 23. Torque-Twist Plots for Furnace Tempered Shafts

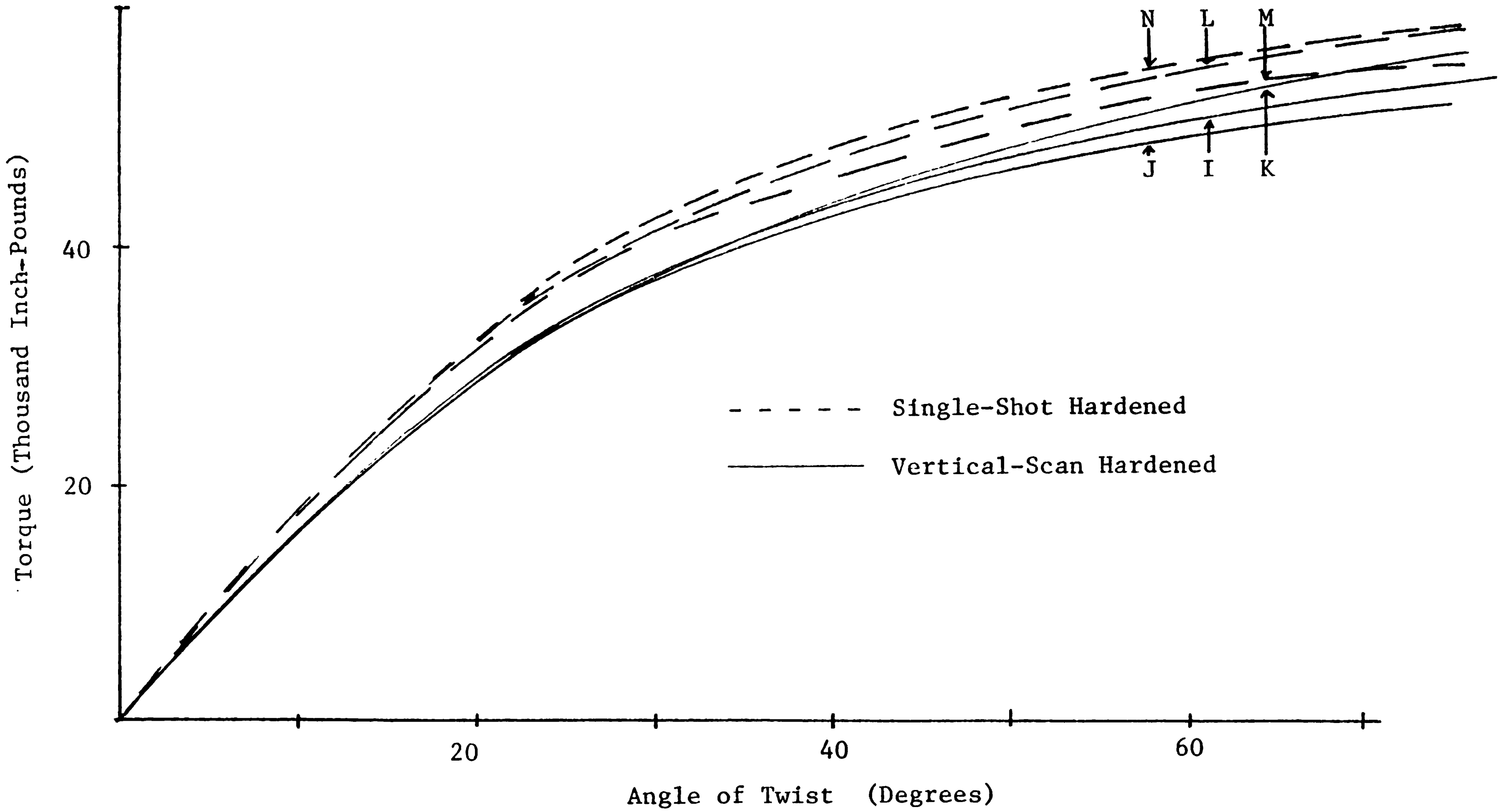

Figure 24. Torque-Twist Plots for Induction Tempered Shafts

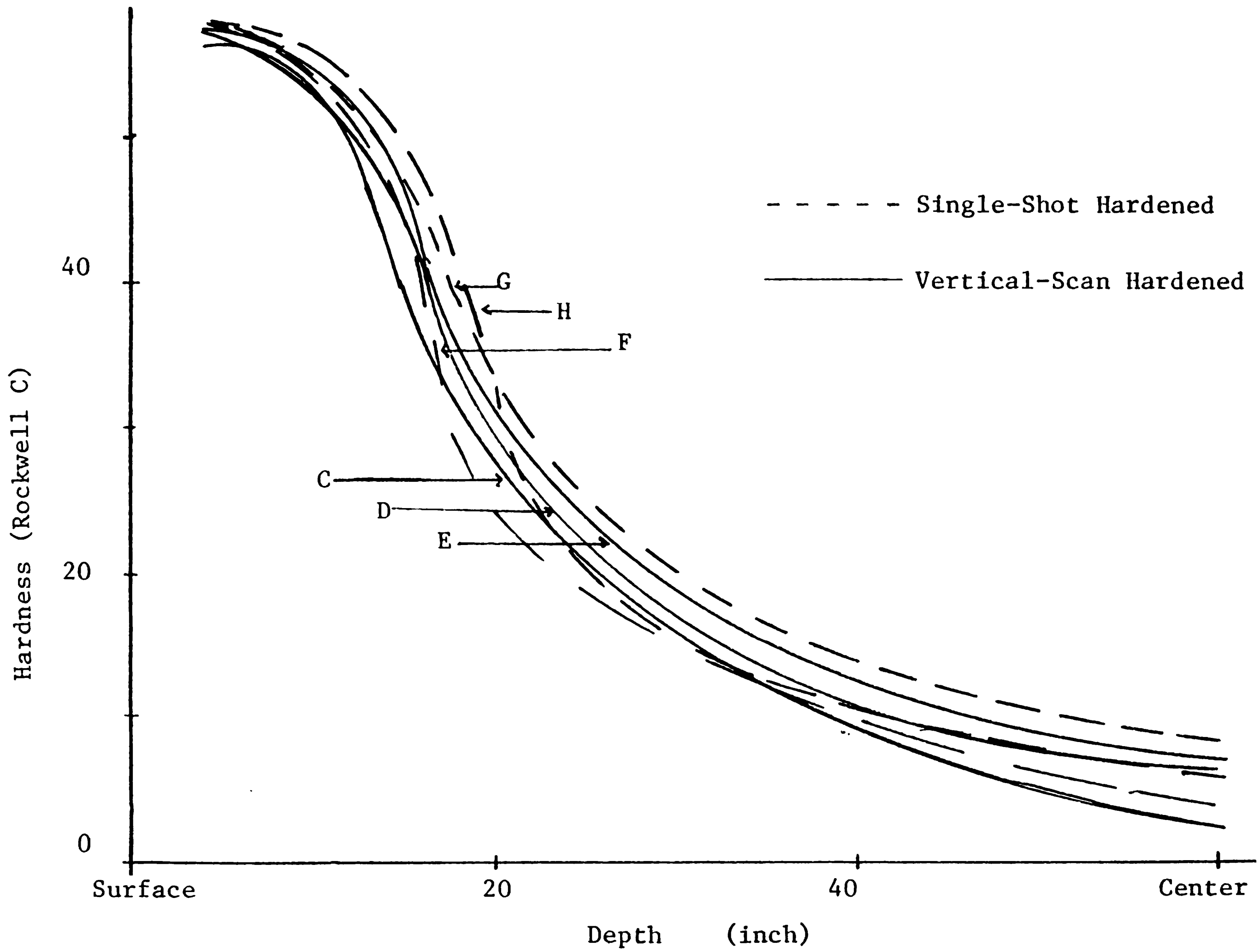

Figure 25. Spline Hardness Traverse for Furnace-Tempered Shafts

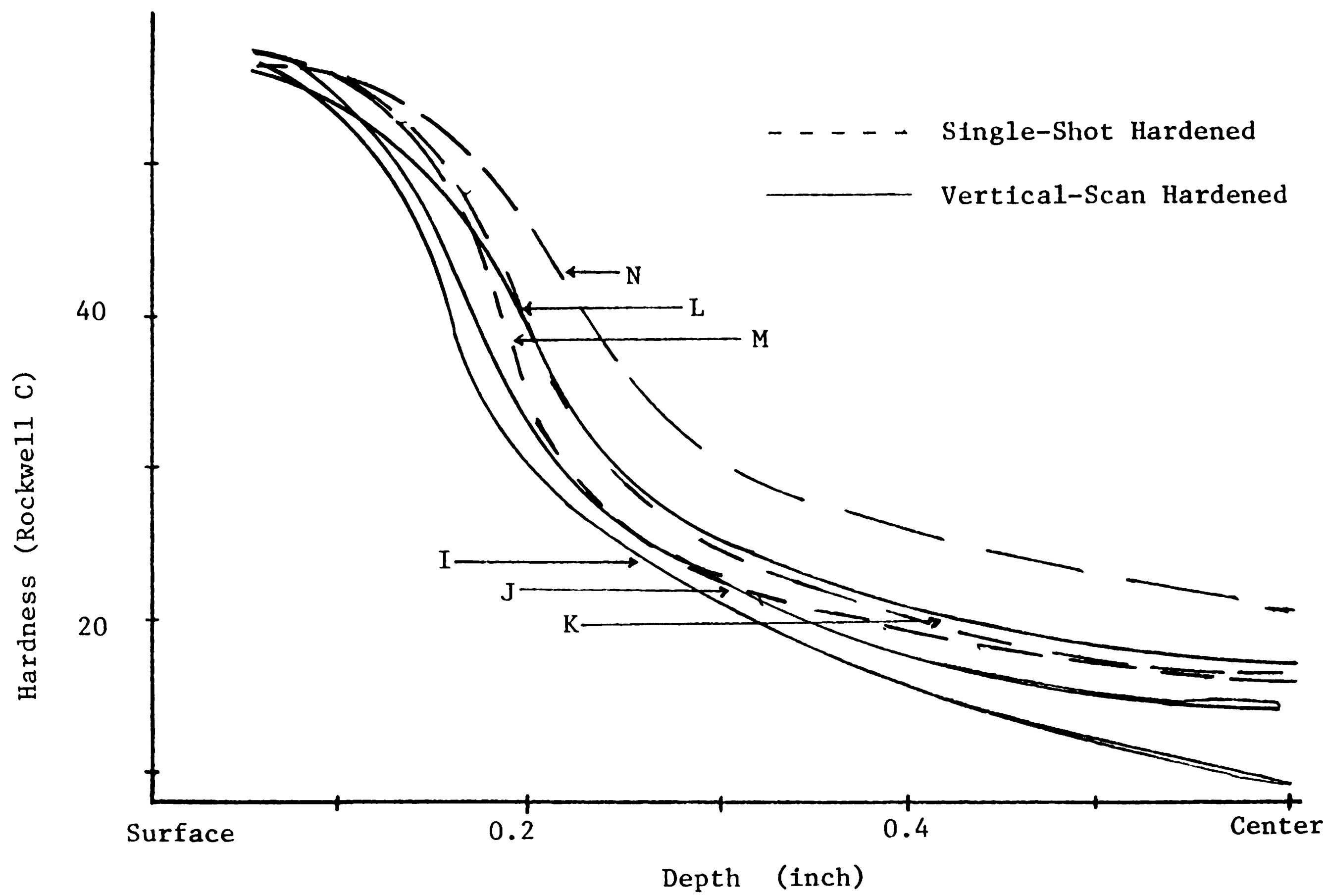

Figure 26. Spline Hardness Traverse for Induction-Tempered Shafts

Table 2 Summary of Experimental Results

TEST NO.	PROCESS CODE	D_I (in)	CASE (Rc)	PHYSICAL PROPERTIES TUS (kip)	TYS (kip)	TYP (kip)	G (kip/°)	θ_F (°)	RESIDUAL STRESS MEAN (ksi	STD DEV compressive)
A	N1VSN	1.73	49	64.1	36.0	20	16.0	164	91.1	8.3
B	N2SSN	1.70	47	62.1	33.0	20	17.1	72	47.4	11.6
C	D4VSF	1.70	40	57.6	35.0	23	17.0	244	101.1	5.8
D	D5VSF	1.68	44	58.6	35.0	24	16.7	232	96.1	4.6
E	D6VSF	1.65	51	57.5	35.5	24	17.0	225	98.4	3.9
F	D2SSF	1.61	40	59.8	33.3	21	16.6	135	79.8	10.1
G	D3SSF	1.63	48	60.4	36.0	23	16.8	126	64.8	9.2
H	D1SSF	1.65	45	60.0	35.4	22	16.7	124	63.9	8.7
I	J1VSI	1.82	40	58.0	30.0	20	16.2	105	53.0	6.3
J	J2VSI	1.85	46	57.0	28.0	18	16.5	110	56.9	5.7
K	J6VSI	1.82	47	58.0	32.5	22	15.9	110	55.0	5.8
L	J3SSI	1.82	49	63.0	39.0	25	17.0	143	74.0	9.2
M	J5SSI	1.78	45	63.0	36.5	26	16.9	122	64.8	14.9
N	J4SSI	1.82	53	63.5	35.0	23	16.0	120	61.3	11.7

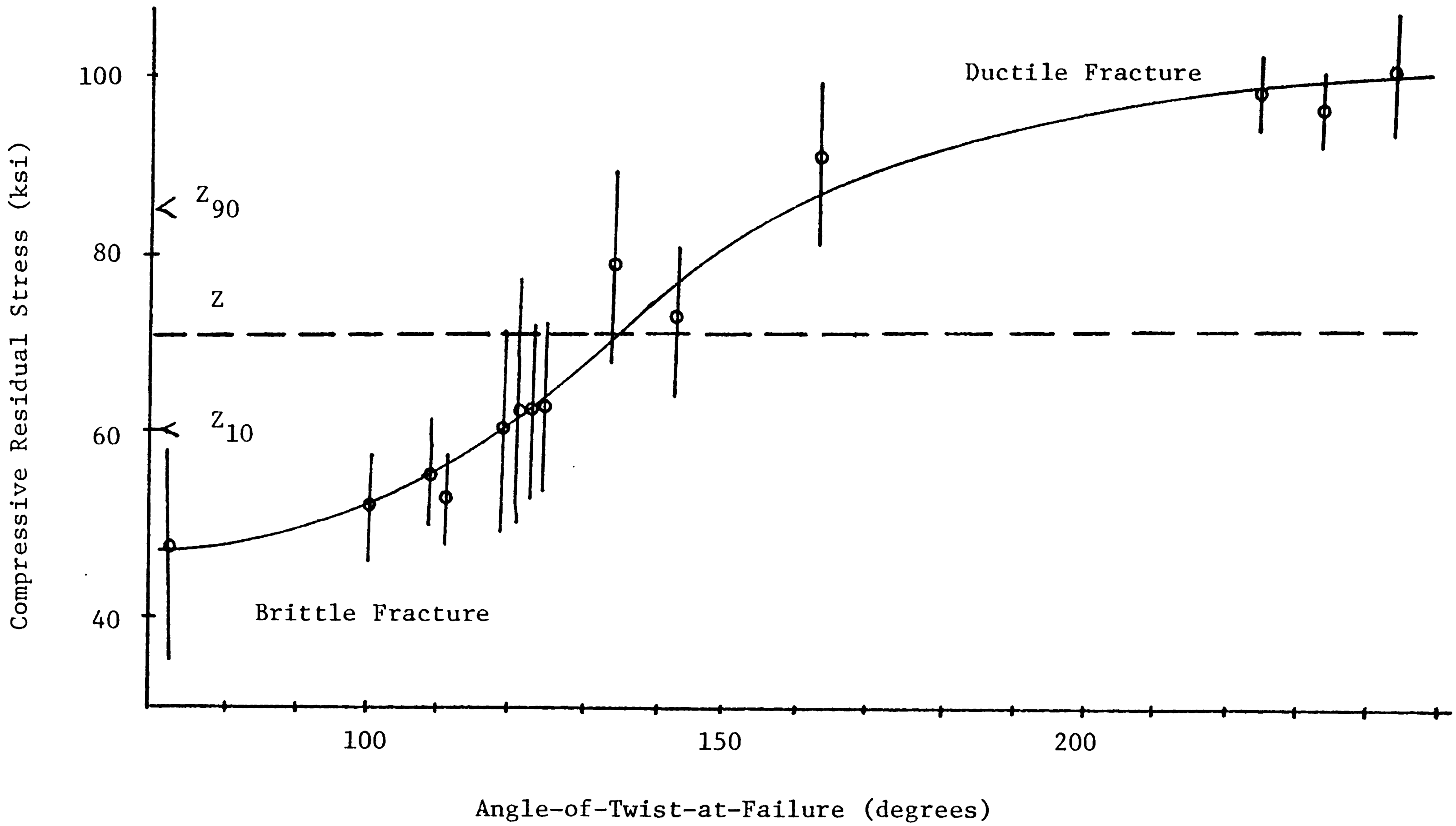

Figure 27. Ultimate Strain Variation with Mean Residual Stress Level

Error bars represent the two sigma variation for each shaft.

identified as Z_{90} and should represent a ductile fracture limit for higher levels of compressive residual stres. Finally, a central limit, chosen at the 50% point in the transition region, was identified as Z, the transition stress level, in order to facilitate further discussion. For those axle shafts represented by the data (Figure 27), interpolation yielded:

$$Z_{10} = 60 \text{ ksi compressive} \qquad (23)$$

$$Z = 70 \text{ ksi compressive, and} \qquad (24)$$

$$Z_{90} = 85 \text{ ksi compressive.} \qquad (25)$$

The existence of the suspected ductile-brittle transition was evaluated by fractography.

3.2.6 Fractography

Analysis of the fracture surfaces on the test samples corroborated the suspected ductile-brittle transition. Evidence for two distinct fracture mechanisms was found. Test samples with low levels of compressive residual stress ($\bar{\sigma}_{RES} < Z_{10}$) failed by a brittle cleavage mechanism whereas samples with high levels of compressive residual stress ($\bar{\sigma}_{RES} > Z_{90}$) failed by a ductile void coalescence process. Those test samples with a mean compressive residual stress level in the transition zone ($Z_{10} < \bar{\sigma}_{RES} < Z_{90}$) ultimately failed by cleavage but exhibited evidence of some void coalescence.

Fractographs were made of sample A to illustrate the morphology of the fracture surface for mean compressive residual stress levels which exceed the ductile limit ($\bar{\sigma}_{RES} > Z_{90}$). Examination of Figure 28 indicated that: first, fracture occurred on a surface that is oriented

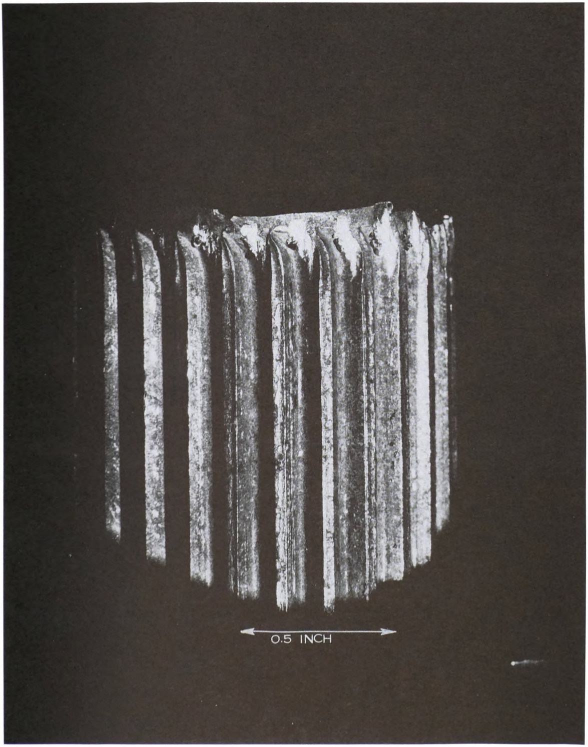

Figure 28. Ductile Mode Fractograph--Radial View of Spline Fracture Surface.

Note transverse fracture, spline distortion and spline root ruptures.

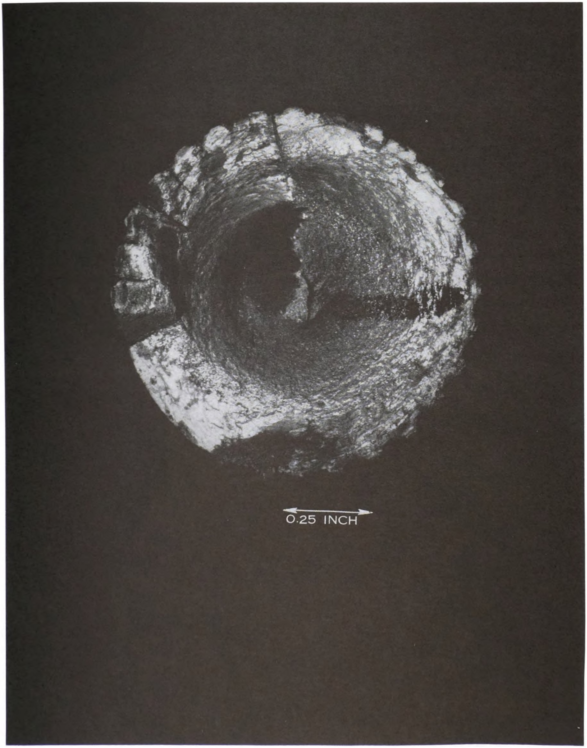

Figure 29 Ductile Mode Fractograph--Axial View of Spline Fracture Surface.

Note radial crack propagation from spline root.

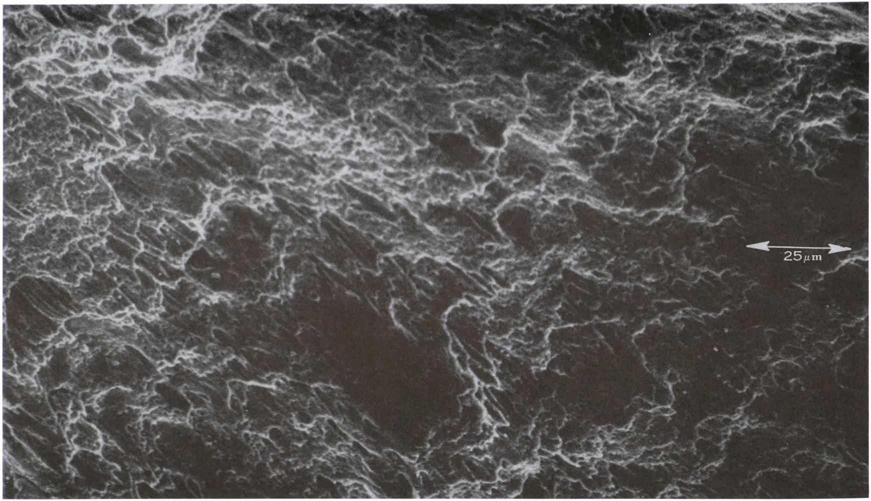

Figure 30 Scanning Electron Micrograph of Ductile Mode Fracture Showing Shear Dimples.

Figure 31 Scanning Electron Micrograph of Ductile Mode Fracture Showing Microvoid Coalescence.

90° to the axle shaft's axis; second, distortion of the spline in the direction of the applied torque was considerable; and third, ruptures in the material's surface occurred at the spline root. Subsequent examination of Figure 29 revealed cracks which extend from the spline root, through a glossy region which was smeared during fracture, and into a region characterized by shear dimples as shown in Figure 30. These cracks terminate in the central fibrous core.

Scanning electron microscopic analysis of the shear dimple region (Figure 31) suggests that the ductile fractures are controlled by a void coalescence mechanism [53]. Apparently, if the mean compressive residual stress level exceeds the ductile limit ($\bar{\sigma}_{RES} > Z_{90}$), surface crack growth is stable or suppressed as the shaft is twisted. This inhibition allows dislocations to pile-up and microvoids to coalesce. This process continues and reduces the effective cross-sectional area until the applied load can no longer be supported. Fracture then occurs. Etch pit studies [50] on torsionally induced fractures in low carbon steels indicate that dislocation motion proceeds along the {100} slip planes.

Fractographs were made of sample B to illustrate the morphology of the fracture surface which results if the mean compressive residual stress level falls below the brittle limit ($\bar{\sigma}_{RES} < Z_{10}$). Examination of Figure 32 indicated that: first, fracture occurred on a surface that is oriented 45° to the axis of the axle shaft; second, distortion of the spline was minimal; third, ruptures in the material's surface occurred at the spline root and extended across the spline teeth; fourth, chevron lines on the outer spiral surface indicated that the fracture originated at the spline root; and fifth, a crack extended to 45° across

Figure 32 Brittle Mode Fractograph--Radial View of Spline Fracture Surface.

Note helical fracture, minimal spline distortion, spline root ruptures, crack propagation at 45°, and chevrons on helical fracture surface.

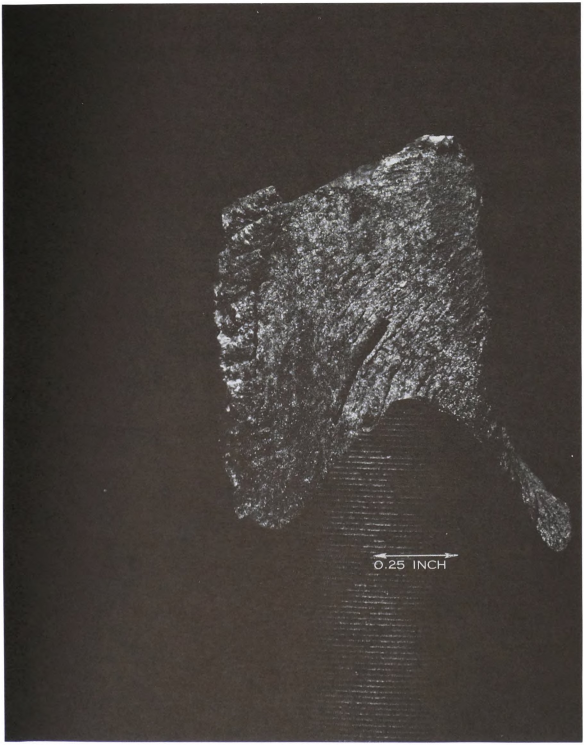

Figure 33 Brittle Mode Fractograph--Radial View of Shaft Fracture Surface.

Note shear lips.

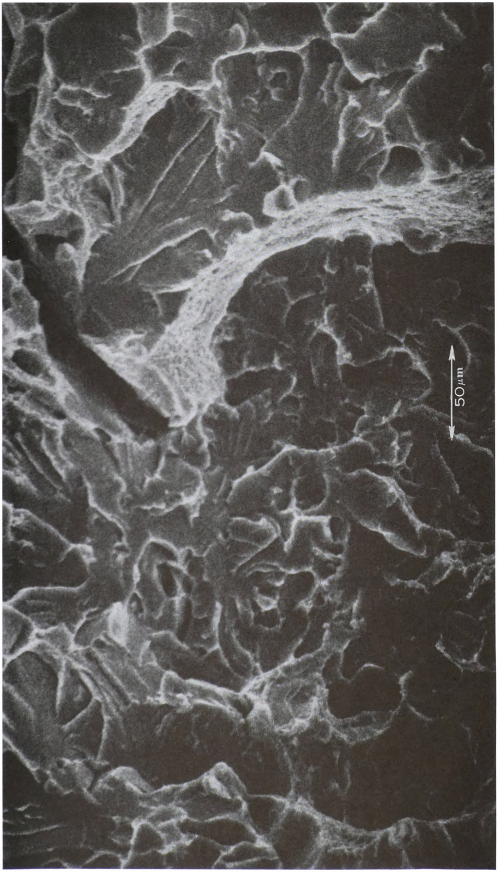

Figure 34 Scanning Electron Micrograph of Brittle Mode Fracture.

Note plateau and ledge morphology.

the spline from this initiation site. Subsequent examination of the mating fracture surface, which is illustrated in Figure 33, suggested that the chevron lines which were referenced in Figure 32 are shear lips which were generated as the crack front propagated.

Scanning electron microscopic analysis of these shear lips (Figure 34) reveals a plateau and ledge morphology that typifies brittle fractures which are controlled by cleavage mechanisms [52]. Apparently, if the mean compressive residual stress level falls below the brittle limit ($\bar{\sigma}_{RES} > Z_{10}$), surface crack growth is suppressed as the shaft is twisted until the maximum shear strain that the material can sustain is reached in the plastic zone at the root of the spline. If twisting continues, these sessile dislocations break loose from the pinning sites. This incipient crack extends a microscopic amount and relieves the local shear strain. At this point, the crack would arrest, except that the material is subject to continually increasing strain. Thus, at the crack tip, the local strain increases until the critical shear strain is reached and, once again, the crack front advances. This process continues until fracture is complete. Etch pit studies [50], indicating dislocation motion along the $\{100\}$ cleavage planes, allow that a Cotrell mechanism [61] may act as the pinning site.

Fractographs were made of sample H to illustrate one of the possible morphologies that the fracture surface may possess if the mean level of the compressive residual stress lies within the transition zone ($Z_{10} < \bar{\sigma}_{RES} < Z_{10}$). Examination of Figure 35 indicated that: first, the fracture occurred on a surface oriented perpendicular to the shaft's axis near the surface and on a surface oriented at 45° to the

Figure 35 Mixed Mode Fractograph--Radial View of Spline Fracture Surface.

Note compound fracture, minimal spline distortion, and spline root ruptures.

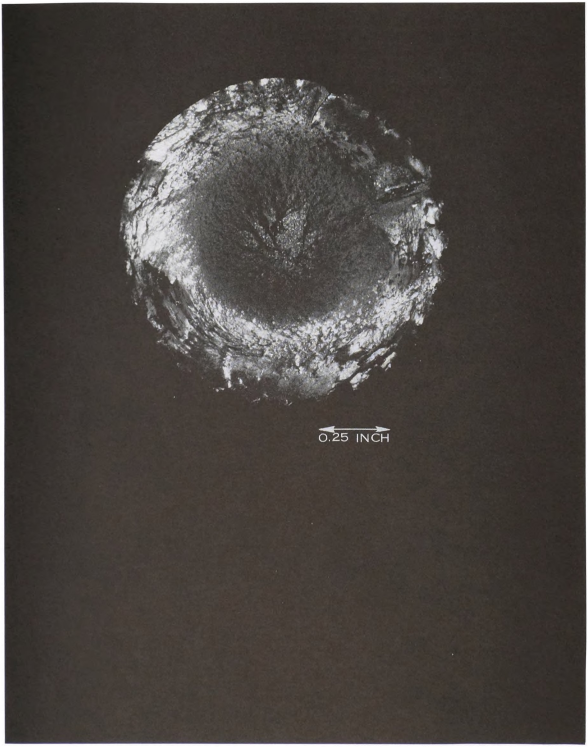

Figure 36 Mixed Mode Fractograph--Axial View of Spline Fracture Surface.

Note radial crack propagation from spline root to central helix.

axle shaft's axis near its central axis; second, distortion of the spline was minimal; and third, ruptures in the material's surface occurred at the spline root. Subsequent examination of Figure 36 revealed that cracks extended radially from the spline root of many teeth and that one, the source of final fracture, extends from the spline root to the edge of the internal spiral.

Apparently, if the mean compressive residual stress level is in this transition region ($Z_{10} < \bar{\sigma}_{RES} < Z_{90}$), the variation in residual stress is sufficient to allow localized dislocation pile-ups as the overall cross section is subject to microvoid coalescence. Once the critical shear strain is exceeded at a pile-up, unstable crack growth and fracture occurs.

IV. ANALYSIS

4.1 Residual Stress--Distribution

Unanticipated residual stresses are recognized as a primary source of failure, but some models used to evaluate the effects of beneficial residual stresses, introduced by chemical, thermal or mechanical processing, neglect the inhomogeneities introduced by the process, material and geometric constraints [62]. Such is the case with induction-hardened axle shafts. Shklyarov [6], and others cited by Almen [63], assume that on equivalent cross sections, the residual stress is a function of depth alone. Further credence to this angular consistency proposition stems from the experimental works of Vatev [26] and Ishii *et al.*[16]. The radial variation which they measured, however, should not be assumed to assure a constant value of residual stresses at a particular depth. Indeed, the experimental evidence indicates that on equivalent cross sections, the residual stress distributions on the surface do differ and that the variation significantly affects failure.

Our residual stress measurements reveal large, local gradients on the surface of induction-hardened axle shafts. These point-to-point residual stress variations reflect local variations in quench conditions. Inspection of the observable quench patterns (Figure 39) indicates that for single-shot hardened shafts (Figure 39a) the quench pattern, as well as the residual stress distribution (Figure 21) appears random, and that for progressively hardened shafts, the quench pattern (Figure 39b,39c) as well as the residual stress distribution (Figure 19) appears periodic. Furthermore, progressively hardened shafts with significant residual stress variation (Figure 21I) exhibited high contrast quench patterns (Figure 39c) whereas those with minimal

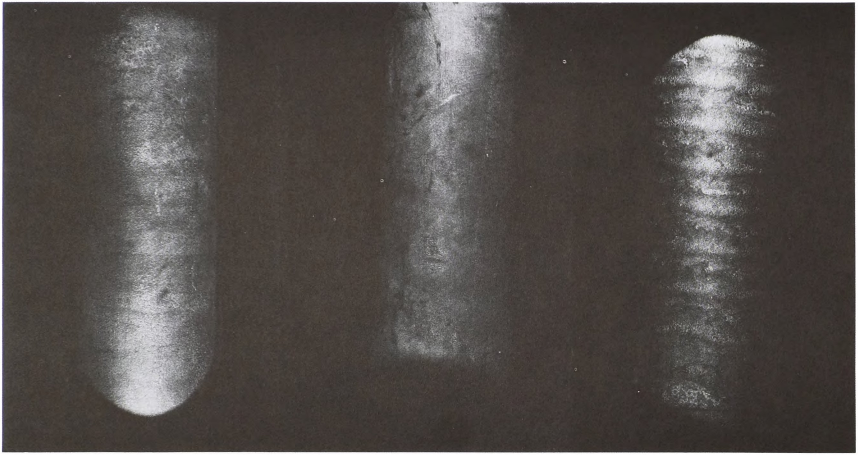

(a) Single-shot hardened

(b) Scan-hardened with uniform quench

(c) Scan-hardened with nonuniform quench

Figure 37 Quench patterns

residual stress variation (Figure 20E) exhibited low contrast quench patterns (Figure 39b).

Quench composition, pressure, temperature, flow and impingement angle are but a few of the variables which affect uniformity. Quench irregularities locally reduce cooling rates and introduce minima into the anticipated uniform residual stress distribution. The minima reduce the mean compressive residual stress level on the surface but, because thermal conduction minimizes cooling rate variations, introduce minimal distortion beneath the surface. Whether increased time, labor and material costs are warranted to increase uniformity should be evaluated by potential reliability enhancement.

In the analysis of Shklyarov,[6] and those cited by Almen [63], the residual stress distribution is treated as uniform at a particular depth. Our physical testing and statistical analyses demonstrate that this assumption is consistent with elastic behavior and failure loads; however, this consistency results not from uniformity of the residual stress distribution on the surface, but from the relative insensitivity of these bulk properties to local surface variations. In order to understand the torsional strain behavior of induction-hardened axle shafts, however, these surface residual stress variations, suspected by Kaplan and Rowell [34], must be considered.

4.2 Residual Stress--First Order Effects

The residual stress variation within this set of similarly processed induction-hardened axle shafts is critical in determining the mode and strain at fracture. Extant models--Littleton for tempered glass[33]--use superposition arguments to explain increased load bearing capability realized with an increase of compressive residual stress on the surface. The success of this model for brittle materials within the linear elastic range does not transfer to the plastic behavior of ductile materials subjected to similar compressive residual stress on the surface. Neither the tests of Shkylarov [6] nor Liss *et al.* [32] successfully relate increased compressive residual stress with improved static fracture resistance. Both, however, show increased fatigue life performance with increased compressive residual stress on the surface. Our experiments suggest that fracture mechanics arguments can resolve these inconsistencies.

Fracture mechanics analyses the growth of pre-existing flaws and establishes failure criteria which depend only on the material toughness, the size and distribution of the flaws present, and the nominal stress. The inherent flaw size and distribution in the test shafts are assumed to depend on those forging and manufacturing operations which precede heat treatment. The insensitivity of the stress sustained before final fracture to prior processing, as indicated in Table 2, is assumed to be evidence that flaw size is constant. Thus, if the variation of strain sustained before failure is combined with this consistency of flaw size, then either the material's unflawed yield strength or toughness controls failure.

Variation in the unflawed yield strength for constant flaw size is illustrated in Figure 38. If the unflawed yield strength is high (Figure 38a), then the failure mechanism is determined by the crack stability criterion (Equation 6). This condition precipitates brittle failure as load increases. If the unflawed yield strength is low (Figure 38b), then the shaft fails as the unflawed yield strength is reached. This criterion determines ductile fracture. These results demand that the mean level of compressive residual stress decrease with increasing yield strength. This conclusion contradicts Littleton's data and, thus, this relation can be rejected.

Illustrated in Figure 39 are two different values of material toughness chosen to test the proposed correspondence between K_{IIIc} and $\bar{\sigma}_{RES}$. If $\bar{\sigma}_{RES}$ is less than the brittle limit (Z_{10}), by assumption, K_{IIIc} is low, and, as indicated in Figure 39a, if the applied stress is increased until failure, unstable crack propagation governs and brittle fracture results. If $\bar{\sigma}_{RES}$ is greater than the ductile limit (Z_{90}), by assumption, K_{IIIc} is large, and as indicated in Figure 49b, if the applied stress is increased until fracture, the unflawed yield strength governs and ductile fracture results. These arguments are consistent with the experimental residual stress results and reduce to the stress superposition model for brittle materials with sufficiently large inherent flaw size.

This residual stress dependent ductile-brittle transition is quite analagous to the temperature induced embrittlement that Yokobori observed [50,51]. Low levels of mean compressive residual stress on the surface yield the least modification of the case martensitic properties. Martensite, a rigid structure with minimal fracture toughness, should

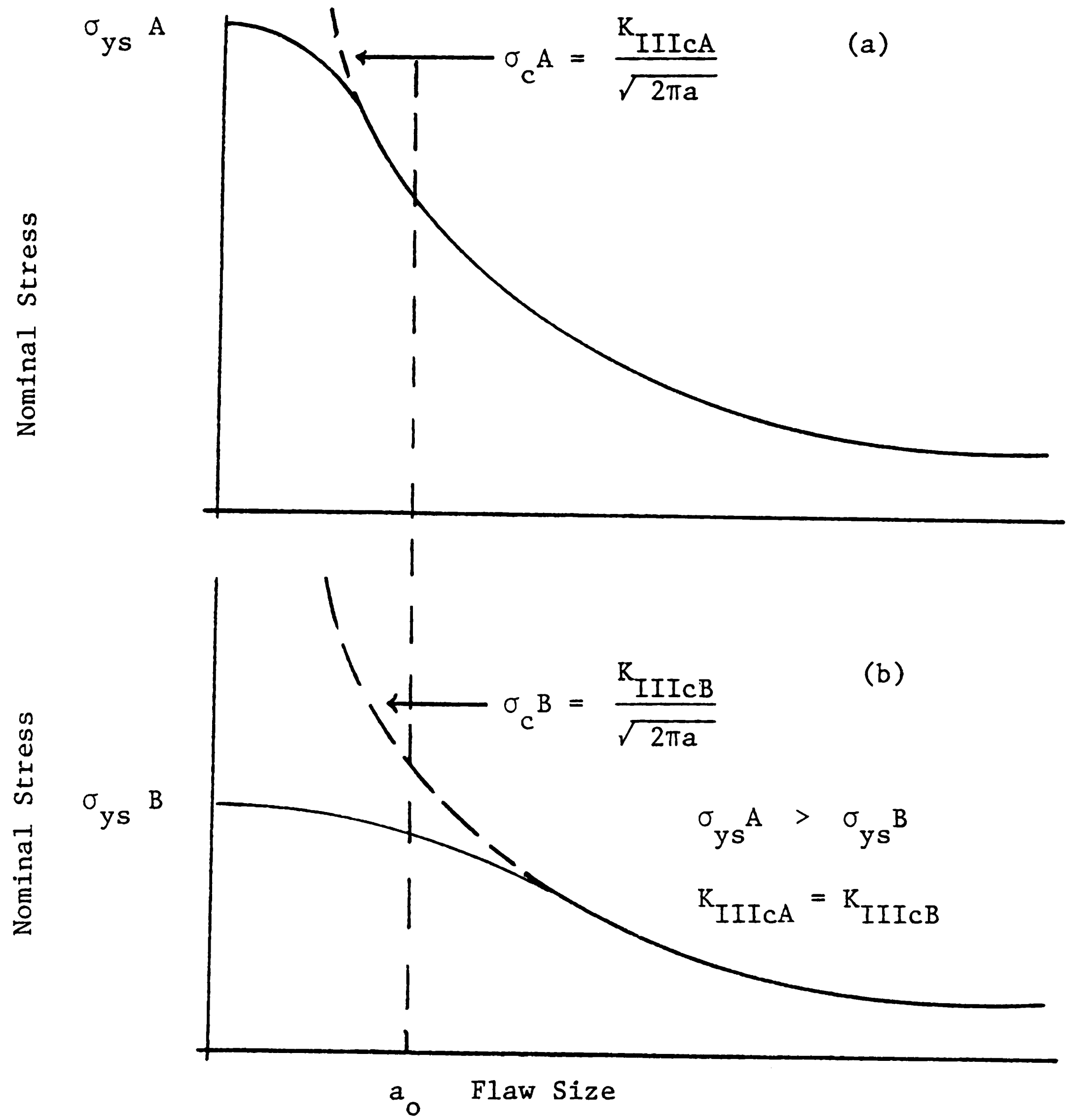

Figure 38. Unflawed Yield Strength and Fracture

(a) For high unflawed yield strength, the flaw line intersects the line representing failure controlled by unstable crack growth.

(b) For low unflawed yield strength, the flaw line intersects the line representing failure controlled by the maximum yield strength.

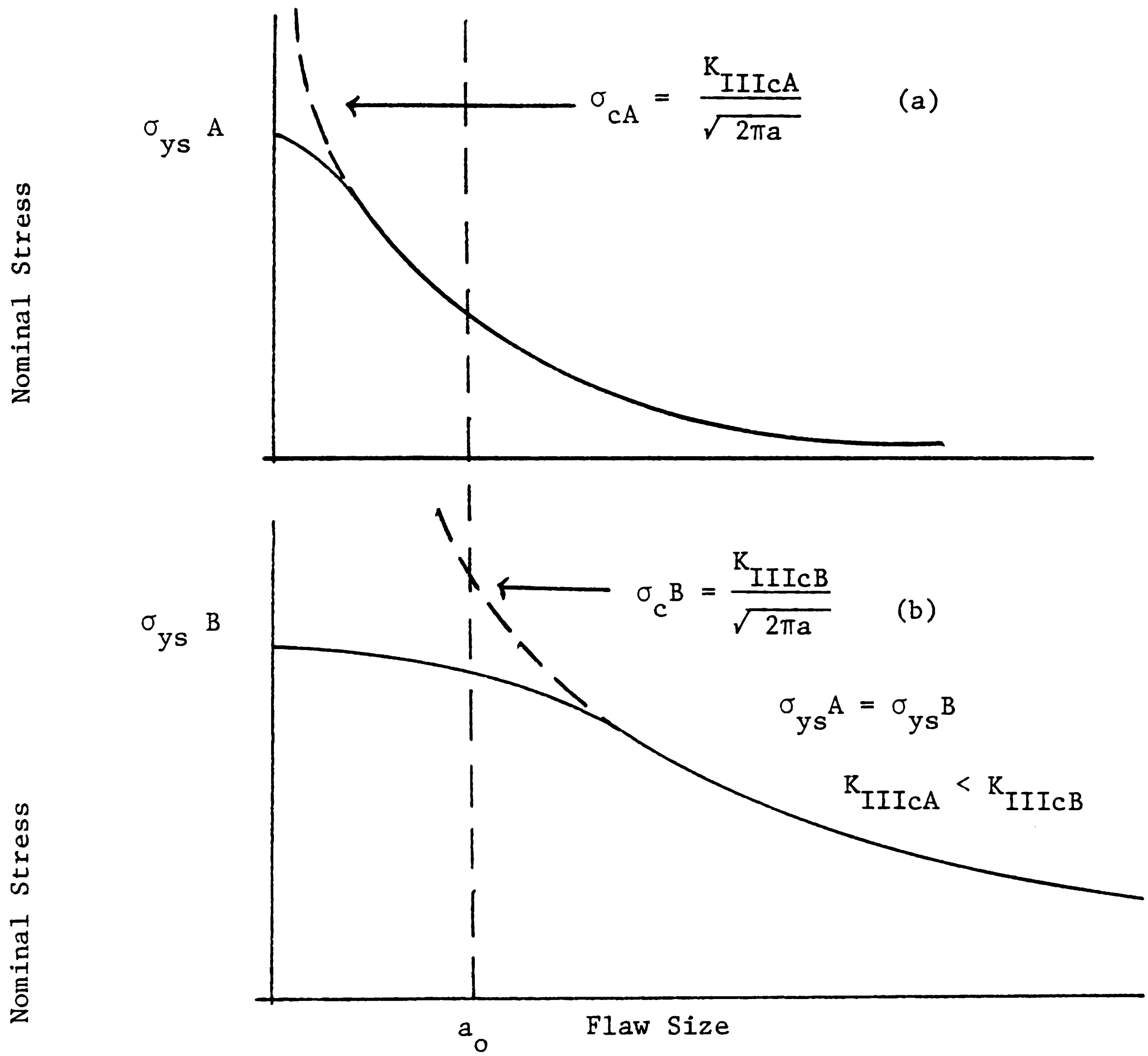

Figure 39. Toughness and Fracture.

a. For low toughness, the flaw line intersects the line representing failure controlled by unstable crack growth.

b. For high toughness, the flaw line intersects the line representing failure controlled by the maximum yield strength.

precipitate a brittle fracture, controlled by cleavage along a helical surface, under extreme torsional loads. This behavior is confirmed by the observed plateau and ledge morphology (Figure 32) on the spiral fracture surface (Figure 34). High levels of mean compressive residual stress on the surface should inhibit crack opening and allow extended crack propagation before fracture. With sufficient stable crack growth, the crack tip will penetrate the core and final fracture should occur as the tough core material ultimately yields to the shear forces on the transverse surface. This crack growth is confirmed by the observed shear dimples (Figure 30) and microvoid coalescence (Figure 31) on the transverse fracture surface (Figure 40)

The effect of compressive residual surface stress on the fracture strain of induction-hardened axle shafts also can be analyzed by stress superposition arguments, provided the inherent non-linearities are included in the analysis and provided fracture is initiated at the surface. Böker's findings[47] that, under sufficient hydrostatic compressive stress, torsional fracture switched from cleavage to shear for brittle materials parallels the conclusions drawn from Figure 27. Both transitions can be understood using the Mohr's envelope analysis which Nadai developed [48] and is reproduced in Figure 11a. This envelope, unlike the fracture toughness criterion, could be established experimentally by residual stress and fracture stress measurements or established by Altiero's calculations [49].

Similarly, Makky's slip-instability arguments [43,46] also allow for dual fracture paths. The only modification required is the realization that processing, in addition to the boundary condition constraints she analyzed, can introduce the tri-axial stresses necessary to switch from

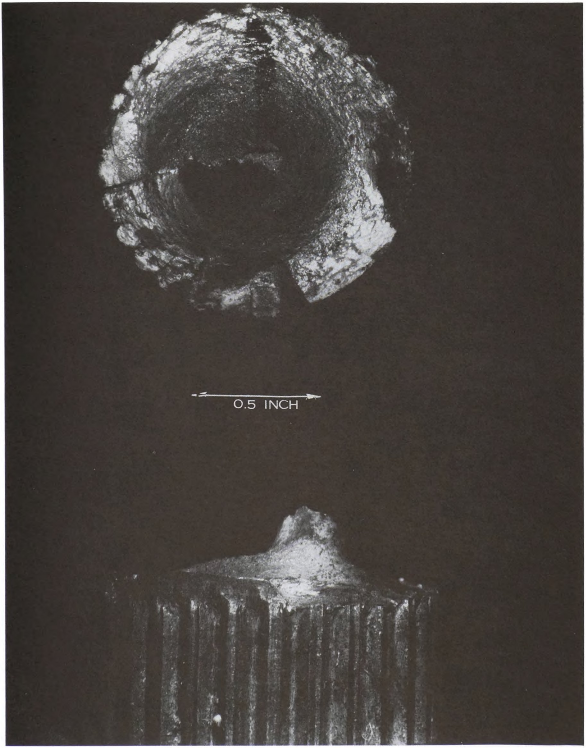

Figure 40 Ductile Mode Fractograph.

the helical to the transverse principle direction. These triaxial stresses disrupt the symmetry of the calculations and allow slip in the z direction. The presence of slip in the z direction favors transverse fracture. Clearly, since similar residual stress distributions, varying primarily in magnitude, exist in both cases, continuum arguments break down and microstructural effects must be considered to evaluate the residual stress influence on z direction slip.

4.3 Residual Stress--Second Order Effects

Analysis of the origins of residual stress and comparison of the surface residual stress with the surface quench pattern indicated that fast quench rates, characterized by a quenchant with high heat capacity, low quenchant temperature and adequate pressure, yield high compressive residual stresses on the surface. For all test induction-hardened axle shafts, cracks initiated at the spline root at the cross-section of minimum area and high levels of compressive residual stress on the surface correspond to extended ultimate strains. These results are consistent with the fracture mechanics, strength of materials, and slip instability analyses. The free body equilibrium condition, however, demands an inhomogeneous residual stress distribution. Both Vatev [29] and Ishii *et al.*[16] measure significant internal tensile residual stresses which these models neglect.

Internal tensile stresses, as noted by Jahsmams *et al.* [40] and Ebert *et al.* [41], produce diminished tensile properties and also increase a shaft's susceptibility to Hertz stress failure [64]. Although no direct comparison between this susceptibility and $\bar{\sigma}_{RES}$ is available, a comparison of quench rates and probability of cracking in a 0.38% carbon steel by Kobasko [65] demonstrated that quench rate, and by analogy, compressive residual surface stress, cannot be chosen arbitrarily. Thus, if internal residual stresses are sufficient, crack initiation and growth occurs internally, and the models proposed to explain the observed compressive residual stress dependence do not apply.

V. CONCLUSIONS

> "Real materials are enormously complex in their response to stress even under isothermal conditions, ... The key to successful analysis or design is to choose the simplest permissible idealization of the behavior of the material not to obtain the best description over the widest range of environmental conditions."
>
> Daniel C. Drucker
> "Edgar Marburg Lecture" (1966)

The primary effects of induction hardening on the fracture of steel axle shafts could be attributed to the increased yield strength in the case. For these similarly processed axle shafts, the maximum loads sustained before failure were distributed normally and exhibited little dispersion. The results of these static torsion tests confirmed the experiments of Wuerful [21,22] and thoeries of Olzak [9]. The deformation at failure, however, could not be anticipated by sole reliance on their analysis. The residual stress, generated during the heat treatment, significantly affected the maximum deformation sustained before failure.

Detailed investigation of the surface residual stress distribution for induction-hardened rear axle shafts reveals significant point-to-point variation in residual stress. These potentially extreme and random local variations eliminate the practical application of any theory that requires complete specification of the stress state. However, if the symmetry inherent in the process and the applied loads allow, a judicious set of measurements can define a mean compressive residual stress level which may prove useful in defining experimentally verifiable fracture criteria. Any model based on this "scalar" $\bar{\sigma}_{RES}$ must be an energy model.

Mohr's envelope, slip instability and fracture mechanics can be applied successfully. The analyses place similar restrictions on crack initiation and growth in static and fatigue torsion. At the crack tip, the compressive residual stress affects the energy release rate which governs whether cleavage or shear fracture occurs. Theoretical evaluation of the critical residual stress level, Z, requires either modification of the Griffith-Orowan-Irwin theory or a statistical mechanics comparison of dislocation motion on competing slip planes.

For those induction hardening processes investigated, the following conclusions are experimentally significant:

1. A mean level of compressive residual stress can be associated with each shaft.
2. Increasing $\bar{\sigma}_{RES}$ increases the torsional strain sustained before fracture.
3. A critical value of $\bar{\sigma}_{RES}$ exists such that:
   a. If $\bar{\sigma}_{RES} < Z$, then fracture is governed by a maximum shear strain mechanism and appears brittle; and,
   b. If $\bar{\sigma}_{RES} > Z$, then fracture is governed by a void coalescence mechanism and appears ductile.
4. The value of $\bar{\sigma}_{RES}$ can be controlled through the quench process variables.

This experimental relationship between the mean level of compressive residual stress on the surface and the angle-of-twist-at-failure implies that if residual stress measurements are made prior to torsional testing, the mode of fracture and the ultimate strain can be predicted. For this to be valid, the axle shafts tested must meet specification. Eddy current inspection to evaluate case depth and ultrasonic inspection to verify material integrity, are non-destructive methods which can be employed prior to torsional testing to determine whether specification is met.

This work demonstrates that residual stress measurements are necessary to characterize fracture behavior of induction-hardened axle shafts. Extension to different heat treatment specifications, forging conditions, materials and geometries requires the development of an extensive $\bar{\sigma}_{RES}$ data base and a complementary theory relating K_{IIIc} with $\bar{\sigma}_{RES}$.

APPENDIX I

PHYSICAL DATA

PHYSICAL DATA

ANG FAIL DEG	ULT TOR KIP	YS TOR KIP	YP TOR KIP	HARD 0.05 Rc	HARD 0.15 Rc	HARD CORE Rc	CASE Rc45 INCH	Di INCH	STEP APPX RcIn2	RAMP APPX RcIn2
116	61.0	37.0	25.0	56.0	38.0	10.0	.132	.634	32.44	44.50
88	68.1	34.0	20.0	57.0	56.0	15.2	****	.717	*****	56.77
193	57.7	34.3	20.0	54.0	36.0	8.0	.127	****	29.41	42.17
107	63.8	39.0	27.0	56.0	40.0	10.0	.140	.709	33.54	45.70
50	54.0	36.0	24.0	54.0	44.0	11.5	.140	.669	33.63	47.73
90	54.1	24.0	19.8	57.0	41.0	10.0	.133	.669	33.04	46.65
94	59.6	37.0	21.0	57.0	32.0	10.0	.125	.634	31.90	41.26
123	60.3	33.5	21.0	57.0	31.0	11.5	.112	.654	31.18	41.00
195	50.3	33.3	24.0	55.0	34.0	9.0	.123	.701	30.02	41.54
146	52.3	32.5	24.0	54.0	37.0	5.4	.130	.661	27.95	42.19
95	61.3	40.0	27.0	55.0	40.0	11.5	.137	.665	33.78	45.68
115	62.6	31.5	23.0	58.0	55.0	12.7	****	.701	*****	55.97
300	53.4	32.0	26.0	53.0	28.0	8.0	****	.579	*****	37.03
135	53.3	37.0	29.0	55.0	53.0	13.8	****	****	*****	53.97
168	61.7	38.0	27.5	49.0	52.0	8.5	****	.654	*****	50.10
195	62.5	40.0	29.0	56.0	49.0	10.0	****	****	*****	51.08
175	65.0	32.0	27.0	54.0	52.0	9.0	****	****	*****	51.96
205	61.3	36.5	27.0	55.0	53.0	11.5	****	.756	*****	53.46
134	60.1	37.5	26.5	55.0	41.0	8.0	.135	.492	30.98	45.51
157	58.6	37.0	26.0	49.0	39.0	8.0	.120	.598	26.35	42.21
100	55.8	36.0	26.5	54.0	49.0	12.7	****	.748	*****	50.98
148	55.0	36.5	25.0	54.0	****	10.0	****	.642	*****	*****
190	52.0	34.5	23.0	54.0	****	12.7	.150	****	35.67	*****
259	51.0	32.6	24.5	54.0	32.0	8.0	.090	.642	24.05	39.77
160	52.2	34.6	25.0	54.0	38.0	11.5	.130	.764	32.36	44.14
180	57.3	34.5	24.0	54.0	41.0	11.5	.140	.764	33.63	45.93
240	58.0	37.0	29.6	56.0	39.0	12.7	.133	.622	34.51	45.70
170	50.0	35.0	28.0	56.0	34.0	8.0	.127	.543	30.28	41.67
180	56.0	36.0	28.0	56.0	****	12.7	.140	.543	35.41	*****
370	59.6	33.0	24.0	57.0	****	12.7	.128	.543	34.30	*****
195	53.5	34.0	28.0	53.0	27.0	10.0	.090	.543	25.43	36.88
180	58.5	36.0	28.0	54.0	36.0	12.7	.130	.622	33.23	43.21
146	57.6	30.0	21.0	50.0	33.0	12.7	.137	.543	32.23	40.02
177	56.3	38.0	31.0	50.0	35.0	10.0	.107	.563	26.66	40.61
198	55.4	36.0	28.0	55.0	34.0	12.7	.117	.701	32.00	42.36
194	51.5	37.5	28.0	54.0	28.0	8.0	.092	.654	24.42	37.38
273	57.6	31.2	15.2	54.0	40.0	11.5	.127	****	31.98	45.33
233	54.9	26.2	37.1	51.0	28.0	8.0	.103	****	24.89	36.33
270	56.1	39.9	28.4	53.0	40.0	12.7	.122	****	31.87	45.25
147	59.9	39.1	22.6	52.0	****	10.0	.100	****	26.47	*****
182	59.1	38.9	22.0	48.0	****	10.0	.100	****	25.06	*****
115	54.5	36.0	22.0	53.0	****	5.4	.123	****	26.49	*****
287	51.6	33.3	26.0	49.0	****	8.0	.070	****	19.72	*****
146	56.3	50.4	34.0	52.0	****	12.7	.137	****	33.16	*****
183	54.0	36.2	24.0	50.0	****	11.4	.093	****	26.04	*****

PHYSICAL DATA

ANG FAIL DEG	ULT TOR KIP	YS TOR KIP	YP TOR KIP	HARD 0.05 Rc	HARD 0.15 Rc	HARD CORE Rc	CASE Rc45 INCH	Di INCH	STEP APPX RcIn2	RAMP APPX RcIn2
95	55.0	37.0	30.0	51.0	45.0	20.5	.150	****	39.34	49.27
120	63.2	36.5	26.0	56.0	44.0	6.4	.145	****	31.77	47.29
120	56.7	36.5	27.5	54.0	****	20.5	.120	****	37.86	*****
170	56.6	34.0	27.0	53.0	44.0	15.2	.140	****	35.72	48.20
125	58.2	37.0	28.0	54.0	41.0	20.5	.140	****	39.88	47.93
105	59.3	36.0	27.0	54.0	42.0	18.8	.135	****	38.17	48.15
130	54.3	39.0	30.0	54.0	****	18.8	.133	****	37.96	*****
135	55.0	36.0	29.5	53.0	****	15.2	.120	****	33.44	*****
245	60.7	34.5	26.5	55.0	41.0	10.0	.145	****	33.73	45.95
120	53.0	40.5	34.5	50.0	****	20.5	.120	****	36.20	*****
185	55.5	34.5	27.5	52.0	****	21.7	.135	****	39.31	*****
260	59.0	34.0	28.0	55.0	****	15.2	.132	****	35.79	*****
165	57.0	41.5	35.0	50.0	48.0	20.5	****	****	*****	50.72
105	56.6	40.0	32.8	53.0	****	20.5	.130	****	38.43	*****
192	56.0	37.0	31.0	50.0	****	8.0	.115	****	26.12	*****
200	57.5	35.0	28.0	53.0	****	10.0	.126	****	30.31	*****
237	57.5	36.0	28.0	54.0	50.0	11.5	****	****	*****	51.32
184	57.5	38.0	31.0	55.0	48.0	10.0	****	****	*****	50.14
77	52.4	35.0	24.0	54.0	42.0	15.2	.125	****	34.45	47.35
63	54.7	37.5	24.0	54.0	47.0	18.8	****	****	*****	51.14
116	59.7	35.8	23.0	56.0	48.0	20.5	****	****	*****	52.81
94	53.6	35.5	26.5	55.0	45.0	17.5	.150	****	39.37	50.00
67	54.6	35.0	22.0	54.0	48.0	16.0	****	****	*****	51.12
84	55.3	34.5	22.0	54.0	48.0	20.5	****	****	*****	52.11
58	51.2	32.5	18.0	54.0	46.0	18.8	****	****	*****	50.54
122	56.7	35.5	24.0	52.0	43.0	17.5	.145	****	37.35	47.76
105	58.5	30.5	17.5	55.0	47.0	18.8	****	****	*****	51.49
139	58.2	34.0	19.0	54.0	49.0	21.7	****	****	*****	52.98
136	52.5	34.5	24.0	55.0	46.0	15.2	****	****	*****	50.09
73	52.0	32.5	21.0	52.0	****	17.5	****	****	*****	*****
60	57.0	41.5	35.0	56.0	50.0	20.5	****	****	*****	54.01
65	52.0	33.5	21.0	53.0	37.0	15.2	****	****	*****	44.01
125	57.0	33.5	22.0	51.0	52.0	15.2	****	****	*****	52.28
91	55.0	31.0	20.0	54.0	44.0	8.0	.150	****	32.55	46.95
96	53.8	31.0	17.0	54.0	45.0	8.0	.150	****	32.55	47.55
74	57.8	35.0	19.0	54.0	44.0	10.0	.140	****	32.59	47.39
265	54.9	35.5	28.0	55.0	44.0	9.0	.145	****	33.05	47.52
74	60.7	36.3	21.0	56.0	45.0	20.5	.150	****	41.86	51.02
195	52.5	39.0	31.0	53.0	50.0	8.5	****	****	*****	50.30
55	54.6	33.0	22.0	56.0	52.0	12.6	****	****	*****	53.45
80	57.7	34.0	22.0	51.0	51.0	12.7	****	****	*****	51.13
80	57.9	32.0	20.0	59.0	49.0	10.0	****	****	*****	52.13
75	61.1	36.0	24.0	51.0	50.0	12.1	.130	****	31.46	50.40
82	56.9	34.6	26.0	55.0	42.0	10.0	****	****	*****	46.55
188	60.2	39.0	30.0	56.0	53.0	13.8	.145	****	36.80	54.32

PHYSICAL DATA

ANG FAIL	ULT TOR	YS TOR	YP TOR	HARD 0.05	HARD 0.15	HARD CORE	CASE Rc45	Di	STEP APPX	RAMP APPX
DEG	KIP	KIP	KIP	Rc	Rc	Rc	INCH	INCH	RcIn2	RcIn2
198	59.4	38.0	28.5	56.0	44.0	15.2	****	****	*****	49.24
75	59.2	35.0	22.0	55.0	46.0	15.2	****	****	*****	50.09
206	64.7	41.0	31.0	58.0	55.0	12.7	****	****	*****	55.97
200	57.6	32.0	27.0	56.0	52.0	12.7	****	****	*****	53.48
88	57.6	33.0	20.0	55.0	53.0	10.0	.098	****	27.23	53.13
100	57.2	34.0	21.0	55.0	48.0	10.0	****	****	*****	50.14
107	63.8	39.0	27.0	56.0	40.0	10.0	.140	****	33.54	45.70
244	57.6	35.0	23.0	56.0	40.0	10.0	.135	.669	32.86	45.70
225	59.5	35.3	24.0	53.0	51.0	10.0	.175	.650	36.39	51.23
232	58.6	35.0	24.0	56.0	44.0	10.0	.145	.654	34.22	48.09
126	60.4	36.0	23.0	56.0	48.0	9.0	.175	.642	37.52	50.26
135	59.8	33.3	21.0	55.0	40.0	9.0	.140	.634	32.37	45.13
124	60.0	35.4	22.0	57.0	45.0	9.0	.150	.650	34.72	48.82
193	57.7	34.3	20.0	54.0	36.0	8.0	.125	****	29.13	42.17
105	58.0	30.0	20.0	56.0	40.0	10.0	.140	.717	33.54	45.70
110	58.0	32.5	22.0	54.0	47.0	8.0	.165	.717	34.51	48.75
110	57.0	28.0	18.0	57.0	46.0	9.0	.155	.728	35.41	49.42
122	63.0	36.0	26.0	56.0	45.0	8.0	.150	.701	33.55	48.25
120	63.5	34.0	23.0	56.0	53.0	8.0	.200	.717	40.11	53.03
143	63.0	39.0	25.0	56.0	49.0	8.0	.170	.724	36.27	50.64
60	60.7	36.0	20.0	58.0	47.0	12.7	****	****	*****	51.18
229	56.8	33.0	22.0	54.0	43.0	8.0	.145	****	31.88	46.35
107	64.0	34.0	23.0	56.0	49.0	8.0	****	****	*****	50.64
171	64.6	36.0	25.0	57.0	54.0	8.0	****	****	*****	53.98
83	62.0	39.0	25.0	56.0	50.0	8.0	****	****	*****	51.24
264	59.1	34.0	23.0	58.0	47.0	8.0	****	****	*****	50.14
114	71.6	39.0	29.0	59.0	54.0	12.7	****	****	*****	55.72
166	59.0	30.0	18.0	55.0	49.0	6.4	****	****	*****	49.94
120	61.5	34.0	21.0	57.0	41.0	12.7	.135	****	35.23	47.25
237	60.0	35.0	25.0	56.0	47.0	12.7	****	****	*****	50.49
162	72.0	36.0	24.0	60.0	43.0	15.2	.142	****	39.31	50.04
95	60.4	38.0	22.0	54.0	34.0	8.0	.142	****	31.47	40.97
110	61.1	31.0	19.0	55.0	37.0	9.0	.135	****	31.69	43.33
202	56.4	33.0	21.0	55.0	36.0	8.0	.129	****	30.13	42.51
102	56.5	28.5	16.0	50.0	49.0	6.4	****	****	*****	48.19
96	52.5	30.0	18.0	54.0	49.0	6.4	****	****	*****	49.59
113	60.5	39.0	24.0	55.0	39.0	8.0	.130	****	30.27	44.31
268	59.8	36.0	24.0	56.0	44.0	8.0	.150	****	33.55	47.65
116	61.0	37.0	25.0	56.0	38.0	10.0	.130	****	32.17	44.50
88	68.1	34.0	20.0	57.0	36.0	15.2	.156	****	39.57	44.81
107	63.8	39.0	27.0	56.0	40.0	10.0	.140	****	33.54	45.70

APPENDIX II

"ERRROR" PROGRAM

ERRROR

```
1000 REM  STATISTICS AND NORMALITY TESTS BY S. A. ZAYAC
1010 PRINT 'INSTRUCTIONS (1=YES)';
1020 INPUT G4
1030 IF G4<>1 GOTO 1190
1040 PRINT
1050 PRINT 'THIS PROGRAM CALCULATES MEAN, STANDARD DEVIATION, SKEWNESS'
1060 PRINT 'AND KURTOSIS (IF REQUESTED), SAMPLE LOW, SAMPLE HIGH, SAMPLE'
1070 PRINT 'RANGE, LOWER 3-SIGMA LIMIT, UPPER 3-SIGMA LIMIT, AND 6-SIGMA'
1080 PRINT 'RANGE.  IF REQUESTED, COMPARES DISTRIBUTION WITH SPECIFICATION--'
1090 PRINT 'COUNT, ACTUAL PERCENTAGE, AND PROBABLE PERCENTAGE BELOW AND'
1100 PRINT 'ABOVE SPECIFICATION ARE INDICATED.  IF REQUESTED, COMPARES'
1110 PRINT 'DISTRIBUTION WITH NORMAL DISTRIBUTION FUNCTION USING THE'
1120 PRINT 'CORRECTED KOLMOGOROV-SMIRNOV D STATISTIC.'
1130 PRINT
1140 PRINT 'INPUT DATA (USE LINES 1 THROUGH 999)'
1150 PRINT '  FOR RAW DATA ENTER:  A(1),A(2),...,A(N),B(1),B(2),...B(N),...'
1160 PRINT '                ENTER:  909090 FOR MISSING DATA WITHIN SET'
1170 PRINT '  FOR FREQUENCIED DATA ENTER:  F(1),X(1),F(2),X(2),...,F(N),X(N)'
1180 GOTO 4980
1190 DATA 999999
1200 DIM V(20),F(20),W(20,5),B(5),C(999),T(999),E2(20)
1210 DIM O(999)
1220 S=S7=S8=R=B6=F5=F6=L0=H1=I5=0
1230 Y=I1=1
1240 PRINT 'DATA:  0=RAW OR 1=WEIGHTED';
1250 INPUT E4
1260 PRINT 'OUTPUT (1=HISTOGRAM & STATISTICS or 2=STATISTICS ONLY)';
1270 INPUT E5
1280 O9=2*E4+E5
1290 PRINT 'UNITS OF MEASURE (10 CHARACTER FIELD)';
1300 INPUT U4$
1310 PRINT 'CALCULATE SKEWNESS?  KURTOSIS (1=YES)';
1320 INPUT G1,G2
1330 PRINT 'TEST NORMALITY OF SAMPLE (1=YES)';
1340 INPUT G3
1350 IF O9>2 GOTO 1380
1360 PRINT 'NUMBER ASSOCIATED DATA POINTS?  VARIABLE ANALYZED';
1370 INPUT E1,E3
1380 PRINT 'SPECIFICATION LIMITS (LOW,HIGH) (ENTER  0  IF NONE)';
1390 INPUT B9,B8
1400 IF  O9<3  GOTO 1450
1410 PRINT 'DATA ADDITIVE CONSTANT';
1420 INPUT B6
1430 PRINT 'DATA MULTIPLICATIVE CONSTANT';
1440 INPUT Y
1450 IF E5<>1 GOTO 1500
1460 PRINT 'HISTOGRAM LOW LIMIT-USE 1 MORE DECIMAL DIGIT THEN REST OF DATA';
1470 INPUT F5
1480 PRINT 'HISTOGRAM INTERVAL-USE SAME NUMBER OF DECIMAL DIGITS AS DATA';
1490 INPUT F6
1500 PRINT 'DATE';
1510 INPUT U1$
1520 PRINT 'TITLE';
1530 INPUT U2$
1540 PRINT 'ENTER ANY CHARCATER.  POSITION PAPER.  PRESS RETURN.  ';
1550 INPUT U3$
1560  PRINT
1570 IF O9<3 GOTO 1710
1580 READ W
1590 IF W=999999 GOTO 1840
```

ERRROR

```
1600 READ Z
1610 IF Z=>B9 GOTO 1630
1620 LO=LO+W
1630 IF Z<=B8 GOTO 1650
1640 H1=H1+W
1650  FOR I=I1 TO I1+W-1
1660  LET C(I)=Z
1670  LET I2=I
1680  NEXT I
1690  LET I1=I1+W
1700  GOTO 1580
1710 FOR E0=1 TO E1
1720 READ E2(E0)
1730 IF E2(1)=999999 GOTO 1840
1740 IF E2(E0)=999999 GOTO 4960
1750 NEXT E0
1760 IF E2(E3)=909090 GOTO1710
1770 C(I1)=E2(E3)
1780 IF C(I1)=>B9 GOTO 1800
1790 LO=LO+1
1800 IF C(I1)<=B8 GOTO 1820
1810 H1=H1+1
1820 I1=I1+1
1830 GOTO 1710
1840 I2=I1-1
1850 N1=I2
1860 IF O9>2 GOTO 1950
1870 FOR J=1 TO N1
1880 FOR I=1 TO N1-1
1890 IF C(I)<C(I+1) GOTO 1930
1900 E6=C(I)
1910 C(I)=C(I+1)
1920 C(I+1)=E6
1930 NEXT I
1940 NEXT J
1950 E9=C(1)
1960 E8=C(N1)
1970  FOR I=1 TO N1
1980  LET C(I)=C(I)*Y+B6
1990  LET S=S+C(I)^2
2000  LET R=R+C(I)
2010  LET T(I)=C(I)
2020 O(I)=C(I)
2030  NEXT I
2040  LET A=R/N1
2050  LET C=S/N1
2060  LET D=A^2
2070  LET G=(N1*C-N1*D)/(N1-1)
2080  S1=0
2090  FOR I=1 TO N1
2100  S1=S1+(C(I)-A)*(C(I)-A)
2110  NEXT I
2120  K1=SQR(S1/(N1-1))
2130 G8=K1
2140  LET L3=A-3*K1
2150  LET U3=A+3*K1
2160 GOTO 2970
2170  PRINT
2180  LET V9=1
2190  LET L=1
```

ERRROR

```
2200  LET V(L)=F5
2210  FOR L=2 TO 20
2220  LET V(L)=V(L-1)+F6
2230  NEXT L
2240  LET F8=0
2250  FOR L=1 TO 20
2260  LET F9=0
2270  LET I=1
2280  IF C(I)>V(L)+.000001 THEN 2310
2290  LET F9=F9+1
2300  LET C(I)=100000.
2310  LET I=I+1
2320  IF I <= N1 THEN 2280
2330  LET F(L)=F9
2340  LET F8=F8+F9
2350  IF F(L)>81 THEN 2850
2360  IF V9=4 THEN 2400
2370  IF F(L)>54 THEN 2830
2380  IF V9=3 THEN 2400
2390  IF F(L)>27 THEN 2810
2400  NEXT L
2410 G9=0
2420 G9=G9+1
2430 IF G9=1 GOTO 2660
2440 PRINT TAB(13),'CELL MAX PRCT QUAN :....:....:....:....:....:....'
2450  FOR L=1 TO 20
2460  IF L=20 THEN 2770
2470  IF ABS(V(L))<.000001 THEN 2890
2480 PRINT USING 2490,V(L);100*F(L)/N1;F(L);
2490 :           #####.####  ###  ###
2500 IF F(L)=0 THEN 2600
2510  FOR M=1 TO INT((F(L)+1)/V9+.5)
2520  IF M=INT((F(L)+1)/V9+.5) THEN 2590
2530 IF M>1 THEN 2560
2540 PRINT ':';
2550 GO TO 2570
2560 PRINT '*';
2570 IF M=27 THEN 2870
2580 NEXT M
2590 IF M>1 THEN 2620
2600 PRINT ':'
2610 GO TO 2630
2620 PRINT '*'
2630 IF ABS(V(L))<.000001 THEN 2920
2640 NEXT L
2650 PRINT TAB(13),'CELL MAX PRCT QUAN :....:....:....:....:....:....'
2660  IF V9=4 THEN 2750
2670  IF V9=3 THEN 2730
2680  IF V9=2 THEN 2710
2690 PRINT TAB(32),'0    5   10   15   20   25   30'
2700 ON G9 GOTO 2420,4580
2710 PRINT TAB(32),'0   10   20   30   40   50   60'
2720 ON G9 GOTO 2420,4580
2730 PRINT TAB(32),'0   15   30   45   60   75   90'
2740 ON G9 GOTO 2420,4580
2750 PRINT TAB(32),'0   20   40   60   80  100  120'
2760 ON G9 GOTO 2420,4580
2770 PRINT USING 2780,100*(N1-F8+F(L))/N1;N1-F8+F(L);
2780 :                 ABOVE  ###  ###
2790  LET F(L)=N1-F8+F(L)
```

ERRROR

```
2800  GOTO 2500
2810  LET V9=2
2820  GOTO 2400
2830  LET V9=3
2840  GOTO 2400
2850  LET V9=4
2860  GOTO 2400
2870  PRINT ">"
2880  GOTO 2630
2890 PRINT USING 2900,100*F(L)/N1;F(L);
2900 :                0.0000  ###  ###
2910  GOTO 2510
2920 PRINT USING 2930,V(L+1);100*F(L+1)/N1;F(L+1);
2930 :            #####.####  ###  ###
2940  LET L=L+1
2950  GOTO 2500
2960  PRINT
2970  FOR I=1 TO N1
2980  LET C(I)=T(I)
2990  LET S9=C(I)-A
3000  LET S8=S8+S9^3
3010  LET S7=S7+S9^4
3020  NEXT I
3030  LET S6=K1^2
3040  LET S8=S8/(N1-1)
3050  LET S8=S8/(S6*K1)
3060  LET S7=S7/(N1-1)
3070  LET S7=S7/(S6^2)
3080  FOR M=1 TO 20
3090  FOR M1=1 TO 5
3100  READ W(M,M1)
3110  NEXT M1
3120  NEXT M
3130  DATA .3,.319,.352,.381,.417,.285,.299,.315,.337,.405
3140  DATA .265,.277,.294,.319,.364,.247,.258,.276,.3,.348
3150  DATA .233,.244,.261,.285,.331,.223,.233,.249,.271,.313
3160  DATA .215,.224,.239,.258,.294,.206,.217,.23,.249,.284
3170  DATA .199,.212,.223,.242,.275,.19,.202,.214,.234,.268
3180  DATA .183,.194,.207,.227,.261,.177,.187,.201,.22,.257
3190  DATA .173,.182,.195,.213,.25,.169,.177,.189,.206,.245
3200  DATA .166,.173,.184,.2,.239,.163,.169,.179,.195,.235
3210  DATA .16,.166,.174,.19,.231,.149,.153,.165,.18,.203
3220  DATA .131,.136,.144,.161,.187,.736,.768,.805,.886,1.031
3230  LET B(1)=.25483
3240  LET B(2)=-.284497
3250  LET B(3)=1.42141
3260  LET B(4)=-1.45315
3270 LET B(5)=1.0614
3280  LET P=.327591
3290  LET K1=K1*1.41421
3300  LET Z=(A-B9)/K1
3310 IF (B8+B9)=0 GOTO 3330
3320  IF Z <= 0 THEN 4930
3330  GOSUB 4660
3340  LET A3=50-50*E2
3350  LET Z=(B8-A)/K1
3360 IF (B8+B9)=0 GOTO 3380
3370  IF Z <= 0 THEN 4930
3380  GOSUB 4660
3390  LET A2=50-50*E2
```

ERRROR

```
3400  FOR I3=1 TO N1
3410  LET C(I3)=T(1)
3420  LET K0=1
3430  FOR I4=2 TO N1
3440  IF C(I3) <= T(I4) THEN 3470
3450  LET K0=I4
3460  LET C(I3)=T(I4)
3470  NEXT I4
3480  LET T(K0)=1.E+25
3490  NEXT I3
3500  LET Z=(A-C(1))/K1
3510  GOSUB 4660
3520  LET D5=.5-E2*.5
3530  LET I6=1
3540  FOR I=I6 TO N1
3550  IF C(I)>C(I6) THEN 3580
3560  IF I=N1 THEN 3790
3570  NEXT I
3580  LET Z=(ABS(C(I-1)-A))/K1
3590  GOSUB 4660
3600  IF C(I-1)<A THEN 3630
3610  LET D6=.5+E2*.5
3620  GOTO 3640
3630  LET D6=.5-E2*.5
3640  LET Q2=(I-1)/N1
3650  LET D6=ABS(Q2-D6)
3660  IF D5>D6 THEN 3680
3670  LET D5=D6
3680  LET Z=(ABS(C(I)-A))/K1
3690  GOSUB 4660
3700  IF C(I)<A THEN 3730
3710  LET D6=.5+E2*.5
3720  GOTO 3740
3730  LET D6=.5-E2*.5
3740  LET D6=ABS(Q2-D6)
3750  IF D5>D6 THEN 3770
3760  LET D5=D6
3770  LET I6=I
3780  GOTO 3540
3790  LET Z=(C(N1)-A)/K1
3800  GOSUB 4660
3810  LET D6=.5+.5*E2
3820  LET D6=1-D6
3830 IF D5>D6 GOTO 3850
3840  LET D5=D6
3850 I5=I5+1
3860 IF I5=6 GOTO 4050
3870 I3=18
3880  IF N1 <= 20 THEN 3920
3890  IF N1=30 THEN 3940
3900  IF N1>30 THEN 3960
3910  GOTO 3970
3920  LET I3=N1-3
3930  GOTO 3970
3940  LET I3=19
3950  GOTO 3970
3960  LET I3=20
3970  LET D6=W(I3,I5)
3980 IF I3<20 GOTO 4000
3990  LET D6=D6/SQR(N1)
```

ERRROR

```
4000 IF D6<=D5 GOTO 3850
4010 C2=.20-.05*(I5-1)
4020 IF C2<>0 GOTO 4060
4030 C2=.01
4040 GOTO4060
4050 C2=0
4060 PRINT
4070 PRINT TAB(17),U1$
4080 PRINT
4090 PRINT TAB(17),U2$
4100 PRINT
4110 PRINT USING 4120
4120 :        -------------------------------------------------------
4130 PRINT
4140 PRINT TAB(17),'SAMPLE DESCRIPTION'
4150 PRINT USING 4160,N1
4160 :                QUANTITY MEASURED.............. ##########
4170 PRINT USING 4180,U4$
4180 :                UNITS OF MEASURE............... 'CCCCCCCCCC
4190 PRINT TAB(17),'STATISTICAL MEASURES'
4200 PRINT USING 4210,A
4210 :                THE MEAN....................... #####.####
4220 PRINT USING 4230,G8
4230 :                STANDARD DEVIATION............. #####.####
4240 IF G1<>1 GOTO 4270
4250 PRINT USING 4260,S8
4260 :                SKEWNESS (-1 TO +1 NORMAL)..... #####.####
4270 IF G2<>1 GOTO 4300
4280 PRINT USING 4290,S7
4290 :                KURTOSIS (+2 TO +4 NORMAL)..... #####.####
4300 PRINT TAB(17),'DISTRIBUTION       LOW       HIGH      RANGE'
4310 IF (B8+B9)=0 GOTO 4340
4320 PRINT USING 4330,B9,B8,B8-B9
4330 :                SPECIFIED. ####.####  ####.####  ####.####
4340 PRINT USING 4350,E9,E8,E8-E9
4350 :                ACTUAL.... ####.####  ####.####  ####.####
4360 PRINT USING 4370,L3,U3,6*G8
4370 :                6-SIGMA... ####.####  ####.####  ####.####
4380 IF (B8+B9)=0 GOTO 4460
4390 PRINT TAB(17),'SPECIFICATION COMPARISON     BELOW     ABOVE'
4400 PRINT USING 4410,L0,H1
4410 :                ACTUAL COUNT..........     #####     #####
4420 PRINT USING 4430,L0*100/N1,H1*100/N1
4430 :                ACTUAL PERCENTAGE.....     ###.#     ###.#
4440 PRINT USING 4450,A3,A2
4450 :                PROBABLE PERCENTAGE...     ###.#     ###.#
4460 IF G3<>1 GOTO 4550
4470 IF C2<>0 GOTO 4520
4480 PRINT TAB(17),'NORMALITY TEST-REJECT @ .01 CONFIDENCE LEVEL'
4490 PRINT USING 4500,D5
4500 :                KOLMOGOROV-SMIRNOV D........... #####.####
4510 GOTO 4550
4520 PRINT USING 4530,C2
4530 :              NORMALITY TEST-ACCEPT @ .## CONFIDENCE LEVEL
4540 PRINT USING 4500,D5
4550 PRINT
4560 PRINT USING 4120
4570 IF E5=1 GOTO 2170
4580 FOR I=1TO 15
4590 PRINT '
          ';
```

ERRROR

```
4600 NEXT I
4610  IF S8<-1.1 THEN 4750
4620  IF S8>1.1 THEN 4750
4630  IF S7<2 THEN 4750
4640  IF S7>4 THEN 4750
4650 GO TO 4980
4660  LET T3=1/(1+P*Z)
4670  LET P2=0
4680  FOR J2=1 TO 5
4690  LET J3=6-J2
4700  LET P2=P2*T3+B(J3)
4710  NEXT J2
4720  LET P2=P2*T3
4730  LET E2=1-P2*EXP(-Z^2)
4740  RETURN
4750 PRINT 'PRINT MEDIAN RANKS (1=YES)';
4760 INPUT E7
4770 IF E7<>1 GOTO 4980
4780 PRINT
4790 PRINT U1$
4800 PRINT
4810 PRINT U2$
4820 PRINT
4830 PRINT 'THE SKEWNESS-KURTOSIS TEST FOR NORMALITY HAS'
4840  PRINT 'IMPLIED NON-NORMALITY. MEDIAN RANKS WILL BE GIVEN.'
4850  PRINT
4860  PRINT '      NUMBER    OBSERVATION    MEDIAN RANK'
4870  PRINT
4880  FOR Q7=1 TO N1
4890  LET Q3=(Q7-.3)/(N1+.4)
4900 PRINT Q7,O(Q7),Q3
4910  NEXT Q7
4920 GO TO 4980
4930  PRINT '*****UPPER SPEC LIMIT < MEAN OR LOWER SPEC LIMIT > MEAN.'
4940  PRINT '*****CHECK YOUR DATA AND TRY AGAIN.'
4950 GO TO 4980
4960 PRINT
4970 PRINT'ERROR IN INPUT DATA  .  DATA DOES NOT CORRESPOND TO GROUP SIZE.'
4980END
```

APPENDIX III

"COMPARE" PROGRAM

COMPARE

```
1000 REM  LINEAR REGRESSION ANALYSIS OF Y ON X BY S. A. ZAYAC
1010 REM   INPUT:  ENTER DATA LINES 1 THRU 999
1020 REM   INPUT:  ENTER PAIRED DATA SEQUENTIALLY
1030 REM   INPUT:  EXAMPLE (A1,A2,.....,AN,B1,B2,.....,BN,C1,C2,....CN)
1040 REM   INPUT:  ENTER 909090 FOR MISSING DATA WITHIN SET
1050 REM  OUTPUT: R, SIGMA(YX), Y=AX+B, PLOT(X,Y)
1060 X1=X2=Y1=Y2=Z=N=0
1070 W=1
1080 DIM X(9999), Y(9999)
1090 PRINT 'NUMBER OF ASSOCIATED DATA POINTS Z(1)....Z(K) WHERE K = ';
1100 INPUT K
1110 PRINT 'LET X = Z(I) IF I = ';
1120 INPUT L
1130 PRINT 'LET Y = Z(I) IF I = ';
1140 INPUT M
1150 FOR J = 1 TO 9999
1160 FOR I = 1 TO K
1170 READ Z(I)
1180 IF Z(1) = 999999 GOTO 1400
1190 IF Z(I)<>999999 GOTO 1230
1200 PRINT
1210 PRINT 'ERROR IN INPUT DATA.  DATA DOES NOT CORRESPOND TO GROUP SIZE.'
1220 GOTO 1520
1230 X=Z(L)
1240 Y=Z(M)
1250 NEXT I
1260 IF X=909090 GOTO 1280
1270 IF Y<>909090 GOTO 1310
1280 X(J)=909090
1290 Y(J)=909090
1300 GOTO 1390
1310 X(J)=X
1320 Y(J)=Y
1330 X1=X1+X
1340 Y1=Y1+Y
1350 X2=X2+X*X
1360 Y2=Y2+Y*Y
1370 Z=Z+X*Y
1380 N=N+1
1390 NEXT J
1400 S1=N*X2-X1*X1
1410 S2=N*Y2-Y1*Y1
1420 S3=N*Z-X1*Y1
1430 A0=(Y1*X2-X1*Z)/S1
1440 A1=S3/S1
1450 R=S3/(SQR(S1)*SQR(S2))
1460 S4=SQR((Y2-A0*Y1-A1*Z)/(N-2))
1470 PRINT
1480 PRINT 'DISPLAY DATA';
1490 INPUT T1
1500 PRINT
1510 IF T1<>1 GOTO 1660
1520 PRINT
1530 PRINT '           NO.','      PT.NO.','          X','           Y'
1540 E=N
1550 FOR J=1 TO E
1560 IF X(J)=909090 GOTO 1580
1570 IF Y(J)<>909090 GOTO 1600
1580 E=E+1
1590 GOTO 1620
```

COMPARE

```
1600 PRINT W,J,X(J),Y(J)
1610 W=W+1
1620 NEXT J
1630 IF Z(1)=999999 GOTO 1650
1640 GOTO 2570
1650 PRINT
1660 RESTORE
1670 PRINT 'VARIABLE NAME?, X UNITS?, TABLE NUMBER';
1680 INPUT X$,U$,T$
1690 PRINT 'VARIABLE ANALYZED?, FIRST CELL?, CELL WIDTH';
1700 INPUT X,X0,W
1710 S0=N
1720 S1=R
1730 S2=S4
1740 A=A1
1750 B=A0
1760 PRINT 'ENTER ANY CHARACTER.  POSITION PAPER. PRESS RETURN.';
1770 INPUT S$
1780 PRINT TAB(17),T$
1790 PRINT
1800 PRINT TAB(17),'ANGLE-OF-TWIST-AT-FAILURE'
1810 PRINT TAB(17),'CORRELATION WITH'
1820 PRINT TAB(17),X$
1830 PRINT
1840 PRINT USING 1850
1850 :             -------------------------------------------------------
1860 PRINT
1870 PRINT USING 1880,S0
1880 :                   SAMPLE SIZE.................          ###
1890 PRINT USING 1900,S1
1900 :                   CORRELATION COEFFICIENT.....       ##.###
1910 PRINT USING 1920,U$
1920 :                   UNITS TO MEASURE X..........  'RRRRRRRRRR
1930 PRINT TAB(17),'UNITS TO MEASURE Y..........       DEGREES'
1940 PRINT USING 1950,S2
1950 :                   STANDARD DEVIATION (YX)..... ##.# DEGREES
1960 PRINT
1970 PRINT USING 1850
1980 PRINT
1990 PRINT USING 2000,X0,X0+10*W,X0+20*W,X0+30*W
2000 :                     ###.#      ###.#      ###.#      ###.#
2010 PRINT TAB(19),'0 :....:....:....:....:....:....:'
2020 FOR N=1 TO 15
2030 D=25*N
2040 PRINT USING 2050,D;
2050 :                   ###
2060 PRINT ':';
2070 FOR M=1 TO 29
2080 C=0
2090 FOR L=1 TO 131
2100 READ Z(1),Z(2),Z(3),Z(4),Z(5),Z(6),Z(7),Z(8),Z(9)
2110 Y=3.14159*(Z(7)*(1220*Z(9)-Z(9)^2)+Z(8)*(610-Z(9))^2)/1000000
2120 IF Y>100 GOTO 2180
2130 IF Z(5)<25*(N-1) GOTO 2180
2140 IF Z(5)>=25*N GOTO 2180
2150 IF Z(X)<X0+W*(M-1) GOTO 2180
2160 IF Z(X)>=X0+W*M GOTO 2180
2170 C=C+1
2180 NEXT L
2190 RESTORE
```

COMPARE

```
2200 ON C+1 GOTO 2210,2230,2250,2270,2290,2310,2330,2350,2370,2390,2410,2430
2210 PRINT ' ';
2220 GOTO 2440
2230 PRINT 'A';
2240 GOTO 2440
2250 PRINT 'B';
2260 GOTO 2440
2270 PRINT 'C';
2280 GOTO 2440
2290 PRINT 'D';
2300 GOTO 2440
2310 PRINT 'E';
2320 GOTO 2440
2330 PRINT 'F';
2340 GOTO2440
2350 PRINT 'G';
2360 GOTO 2440
2370 PRINT 'H';
2380 GOTO 2440
2390 PRINT 'I';
2400 GOTO 2440
2410 PRINT 'J';
2420 GOTO 2440
2430 PRINT 'K';
2440 NEXT M
2450 PRINT ':'
2460 NEXT N
2470 PRINT TAB(17),'400 :....:....:....:....:....:....!'
2480 PRINT USING 2000,X0,X0+10*W,X0+20*W,X0+30*W
2490 PRINT
2500 PRINT TAB(17),'LEAST-SQUARES LINEAR APPROXIMATION'
2510 PRINT USING 2520,A,B
2520 :                     Y = (##.##) X + (###)
2530 FOR O=1 TO 20
2540 PRINT '
          '
2550 NEXT O
2560 DATA 999999
2570 END
```

APPENDIX IV

STATISTICAL RESULTS

TABLE 1

ANGLE-OF-TWIST-AT-FAILURE DISTRIBUTION

```
----------------------------------------------------------------

     SAMPLE DESCRIPTION
       QUANTITY MEASURED..............          131
       UNITS OF MEASURE...............      DEGREES
     STATISTICAL MEASURES
       THE MEAN.......................     148.1603
       STANDARD DEVIATION.............      62.4557
       SKEWNESS (-1 TO +1 NORMAL).....        .7537
       KURTOSIS (+2 TO +4 NORMAL).....       3.1724
     DISTRIBUTION         LOW        HIGH       RANGE
       ACTUAL....     50.0000    370.0000    320.0000
       6-SIGMA...    -39.2069    335.5275    374.7344
     NORMALITY TEST-REJECT @ .01 CONFIDENCE LEVEL
       KOLMOGOROV-SMIRNOV D...........        .1272

----------------------------------------------------------------

                           0    10   20   30   40   50   60
 CELL MAX PRCT QUAN :....:....:....:....:....:....:....:....
  25.0000    0    0 :
  50.0000    1    1 :
  75.0000    9   12 :******
 100.0000   15   20 :**********
 125.0000   23   30 :***************
 150.0000   11   14 :*******
 175.0000    8   10 :*****
 200.0000   17   22 :***********
 225.0000    3    4 :**
 250.0000    6    8 :****
 275.0000    5    7 :***
 300.0000    2    2 :*
 325.0000    0    0 :
 350.0000    0    0 :
 375.0000    1    1 :
 400.0000    0    0 :
 425.0000    0    0 :
 450.0000    0    0 :
 475.0000    0    0 :
    ABOVE    0    0 :
 CELL MAX PRCT QUAN :....:....:....:....:....:....:....:....
                           0    10   20   30   40   50   60
```

TABLE 2

TORSIONAL ULTIMATE STRENGTH DISTRIBUTION

```
---------------------------------------------------------

     SAMPLE DESCRIPTION
       QUANTITY MEASURED..............          131
       UNITS OF MEASURE............... 1000IN-LBS
     STATISTICAL MEASURES
       THE MEAN......................      57.9298
       STANDARD DEVIATION............       4.0685
       SKEWNESS (-1 TO +1 NORMAL).....       .6470
       KURTOSIS (+2 TO +4 NORMAL).....      3.9769
     DISTRIBUTION        LOW        HIGH       RANGE
       ACTUAL....   50.0000    72.0000    22.0000
       6-SIGMA...   45.7243    70.1352    24.4109
     NORMALITY TEST-ACCEPT @ .20 CONFIDENCE LEVEL
       KOLMOGOROV-SMIRNOV D...........        .0580

---------------------------------------------------------

                           0    15   30   45   60   75   90
 CELL MAX PRCT QUAN :....:....:....:....:....:....:....:....
   5.0000    0    0 :
  10.0000    0    0 :
  15.0000    0    0 :
  20.0000    0    0 :
  25.0000    0    0 :
  30.0000    0    0 :
  35.0000    0    0 :
  40.0000    0    0 :
  45.0000    0    0 :
  50.0000    1    1 :
  55.0000   26   34 :***********
  60.0000   47   61 :********************
  65.0000   24   31 :**********
  70.0000    2    2 :
  75.0000    2    2 :
  80.0000    0    0 :
  85.0000    0    0 :
  90.0000    0    0 :
  95.0000    0    0 :
    ABOVE    0    0 :
 CELL MAX PRCT QUAN :....:....:....:....:....:....:....:....
                    0    15   30   45   60   75   90
```

TABLE 3

TORSIONAL YIELD STRENGTH DISTRIBUTION

```
-------------------------------------------------------

SAMPLE DESCRIPTION
  QUANTITY MEASURED..............          131
  UNITS OF MEASURE............... 1000IN-LBS
STATISTICAL MEASURES
  THE MEAN.......................      35.2863
  STANDARD DEVIATION.............       3.2809
  SKEWNESS (-1 TO +1 NORMAL).....        .2515
  KURTOSIS (+2 TO +4 NORMAL).....       6.3572
DISTRIBUTION        LOW        HIGH       RANGE
  ACTUAL....    24.0000    50.4000     26.4000
  6-SIGMA...    25.4436    45.1289     19.6852
NORMALITY TEST-ACCEPT @ .01 CONFIDENCE LEVEL
  KOLMOGOROV-SMIRNOV D...........        .0880

-------------------------------------------------------

                       0    15   30   45   60   75   90
CELL MAX PRCT QUAN :....:....:....:....:....:....:....
   5.0000    0    0 :
  10.0000    0    0 :
  15.0000    0    0 :
  20.0000    0    0 :
  25.0000    1    1 :
  30.0000    5    7 :**
  35.0000   44   57 :******************
  40.0000   47   61 :********************
  45.0000    3    4 :*
  50.0000    0    0 :
  55.0000    1    1 :
  60.0000    0    0 :
  65.0000    0    0 :
  70.0000    0    0 :
  75.0000    0    0 :
  80.0000    0    0 :
  85.0000    0    0 :
  90.0000    0    0 :
  95.0000    0    0 :
    ABOVE    0    0 :
CELL MAX PRCT QUAN :....:....:....:....:....:....:....
                   0    15   30   45   60   75   90
```

TABLE 4

TORSIONAL YIELD POINT DISTRIBUTION

```
--------------------------------------------------------

     SAMPLE DESCRIPTION
       QUANTITY MEASURED..............          131
       UNITS OF MEASURE............... 1000IN-LBS
     STATISTICAL MEASURES
       THE MEAN.......................      24.6981
       STANDARD DEVIATION.............       4.1861
       SKEWNESS (-1 TO +1 NORMAL).....        .3456
       KURTOSIS (+2 TO +4 NORMAL).....       3.0192
     DISTRIBUTION         LOW        HIGH      RANGE
       ACTUAL....    15.2000    37.1000    21.9000
       6-SIGMA...    12.1397    37.2565    25.1168
     NORMALITY TEST-ACCEPT @ .01 CONFIDENCE LEVEL
       KOLMOGOROV-SMIRNOV D...........        .0853

--------------------------------------------------------

                          0    15   30   45   60   75   90
 CELL MAX PRCT QUAN :....:....:....:....:....:....:....
   5.0000    0    0 :
  10.0000    0    0 :
  15.0000    0    0 :
  20.0000   16   21 :******
  25.0000   43   56 :******************
  30.0000   33   43 :**************
  35.0000    8   10 :***
  40.0000    1    1 :
  45.0000    0    0 :
  50.0000    0    0 :
  55.0000    0    0 :
  60.0000    0    0 :
  65.0000    0    0 :
  70.0000    0    0 :
  75.0000    0    0 :
  80.0000    0    0 :
  85.0000    0    0 :
  90.0000    0    0 :
  95.0000    0    0 :
    ABOVE    0    0 :
 CELL MAX PRCT QUAN :....:....:....:....:....:....:....
                    0    15   30   45   60   75   90
```

TABLE 5

SURFACE HARDNESS DISTRIBUTION

```
--------------------------------------------------------

SAMPLE DESCRIPTION
  QUANTITY MEASURED..............          131
  UNITS OF MEASURE............... Rc@0.050IN
STATISTICAL MEASURES
  THE MEAN.......................      54.4198
  STANDARD DEVIATION.............       2.2359
  SKEWNESS (-1 TO +1 NORMAL).....       -.5611
  KURTOSIS (+2 TO +4 NORMAL).....       3.3815
DISTRIBUTION          LOW        HIGH       RANGE
  ACTUAL....   48.0000    60.0000     12.0000
  6-SIGMA...   47.7121    61.1276     13.4155
NORMALITY TEST-REJECT @ .01 CONFIDENCE LEVEL
  KOLMOGOROV-SMIRNOV D...........        .1812

--------------------------------------------------------

                     0    15   30   45   60   75   90
CELL MAX PRCT QUAN :....:....:....:....:....:....:....:....
  5.0000    0    0 :
 10.0000    0    0 :
 15.0000    0    0 :
 20.0000    0    0 :
 25.0000    0    0 :
 30.0000    0    0 :
 35.0000    0    0 :
 40.0000    0    0 :
 45.0000    0    0 :
 50.0000    8   11 :***
 55.0000   57   75 :************************
 60.0000   34   45 :**************
 65.0000    0    0 :
 70.0000    0    0 :
 75.0000    0    0 :
 80.0000    0    0 :
 85.0000    0    0 :
 90.0000    0    0 :
 95.0000    0    0 :
   ABOVE    0    0 :
CELL MAX PRCT QUAN :....:....:....:....:....:....:....:....
                     0    15   30   45   60   75   90
```

TABLE 6

CASE HARDNESS DISTRIBUTION

```
---------------------------------------------------------

     SAMPLE DESCRIPTION
       QUANTITY MEASURED..............        111
       UNITS OF MEASURE............... Rc@0.150IN
     STATISTICAL MEASURES
       THE MEAN.......................    43.7207
       STANDARD DEVIATION.............     6.7233
       SKEWNESS (-1 TO +1 NORMAL).....     -.4184
       KURTOSIS (+2 TO +4 NORMAL).....     2.5460
     DISTRIBUTION         LOW        HIGH       RANGE
       ACTUAL....    27.0000    56.0000     29.0000
       6-SIGMA...    23.5507    63.8907     40.3399
     NORMALITY TEST-ACCEPT @ .01 CONFIDENCE LEVEL
       KOLMOGOROV-SMIRNOV D...........      .0841

---------------------------------------------------------

                          0    10   20   30   40   50   60
 CELL MAX PRCT QUAN :....:....:....:....:....:....:....
   5.0000    0    0 :
  10.0000    0    0 :
  15.0000    0    0 :
  20.0000    0    0 :
  25.0000    0    0 :
  30.0000    4    4 :**
  35.0000    8    9 :****
  40.0000   21   23 :***********
  45.0000   24   27 :*************
  50.0000   28   31 :***************
  55.0000   14   16 :********
  60.0000    1    1 :
  65.0000    0    0 :
  70.0000    0    0 :
  75.0000    0    0 :
  80.0000    0    0 :
  85.0000    0    0 :
  90.0000    0    0 :
  95.0000    0    0 :
    ABOVE    0    0 :
 CELL MAX PRCT QUAN :....:....:....:....:....:....:....
                    0    10   20   30   40   50   60
```

TABLE 7

CORE HARDNESS DISTRIBUTION

```
----------------------------------------------------------

    SAMPLE DESCRIPTION
      QUANTITY MEASURED..............         131
      UNITS OF MEASURE............... RcCORE@FLG
    STATISTICAL MEASURES
      THE MEAN.......................     11.9160
      STANDARD DEVIATION.............      4.1265
      SKEWNESS (-1 TO +1 NORMAL).....       .8349
      KURTOSIS (+2 TO +4 NORMAL).....      2.7347
    DISTRIBUTION        LOW        HIGH       RANGE
      ACTUAL....     5.4000     21.7000     16.3000
      6-SIGMA...     -.4636     24.2956     24.7592
    NORMALITY TEST-REJECT @ .01 CONFIDENCE LEVEL
      KOLMOGOROV-SMIRNOV D...........       .1902

----------------------------------------------------------

                          0    15   30   45   60   75   90
CELL MAX PRCT QUAN :....:....:....:....:....:....:....
   5.0000    0    0 :
  10.0000   51   67 :**********************
  15.0000   24   31 :**********
  20.0000   16   21 :******
  25.0000    9   12 :***
  30.0000    0    0 :
  35.0000    0    0 :
  40.0000    0    0 :
  45.0000    0    0 :
  50.0000    0    0 :
  55.0000    0    0 :
  60.0000    0    0 :
  65.0000    0    0 :
  70.0000    0    0 :
  75.0000    0    0 :
  80.0000    0    0 :
  85.0000    0    0 :
  90.0000    0    0 :
  95.0000    0    0 :
    ABOVE    0    0 :
CELL MAX PRCT QUAN :....:....:....:....:....:....:....
                    0    15   30   45   60   75   90
```

TABLE 8

DEPTH TO Rc 45 DISTRIBUTION

SAMPLE DESCRIPTION			
QUANTITY MEASURED...............			86
UNITS OF MEASURE...............			IN/1000
STATISTICAL MEASURES			
THE MEAN.......................			133.1977
STANDARD DEVIATION.............			20.0451
SKEWNESS (-1 TO +1 NORMAL).....			-.1988
KURTOSIS (+2 TO +4 NORMAL).....			4.6899
DISTRIBUTION	LOW	HIGH	RANGE
ACTUAL....	70.0000	200.0000	130.0000
6-SIGMA...	73.0623	193.3331	120.2708
NORMALITY TEST-REJECT @ .01 CONFIDENCE LEVEL			
KOLMOGOROV-SMIRNOV D...........			.1196

CELL MAX	PRCT	QUAN	0 5 10 15 20 25 30
10.0000	0	0	:
20.0000	0	0	:
30.0000	0	0	:
40.0000	0	0	:
50.0000	0	0	:
60.0000	0	0	:
70.0000	1	1	:*
80.0000	0	0	:
90.0000	2	2	:**
100.0000	6	5	:*****
110.0000	2	2	:**
120.0000	8	7	:*******
130.0000	22	19	:*******************
140.0000	29	25	:*************************
150.0000	21	18	:******************
160.0000	2	2	:**
170.0000	2	2	:**
180.0000	2	2	:**
190.0000	0	0	:
ABOVE	1	1	:*
CELL MAX	PRCT	QUAN	0 5 10 15 20 25 30

TABLE 9

HARDENABILITY DISTRIBUTION

SAMPLE DESCRIPTION				
QUANTITY MEASURED..............				43
UNITS OF MEASURE...............				Di-IN/1000
STATISTICAL MEASURES				
THE MEAN.......................				654.2558
STANDARD DEVIATION.............				67.4357
SKEWNESS (-1 TO +1 NORMAL).....				-.4493
KURTOSIS (+2 TO +4 NORMAL).....				2.5229
DISTRIBUTION	LOW	HIGH	RANGE	
ACTUAL....	492.0000	764.0000	272.0000	
6-SIGMA...	451.9487	856.5629	404.6143	
NORMALITY TEST-ACCEPT @ .05 CONFIDENCE LEVEL				
KOLMOGOROV-SMIRNOV D...........				.1261

```
                            0    5    10   15   20   25   30
CELL MAX PRCT QUAN :....:....:....:....:....:....:....
400.0000     0    0 :
425.0000     0    0 :
450.0000     0    0 :
475.0000     0    0 :
500.0000     2    1 :*
525.0000     0    0 :
550.0000    12    5 :*****
575.0000     2    1 :*
600.0000     5    2 :**
625.0000     5    2 :**
650.0000    19    8 :********
675.0000    21    9 :*********
700.0000     0    0 :
725.0000    23   10 :**********
750.0000     5    2 :**
775.0000     7    3 :***
800.0000     0    0 :
825.0000     0    0 :
850.0000     0    0 :
   ABOVE     0    0 :
CELL MAX PRCT QUAN :....:....:....:....:....:....:....
                    0    5    10   15   20   25   30
```

TABLE 10

STEP APPROXIMATION DISTRIBUTION

```
----------------------------------------------------------------------

SAMPLE DESCRIPTION
  QUANTITY MEASURED...............              86
  UNITS OF MEASURE................         Rc-IN^2
STATISTICAL MEASURES
  THE MEAN........................         32.7950
  STANDARD DEVIATION..............          4.2760
  SKEWNESS (-1 TO +1 NORMAL)......          -.4305
  KURTOSIS (+2 TO +4 NORMAL)......          3.1564
DISTRIBUTION           LOW         HIGH      RANGE
  ACTUAL....     19.7207      41.8642      22.1435
  6-SIGMA...     19.9669      45.6230      25.6561
NORMALITY TEST-ACCEPT @ .01 CONFIDENCE LEVEL
  KOLMOGOROV-SMIRNOV D............           .1101

----------------------------------------------------------------------

                          0    5    10   15   20   25   30
CELL MAX  PRCT  QUAN  :....:....:....:....:....:....:....
 18.7500     0     0  :
 20.0000     1     1  :*
 21.2500     0     0  :
 22.5000     0     0  :
 23.7500     0     0  :
 25.0000     3     3  :***
 26.2500     5     4  :****
 27.5000     6     5  :*****
 28.7500     1     1  :*
 30.0000     2     2  :**
 31.2500     8     7  :*******
 32.5000    16    14  :**************
 33.7500    21    18  :******************
 35.0000     8     7  :*******
 36.2500     8     7  :*******
 37.5000     5     4  :****
 38.7500     6     5  :*****
 40.0000     7     6  :******
 41.2500     1     1  :*
   ABOVE     1     1  :*
CELL MAX  PRCT  QUAN  :....:....:....:....:....:....:....
                          0    5    10   15   20   25   30
```

TABLE 11

RAMP APPROXIMATION DISTRIBUTION

```
------------------------------------------------------------

   SAMPLE DESCRIPTION
     QUANTITY MEASURED..............          111
     UNITS OF MEASURE...............      Rc-IN^2
   STATISTICAL MEASURES
     THE MEAN.......................      47.8454
     STANDARD DEVIATION.............       4.4571
     SKEWNESS (-1 TO +1 NORMAL).....       -.4521
     KURTOSIS (+2 TO +4 NORMAL).....       2.7606
   DISTRIBUTION         LOW        HIGH     RANGE
     ACTUAL....     36.3324     56.7717   20.4393
     6-SIGMA...     34.4741     61.2168   26.7427
   NORMALITY TEST-REJECT @ .01 CONFIDENCE LEVEL
     KOLMOGOROV-SMIRNOV D...........        .1039

------------------------------------------------------------

                        0    5    10   15   20   25   30
 CELL MAX PRCT QUAN :....:....:....:....:....:....:....
  36.2500    0    0 :
  37.5000    4    4 :****
  38.7500    0    0 :
  40.0000    1    1 :*
  41.2500    4    4 :****
  42.5000    7    8 :********
  43.7500    3    3 :***
  45.0000    5    6 :******
  46.2500   12   13 :*************
  47.5000    7    8 :********
  48.7500   11   12 :************
  50.0000    5    6 :******
  51.2500   23   25 :*************************
  52.5000    5    6 :******
  53.7500    6    7 :*******
  55.0000    4    4 :****
  56.2500    3    3 :***
  57.5000    1    1 :*
  58.7500    0    0 :
    ABOVE    0    0 :
 CELL MAX PRCT QUAN :....:....:....:....:....:....:....
                    0    5    10   15   20   25   30
```

TABLE 12

ANGLE-OF-TWIST-AT-FAILURE
CORRELATION WITH
TORSIONAL ULTIMATE STRENGTH

SAMPLE SIZE.................	131
CORRELATION COEFFICIENT.....	-.076
UNITS TO MEASURE X..........	1000IN-LBS
UNITS TO MEASURE Y..........	DEGREES
STANDARD DEVIATION (YX).....	62.5 DEGREES

```
   45.0      55.0      65.0      75.0
  0 :....:....:....:....:....:....:
 25 :                             :
 50 :                             :
 75 :      AB D  B  B             :
100 :       BBACAC BABA     B     :
125 :        AAADBCBCDAFA      A  :
150 :       BAABABBBB  A          :
175 :     A A   AAAA A  A       A :
200 :     AABAABCDABA A  A        :
225 :           AB   A  A         :
250 :         A ABBAB             :
275 :      A  A AA C              :
300 :      A                      :
325 :        A                    :
350 :                             :
375 :              A              :
400 :....:....:....:....:....:....:
   45.0      55.0      65.0      75.0
```

LEAST-SQUARES LINEAR APPROXIMATION
Y = (-1.16) X + (216)

TABLE 13

ANGLE-OF-TWIST-AT-FAILURE
CORRELATION WITH
TORSIONAL YIELD STRENGTH

```
SAMPLE SIZE.................              131
CORRELATION COEFFICIENT.....             -.010
UNITS TO MEASURE X..........       1000IN-LBS
UNITS TO MEASURE Y..........          DEGREES
STANDARD DEVIATION (YX)..... 62.7 DEGREES
```

```
   22.0      32.0      42.0      52.0
  0 :....:....:....:....:....:....:
 25 :                             :
 50 :                             :
 75 :          BB BCA   A         :
100 :  A     ABAAECABAAA          :
125 :      B BBAADCFB EB          :
150 :        A ABB CC C          A:
175 :        A   BABAA  A         :
200 :          AAF DBDBA          :
225 :          AA AA    A         :
250 :    A      AADAA             :
275 :         AA BAA  A           :
300 :           A                 :
325 :          A                  :
350 :                             :
375 :           A                 :
400 :....:....:....:....:....:....:
   22.0      32.0      42.0      52.0
```

LEAST-SQUARES LINEAR APPROXIMATION
Y = (-.20) X + (155)

TABLE 14

ANGLE-OF-TWIST-AT-FAILURE
CORRELATION WITH
TORSIONAL YIELD POINT

SAMPLE SIZE................	131
CORRELATION COEFFICIENT.....	.284
UNITS TO MEASURE X..........	1000IN-LBS
UNITS TO MEASURE Y..........	DEGREES
STANDARD DEVIATION (YX).....	60.1 DEGREES

```
    10.0      20.0      30.0      40.0
   0 :....:....:....:....:....:....:
  25 :                             :
  50 :                             :
  75 :        AAACB B          A   :
 100 :       AAAEAD BABA  A        :
 125 :      AAAAACCDBBCE A  A A    :
 150 :         A BBABBA ABA   A    :
 175 :        A     ABABA      A   :
 200 :          B AAC  BFAAD       :
 225 :           A     BA  A       :
 250 :            AABAA AA       A :
 275 :     A       AB   C          :
 300 :                A            :
 325 :                A            :
 350 :                             :
 375 :              A              :
 400 :....:....:....:....:....:....:
    10.0      20.0      30.0      40.0
```

LEAST-SQUARES LINEAR APPROXIMATION
Y = (4.24) X + (43)

TABLE 15

ANGLE-OF-TWIST-AT-FAILURE
CORRELATION WITH
SURFACE HARDNESS (Rc @ 0.050 in)

SAMPLE SIZE.................	131
CORRELATION COEFFICIENT.....	-.085
UNITS TO MEASURE X..........	ROCKWELL C
UNITS TO MEASURE Y..........	DEGREES
STANDARD DEVIATION (YX).....	62.5 DEGREES

```
   40.0      50.0      60.0      70.0
  0 :....:....:....:....:....:....:
 25 :                             :
 50 :                             :
 75 :            AAE C A          :
100 :           C  FEAD A         :
125 :          B ABDDKDAA         :
150 :          AABAEDB            :
175 :         BA  AAAAA  A        :
200 :        A C ABGCD            :
225 :             A BA A          :
250 :           A ABAD            :
275 :             ABBA A          :
300 :         A                   :
325 :             A               :
350 :                             :
375 :                 A           :
400 :....:....:....:....:....:....:
   40.0      50.0      60.0      70.0
```

LEAST-SQUARES LINEAR APPROXIMATION
Y = (-2.36) X + (276)

TABLE 16

ANGLE-OF-TWIST-AT-FAILURE
CORRELATION WITH
CASE HARDNESS (Rc @ 0.150 in)

SAMPLE SIZE.................	111
CORRELATION COEFFICIENT.....	-.242
UNITS TO MEASURE X..........	ROCKWELL C
UNITS TO MEASURE Y..........	DEGREES
STANDARD DEVIATION (YX).....	58.9 DEGREES

```
   27.0      37.0      47.0      57.0
  0 :....:....:....:....:....:....:
 25 :                              :
 50 :                              :
 75 :          A      BAABA A A   :
100 :     A A A   AAB ACA ABBA A   :
125 :    A     ABADAAAABABBC   AAA:
150 :      A   A  AB    A AB  AA  :
175 :       A  AA   AA   AA  A A :
200 :AA     BAC    A  A   AAA AA  :
225 :         A               AA A:
250 : A          AAA AA  A  AA    :
275 :     A       B   B  A        :
300 :                              :
325 : A                            :
350 :                              :
375 :                              :
400 :....:....:....:....:....:....:
   27.0      37.0      47.0      57.0
```

LEAST-SQUARES LINEAR APPROXIMATION
Y = (-2.18) X + (239)

TABLE 17

ANGLE-OF-TWIST-AT-FAILURE
CORRELATION WITH
CORE HARDNESS (Rc @ flange)

SAMPLE SIZE..................	131
CORRELATION COEFFICIENT.....	-.265
UNITS TO MEASURE X..........	ROCKWELL C
UNITS TO MEASURE Y..........	DEGREES
STANDARD DEVIATION (YX).....	60.5 DEGREES

```
      .0      10.0      20.0      30.0
  0 :....:....:....:....:....:....:
 25 :                             :
 50 :                             :
 75 :          AAB  AAAB B        :
100 :      A D EAB  D A  B        :
125 :     AB ECGAD    AB D        :
150 :     A  BBB BA C  A AA       :
175 :      A D  A   B    A        :
200 :        EBEBDA A     A       :
225 :        A AAB                :
250 :        B DAB                :
275 :        CA AA  A             :
300 :        A                    :
325 :        A                    :
350 :                             :
375 :            A                :
400 :....:....:....:....:....:....:
      .0      10.0      20.0      30.0
```

LEAST-SQUARES LINEAR APPROXIMATION
Y = (-4.02) X + (196)

TABLE 18

ANGLE-OF-TWIST-AT-FAILURE
CORRELATION WITH
CASE DEPTH (Depth to Rc 45)

SAMPLE SIZE.................	86
CORRELATION COEFFICIENT.....	-.278
UNITS TO MEASURE X..........	INCH/1000
UNITS TO MEASURE Y..........	DEGREES
STANDARD DEVIATION (YX).....	59.5 DEGREES

```
   60.0     110.0     160.0     210.0
  0 :....:....:....:....:....:....:
 25 :                             :
 50 :                             :
 75 :                B A          :
100 :       A     BBAA DA         :
125 :          A C DCDBBA A      A:
150 :        A   A BCB     AA     :
175 :            AAA B            :
200 :      C AA BABAABAA          :
225 :             B               :
250 :        A     AA C     A     :
275 :      A     AAA  AA          :
300 :  A                          :
325 :                             :
350 :                             :
375 :             A               :
400 :....:....:....:....:....:....:
   60.0     110.0     160.0     210.0
```

LEAST-SQUARES LINEAR APPROXIMATION
Y = (-.85) X + (270)

TABLE 19

ANGLE-OF-TWIST-AT-FAILURE
CORRELATION WITH
HARDENABILITY (DI)

```
SAMPLE SIZE.................             43
CORRELATION COEFFICIENT.....          -.345
UNITS TO MEASURE X..........     INCH/1000
UNITS TO MEASURE Y..........       DEGREES
STANDARD DEVIATION (YX)..... 59.2 DEGREES
```

```
  490.0     590.0     690.0     790.0
  0 :....:....:....:....:....:....:
 25 :                             :
 50 :                             :
 75 :                 A           :
100 :              A  B    A      :
125 :              A B    CCA A   :
150 :A    A        AB A     A     :
175 :     A    A     A          A :
200 :     B A     A  A    B     A :
225 :                          A  :
250 :             A  BA           :
275 :               A             :
300 :                             :
325 :        A                    :
350 :                             :
375 :     A                       :
400 :....:....:....:....:....:....:
  490.0     590.0     690.0     790.0
```

LEAST-SQUARES LINEAR APPROXIMATION
Y = (-.32) X + (369)

TABLE 20

ANGLE-OF-TWIST-AT-FAILURE
CORRELATION WITH
STEP APPROXIMATION

SAMPLE SIZE.................	86
CORRELATION COEFFICIENT.....	-.137
UNITS TO MEASURE X..........	Rc-INCH^2
UNITS TO MEASURE Y..........	DEGREES
STANDARD DEVIATION (YX).....	61.4 DEGREES

```
   15.0      25.0      35.0      45.0
  0 :....:....:....:....:....:....:
 25 :                             :
 50 :                             :
 75 :                 AA       A  :
100 :            A   CBBA    C    :
125 :           A   ACBEBBABB A   :
150 :           AA  A BB  AB A    :
175 :           A   A A  A   A    :
200 :         ABC  BAA B BA  A    :
225 :               B             :
250 :         A      AAAB A       :
275 :         A      B B A        :
300 :    A                        :
325 :                             :
350 :                             :
375 :                   A         :
400 :....:....:....:....:....:....:
   15.0      25.0      35.0      45.0
```

LEAST-SQUARES LINEAR APPROXIMATION
Y = (-1.65) X + (183)

TABLE 21

ANGLE-OF-TWIST-AT-FAILURE
CORRELATION WITH
RAMP APPROXIMATION

SAMPLE SIZE................	111
CORRELATION COEFFICIENT.....	-.290
UNITS TO MEASURE X..........	Rc-INCH^2
UNITS TO MEASURE Y..........	DEGREES
STANDARD DEVIATION (YX).....	58.1 DEGREES

```
   30.0      40.0      50.0      60.0
  0 :....:....:....:....:....:....:
 25 :                             :
 50 :                             :
 75 :              A  B  AD AA    :
100 :          AA  AACB BCBBA  A  :
125 :          A  ACD CEACAAA B   :
150 :          A A  B A  C BA     :
175 :           AA A   AAC  A     :
200 :      AA  AACA A   ABB  A    :
225 :            A          B A   :
250 :      A        CA A AB       :
275 :         A     B B  A        :
300 :                             :
325 :       A                     :
350 :                             :
375 :                             :
400 :....:....:....:....:....:....:
   30.0      40.0      50.0      60.0
```

LEAST-SQUARES LINEAR APPROXIMATION
Y = (-3.93) X + (332)

BIBLIOGRAPHY

BIBLIOGRAPHY

1. Forbes, R. J., Metallurgy in Antiquity, Brill, Leiden, 1950.

2. Shot Peening, Wheelabrator-Frye, Mishawaka, Indiana, 1977.

3. Almen, J. O., "Improving Fatigue Strength of Machine Parts," Machine Design, Vol. 14, No. 6, pp. 124-129, 1943.

4. Horger, O. J. and Maulbetsch, J. L., "Improving the Fatigue Strength of Press-Fitted Axle Assemblies by Surface Rolling," A.S.M.E. Transactions, Vol. 48, pp. 91-98, 1936.

5. Osborn, H. B., Jr., "Surface Hardening by Induction," Metals Engineering Quarterly, August 1971.

6. Shklyarov, I. N., "Surface Quenching in the Case of Bulk Induction Heating ZIL-130 Axles," Metal Science and Heat Treatment, 1967, (UDC 621.735.545.4).

7. Smith, D. C., "Rating the 79's," Wards Auto World, Vol. 14, No. 10, p. 39, 1978.

8. Crandall, S. H., Dahl, N. L. and Lardner, T. J., An Introduction to the Mechanics of Solids, McGraw-Hill, 1972, p. 366.

9. Olszak, W., "Non-Homogeneity in Elasticity and Plasticity," I.U.T.A.M. Symposium, Warszawa, 1959, Pergamon Press.

10. Klosowicz, B. and Lurie, K. A., "On the Optimal Nonhomogeneity of a Torsional Elastic Bar," Archives of Mechanics, Vol. 24, No. 2, 1971, p. 239ff.

11. Klosowicz, B., "On the Optimal Nonhomogeneity of an Elastic Bar in Torsion; Numerical Examples," Archives of Mechanics, Vol. 25, No. 6, 1973, p. 945ff.

12. Reichert, V. K., "A Numerical Method to Calculate Induction Heating Installations," Electrowärme International, Bd. 26, Nn. 4, April 1968.

13. Lauers, J. D. and Biringer, P. P., "Induction Heating Calculations-The Effect of Coil Geometry," IEEE Conference Record, 5th Annual Meeting, Industrial and General Applications Group, pp. 299-305, 1970.

14. Kasper, R. J., "Transient Temperature Distribution in Round and Slab-Type Loads Heated by Electric Induction," Transactions of the A.S.M.E.-Journal of Heat Transfer, February 1971, p. 113.

15. "Induction Hardening and Tempering," A.S.M. Metals Handbook, Vol. 2, p. 170, A.S.M., 1971.

16. Ishii, K., Iwamoto, M., Shiriawa, T., and Sakamoto, Y., "Residual Stress in the Induction Hardened Surface of Steel," S.A.E. Paper No. 710280, 1968.

17. "Induction Hardening and Tempering," A.S.M. Metals Handbook, Vol. 2, p. 179, A.S.M., 1971

18. Feurstein, W. J. and Smith, W. K., "Elevation of Critical Temperatures in Steel by High Heating Rates," A.S.M. Transactions, Vol. 46, 1954, p. 1276.

19. Chipman, J., Metallurgical Transactions, Vol. 3, 1972, p. 55.

20. Gregson, V. G. and Sanders, B. A., "A Physical Model of Laser Heat Treatment," Proceedings of the Electro-Optics Conference, November 1974, Prepublication Reprint.

21. Wuerfel, E. R., A.S.M. Educational Seminar, 1960.

22. Wuerfel, R. K., "Characteristics of Induction Hardened Axles," Metals Progress, December 1963.

23. Hodge and Orehoski, Transactions A.I.M.E., Vol. 167, 1946, p. 627.

24. "Hardness Conversion Chart for Hardenable Carbon and Alloy Steels," 1966 S.A.E. Handbook, from "Useful Tables and Charts," International Nickel, December 1972.

25. Evans, E. B., "Metallurgical Instability and Residual Stresses in Hardened Steels," S.A.E. Conference Record, X-ray Fatigue Division, S.A.E. Fatigue Design and Evaluation Committee, Ann Arbor, Michigan, Sept. 24--25, 1968 (S.A.E. 710278).

26. Dolos, J., "The Effect of Grinding on the Residual Surface Stress Distributions in Case Hardened and Induction Hardened Parts," Senior Research Paper, Wayne State University, April 11, 1968.

27. Glenny, E., "Thermal Fatigue," Metallurgical Reviews, Vol. 6, No. 24, pp. 387-405, 1961.

28. Bühler and Scheil, Residual Stress Measurements, A.S.M., 1950, from N. H. Polakowski and E. J. Ripling, Strength and Structure in Engineering Materials, Prentice-Hall, 1966, p. 463.

29. Vatev, E., "Effect of Method of Induction Hardening on the Residual Stress Distribution," Hatere-Technische Mitteilungen, Vol. 29, No. 3, 1974, pp. 192-196.

30. Christenson, A. L., "Measurement of Stress by X-ray," S.A.E. TR-182, New York, NY, Society of Automotive Engineers, 1960.

31. Vatev, E., "Effect of the Tempering Process on the Residual Stress Distribution," Hatere-Technische Mitteilungen, Vol. 29, No. 1, pp. 32-37, 1974.

32. Liss, R. B., Massieon, C. G. and McKloskey, A. S., "The Development of Heat Treat Stresses and Their Effect on Fatigue Strength of Hardened Steels," S.A.E. Transactions, Vol. 74 (part 3), pp. 870-877, 1966.

33. Littleton, J. L., Jr., "A New Method for Measuring the Tensile Strength of Glass," Physical Review, Vol. 22, pp. 510-516, 1923.

34. Kaplan, M. A. and Rowell, G. A., "Shear Constraint and Macroscopic Fracture Criteria for Ductile Metals," A.S.M.E. Transactions - Journal of Applied Mechanics, Vol. 42, pp. 15-24, March 1975.

35. Irwin, "Fracture Mechanics," Structural Mechanics, Pergamon, 1960.

36. Brenner, S. S., Journal of Applied Physics, Vol 27. p. 1484ff, 1956.

37. Griffith, A. A., "The Phenomena of Rupture and Flow in Solids," Philisophical Transactions of the Royal Society, London, Vol. 221, pp. 163-198, 1921.

38. Lawn, B. R. and Wilshaw, T. R., Fracture of Brittle Solids, Cambridge University Press, 1975, pp. 5-78.

39. Polakowski, N. H. and Ripling, E. J., Strength and Structure of Engineering Materials, pp. 227-261, Prentice-Hall, 1966.

40. Jahsman, W. E. and Field, F. A., "The Effect of Residual Stresses on the Critical Crack Length Predicted by the Griffith Theory," Transactions of the A.S.M.E. - Journal of Applied Mechanics, Dec. 1963, pp. 613-616.

41. Ebert, L. J., Krotine, F. T. and Troiano, A. R., "A Behavioral Model for the Fracture of Surface Hardened Components," Transactions of the A.S.M.E. - Journal of Basic Engineering, Dec. 1965, pp. 871-874.

42. Rolfe, S. T. and Barsom, J. M., Fracture and Fatigue Control in Structures, Prentice-Hall, 1977, p. 32.

43. Makky, S. M., "Plastic Flow and Fracture in Round Bard in Pure Torsion," Journal of Mathematics and Mechanics, Vol. 10, No. 2, 1961, p. 199ff.

44. Fractographs 4918, 491 , 5032, A.S.M. Metals Handbook, Vol. 9, A.S.M., 1974.

45. "Interpretation of Light-Microscope Fractographs," A.S.M. Metals Handbook, Vol. 9, pp. 36-48, A.S.M., 1974.

46. Makky, S. M., "Application of the Theory of Fracture on the Surface of Instability," Angew. Math. und Mech., Vol. 46, No. 7, 1966, p. 432ff.

47. Nadai, A., Theory of Flow and Fracture of Solids, Vol. 1, Chap. 17, p. 243ff, McGraw-Hill, N.Y., 1950.

48. Nadai, A., op. cit. Chap. 15.13, p214ff.

49. Altiero, N. J., "On Edge - Fracture Problem of Rock Mechanics," Mechanics Research Committee, Vol. 3, pp. 345-352, Pergamon Press, 1976.

50. Yokobori, T. and Otsuka, T., Proceedings of the First International Congress on Experimental Mechanics, Pergamon Press, 1963, p. 353.

51. Yokobori, T., Takahaski, T. and Kishimoto, H., Journal of the Australian Institute of Metals, Vol. 8, p. 184, 1963.

52. McClintock, F. A., "Plasticity Aspects of Fracture," Fracture, An Advanced Treatise, Vol. III, Academic Press, 1971, p.111ff.

53. Hertzberg, R. W., Deformation and Fracture Mechanics of Engineering Materials, J. Wiley and Sons, 1976, p. 248.

54. Kardos, G., "Design Criterion for Generalized High Strain," Transactions of the ASME - Journal of the Engineering for Industry, Vol. 90, August 1968, pp. 485-490.

55. Jatczak, C. F., "Determining Hardenability from Composition," Metals Progress, September 1971.

56. Lilliefors, H. W., "On the Kolmogorov-Smirnov Test for Normality with Mean and Variance Unknown," American Statistical Association Journal, pp. 399-402, June 1967.

57. Glocker, R., Material Prufung mit Röntgenstrahlen, Springer, 1958, cited in J. T. Norton, "X-ray Determination of Residual Stresses," Materials Evaluation, February 1973, p. 21Aff.

58. Cullity, B. D., Elements of X-ray Diffraction, Addison-Wesley, 1959, p. 431ff.

59. Weinman, E. W., J. E. Hunter and D. D. McCormack, "Determining Residual Stresses Rapidly," Metal Progress, July 1969, p. 88ff.

60. Anderson, K. G., "Practical Accuracy Considerations in Use of the Fastress Residual Stress Analyzer," Chrysler Fastress Seminar, April 4, 1978.

61. Petch, N. J., "Metallurgical Aspects of Fracture," Fracture: An Advance Treatise, Vol. I, Academic Press, 1968, p. 381ff.

62. Cellitti, R. A., "A Study of the Effect of the Induction Hardening Variables on the Residual Stresses and Bending Fatigue Strength of Final Drive Gears," SAE Transactions, Vol. 76, 1968, p. 124ff, (SAE Paper No. 670504).

63. Almen, J. D. and Black, P. H., Residual Stresses and Fatigue in Metals, McGraw-Hill, 1963.

64. Landau, L. D. and E. M. Lifshitz, Theory of Elasticity, Pergamon Press, 1959, p. 30.

65. Kobasko, N. I., "The Development of Quench Cracks in Steel," Metal Science and Heat Treatment, 1971, p. 30.